

---

Electronic Theses and Dissertations, 2004-2019

---

2017

## Load Estimation, Structural Identification and Human Comfort Assessment of Flexible Structures

Ozan Celik  
*University of Central Florida*

 Part of the [Civil Engineering Commons](#), and the [Structural Engineering Commons](#)  
Find similar works at: <https://stars.library.ucf.edu/etd>  
University of Central Florida Libraries <http://library.ucf.edu>

This Doctoral Dissertation (Open Access) is brought to you for free and open access by STARS. It has been accepted for inclusion in Electronic Theses and Dissertations, 2004-2019 by an authorized administrator of STARS. For more information, please contact [STARS@ucf.edu](mailto:STARS@ucf.edu).

---

### STARS Citation

Celik, Ozan, "Load Estimation, Structural Identification and Human Comfort Assessment of Flexible Structures" (2017). *Electronic Theses and Dissertations, 2004-2019*. 5671.  
<https://stars.library.ucf.edu/etd/5671>

LOAD ESTIMATION, STRUCTURAL IDENTIFICATION, AND HUMAN  
COMFORT ASSESSMENT OF FLEXIBLE STRUCTURES

by

OZAN CELIK

B.S. Istanbul Technical University, 2009

M.S. Istanbul Technical University, 2011

A dissertation submitted in partial fulfillment of the requirements  
for the degree of Doctor of Philosophy  
in the Department of Civil and Environmental Engineering  
in the College of Engineering and Computer Science  
at the University of Central Florida  
Orlando, Florida

Fall Term  
2017

Major Professor: F. Necati Catbas

© 2017 Ozan Celik

## **ABSTRACT**

Stadiums, pedestrian bridges, dance floors, and concert halls are distinct from other civil engineering structures due to several challenges in their design and dynamic behavior. These challenges originate from the flexible inherent nature of these structures coupled with human interactions in the form of loading. The investigations in past literature on this topic clearly state that the design of flexible structures can be improved with better load modeling strategies acquired with reliable load quantification, a deeper understanding of structural response, generation of simple and efficient human-structure interaction models and new measurement and assessment criteria for acceptable vibration levels. In contribution to these possible improvements, this dissertation taps into three specific areas: the load quantification of lively individuals or crowds, the structural identification under non-stationary and narrowband disturbances and the measurement of excessive vibration levels for human comfort. For load quantification, a computer vision based approach capable of tracking both individual and crowd motion is used. For structural identification, a noise assisted Multivariate Empirical Mode Decomposition (MEMD) algorithm is incorporated into the operational modal analysis. The measurement of excessive vibration levels and the assessment of human comfort are accomplished through computer vision based human and object tracking, which provides a more convenient means for measurement and computation. All the proposed methods are tested in the laboratory environment utilizing a grandstand simulator and in the field on a pedestrian bridge and on a football stadium. Findings and interpretations from the experimental results are presented. The dissertation is concluded by highlighting the critical findings and the possible future work that may be conducted.

*Dedicated to;*

*My mother, Mahmude Celik*

*My father, Remzi Celik*

*My sister, Sezen Celik*

*And my beloved friends who supported, encouraged, and inspired me*

## ACKNOWLEDGMENTS

I would like to express my profound appreciation to my committee chair and advisor Professor F. Necati Catbas, who has given me the opportunity to be a part of innovative research projects, enlightened me with entrepreneurial vision and taught me the ways of being a proactive, conscientious, and hardworking person. He continually and convincingly conveyed a spirit of adventure in regard to research and scholarship, and excitement in regard to teaching. Without his guidance and persistent help, this dissertation would not have been possible.

To my committee members, Dr. Jeffrey Kauffman, Dr. Hae-bum Yun and Dr. Nicos Makris, for their time and valuable feedback; Dr. Mustafa Gul, Dr. Onur Avci, Dr. Manoj Chopra, Mr. Bora Erbilien and Mr. David Hansen for their help and insight in exchanging ideas and conducting experiments; our former and current research team members of Civil Infrastructure Technologies for Resilience and Safety (CITRS) along with all the undergraduate and graduate researchers who took part in the creation of this work. The hardware support from Mr. Lou Zagst and Mr. Jenner Sequeira of PCB Piezotronics is greatly appreciated.

I also would like to acknowledge the financial support for this research that is provided by Qatar National Research Fund [QNRF (a member of Qatar Foundation)] via the National Priorities Research Program (NPRP), Project Number: NPRP 6-526-2-218 and NSF Division of Civil, Mechanical and Manufacturing Innovation [grant number 1463493].

And last but most certainly not the least, I would like to express my deepest love and gratitude to my family and my great friends for their timeless and priceless support and encouragement through many years of personal, professional, and academic challenges.

# TABLE OF CONTENTS

LIST OF FIGURES .....	x
LIST OF TABLES .....	xiv
CHAPTER ONE: INTRODUCTION.....	1
Current Practices.....	2
Sensing/monitoring of individuals and crowd for load estimation.....	2
Load-time history measurements.....	2
Regeneration of Force Recordings.....	8
Structural Identification.....	10
Human Comfort.....	12
Objective and Scope .....	15
Organization of the Dissertation.....	19
CHAPTER TWO: A COMPUTER VISION APPROACH FOR THE LOAD TIME HISTORY MEASUREMENT OF LIVELY INDIVIDUALS AND CROWDS.....	20
General Remarks.....	20
Force Measurement Using Computer Vision.....	23
Sparse Flow.....	24
Dense Flow .....	28
Conversion of displacement units from image space to real world.....	29

Laboratory Verification.....	31
Experimental Setup.....	31
Dynamic Characterization of The Grandstand Simulator.....	34
Finite Element Model .....	35
Tests Conducted.....	37
Results and Discussion .....	38
Real Life Implementation .....	48
Monitoring and Modeling of the Structure .....	49
Analysis and Results.....	54
Concluding Remarks.....	57
 CHAPTER THREE: MODAL ANALYSIS UNDER HUMAN INDUCED EXCITATIONS USING NOISE ASSISTED AND ADAPTIVELY TRANSFORMED MULTIVARIATE EMPIRICAL MODE DECOMPOSITION.....	
Introduction.....	59
Empirical Mode Decomposition (EMD) Algorithm and Its Improved Variations .....	62
Multivariate Empirical Mode Decomposition (MEMD).....	64
Noise Assisted Adaptive Projection Intrinsically Transformed Multivariate Empirical Mode Decomposition (NA-APIT-MEMD).....	66
Time-Frequency Representation via Hilbert-Huang Transform .....	68

Adaptation to Operational Modal Analysis (OMA) .....	69
Separation of operational modes and applications steps .....	70
Experimental Studies .....	72
Laboratory structure and tests conducted .....	72
Results and Discussion .....	74
Real Life Applications .....	84
Monitoring of a stadium during a football event .....	84
Findings.....	86
Monitoring of a Footbridge.....	90
Findings.....	91
Concluding Remarks.....	94
CHAPTER FOUR: COMPUTER VISION BASED HUMAN COMFORT ASSESSMENT OF STADIA .....	95
Introduction.....	95
Calculation of Human Comfort Indices .....	97
Computer Vision Based Displacement Measurement.....	101
Experimental Studies .....	103
Concluding Remarks.....	107
CHAPTER FIVE: CONCLUSIONS .....	108

LIST OF REFERENCES .....112

## LIST OF FIGURES

Figure 1 Architectural and structural details of a stadium .....	1
Figure 2 Objective and scope of the dissertation .....	18
Figure 3 A: Gaussian Image pyramid; B: Bidirectional error .....	28
Figure 4 A: Scheme showing the measurements to acquire scale ratio; B: Scheme for scale ratio calibration in case of inclined camera.....	30
Figure 5 Force platform and its constituents.....	32
Figure 6 The grandstand simulator along with the details of its elements.....	32
Figure 7 The sensors installed on the simulator.....	32
Figure 8 Plan view showing the locations of sensors placed on the structure .....	33
Figure 9 Frontal and side view of the grandstand finite element model.....	35
Figure 10 A: Single subject on the rigid beam (Lucas-Kanade method); B: Two subjects on the rigid beam (Lucas-Kanade method); C: Four subjects on the flexible grandstand simulator (Lucas-Kanade method); D: Eight subjects on the stiff grandstand simulator (Lucas-Kanade method); E: Eleven subjects on the stiff grandstand simulator (Dense flow method).....	38
Figure 11 A: Displacement history of a single subject on the rigid beam; B: Acceleration time history; C: Comparison of estimated and measured forces; D: Close-up view of the comparison; E: Comparison of estimated and measured forces in the frequency domain.....	39
Figure 12 A: Comparison of estimated and measured forces of the two subjects on the rigid beam; B: Close-up view of the comparison; C: Comparison of estimated and measured forces in the frequency domain.....	41

Figure 13 A: Force time histories of each individual (four subjects) and their sum B: Comparison of estimated and measured forces of the four subjects on the flexible grandstand; C: Close-up view of the comparison; D: Comparison of estimated and measured forces in the frequency domain. 43

Figure 14 A: Comparison of displacements between FEM and LVDT generated by four subjects on the flexible grandstand; B: Comparison of acceleration for the same case ..... 44

Figure 15 A: Force time histories of each individual and their sum B: Comparison of estimated and measured forces of the eight subjects on the stiff grandstand; C: Close-up view of the comparison; D: Comparison of estimated and measured forces in the frequency domain..... 45

Figure 16 A: Comparison of accelerations generated by eight subjects on the stiff grandstand between FEM result and accelerometer; B: Close-up view of the same comparison, C: Comparison of strain values between FEM and strain gage ..... 46

Figure 17 A: Force time histories of each individual and their sum B: Comparison of estimated and measured forces of the eleven subjects on the stiff grandstand with dense flow; C: Close-up view of the comparison; D: Comparison of estimated and measured forces in the frequency domain ..... 47

Figure 18 A: Overlook of the stadium showing the monitored section and the location of the camera; B: Experiment setup; C: The computer controlled industrial camera; D: One sample frame from the camera record ..... 49

Figure 19 A: Accelerometer locations marked on the structure plan; B,D: Picture from the stadium corresponding to accelerometer locations; C: Sample detailed views of sensor-element attachments ..... 51

Figure 20 Finite element model of the monitored section ..... 51

Figure 21 CMIF plot of a sample data taken from stadium under ambient vibration .....	52
Figure 22 Mode shapes of the monitored grandstand.....	53
Figure 23 Overview of force estimation approach for the field study.....	54
Figure 24 Comparison of accelerations generated by the crowd on the monitored portion of the stadium between FEM result and accelerometer at 17 in Figure 19.....	56
Figure 25 Frequency comparison of accelerations generated by the crowd on the monitored portion of the stadium between FEM result and accelerometer at 17 in Figure 19.....	56
Figure 26 Illustration of dyadic filterbank property of MEMD after averaging the IMF spectrums of multiple channel 500 Gaussian white noise realizations .....	67
Figure 27 A, B: The grandstand simulator with accelerometers mounted at the front and at the back side of the structure; C, D: The placement of force washers between the steel grid and the support columns; E: The view of connections after the placement .....	73
Figure 28 An instant from the test as the subjects jump to the song on play and the locations of sensors.....	73
Figure 29 Amplitude spectrum of the recorded force and the white Gaussian noise of the same variance .....	75
Figure 30 The CMIF plot of the first singular value line under ambient testing and jumping excitation.....	76
Figure 31 SSI-COV stability diagram for the grandstand under ambient excitation.....	77
Figure 32 SSI-COV stability diagram for in-service data. ....	78
Figure 33 IMFs that belong to the grandstand jumping test .....	79
Figure 34 Power spectra of each IMF from four different locations on the grandstand.....	80

Figure 35 Estimation of damping from the auto correlation function of IMFs .....	82
Figure 36 Hilbert-Huang spectrum showing the variation of frequency over time .....	83
Figure 37 A: Monitored portion of the stadium; B: An overview of the crowd over the section .	85
Figure 38 The high sensitivity seismic sensors along with their locations on the structure .....	85
Figure 39 Extracted IMFs from the stadium field implementation .....	87
Figure 40 Hilbert-Huang spectrum showing the variation of frequency over time .....	89
Figure 41 A: The side view of the footbridge and locations of accelerometers; B: Name tags for accelerometers on both sides of the bridge .....	90
Figure 42 A: A perspective view from the footbridge and the data collection setup; B: The footbridge under the uncoordinated walking excitation of a group .....	91
Figure 43 Extracted IMFs from the footbridge experiment.....	92
Figure 44 Architectural and structural details of a stadium as a demonstration of their slender nature .....	98
Figure 45 Procedure for vision-based displacement measurement.....	101
Figure 46 SURF feature and Lucas-Kanade tracking: a) extracted SURF features; b) Feature tracking using Lucas-Kanade tracking algorithm .....	102
Figure 47 A demonstration of full field dense optical flow using Farneback algorithm .....	103
Figure 48 Comparison of the displacement records between the camera and the displacement sensor .....	104
Figure 49 Comparison of the acceleration records between the camera and the displacement sensor .....	104
Figure 50 Two structural members monitored for human comfort.....	106

## LIST OF TABLES

Table 1 Modal parameters of the grandstand simulator within 0-100 Hz frequency band.....	34
Table 2 Comparison of dynamic properties of the one-span simply supported structure with EMA parameters.....	36
Table 3 Comparison of dynamic properties of the two-span simply supported structure with EMA parameters.....	37
Table 4 A summary of the identification results for the laboratory grandstand simulator.....	81
Table 5 A summary of the identification results for the stadium structure .....	88
Table 6 A summary of the identification results for the footbridge .....	93
Table 7 Guide for the application of frequency-weighting curves for principal weightings .....	97
Table 8 Parameters of the transfer functions of the principal frequency weightings.....	98
Table 9 RMS Values and corresponding comfort levels (ISO 1997).....	99
Table 10 RMS Values and corresponding comfort levels [141] .....	99
Table 11 VDV Values and corresponding comfort levels [142] .....	100
Table 12 RMS & VDV Values and corresponding comfort levels [41].....	100
Table 13 Test scenarios for the measurement of comfort levels .....	103
Table 14 Comparison of the Evaluation of Each Case Based on RMS Acceleration for the grandstand.....	105
Table 15 Comparison of the Evaluation of Each Case Based on VDV Perception Ranges for the grandstand.....	105
Table 16 Comparison of the Evaluation of Each Case Based on RMS Acceleration for the stadium .....	106

Table 17 Comparison of the Evaluation of Each Case Based on VDV Perception Ranges for the stadium..... 107

## CHAPTER ONE: INTRODUCTION

Structures such as footbridges, dance floors, concert venues and especially stadia are usually designed with the intent to hold large numbers of people. The recent population growth and expansion of the entertainment industry, demand for such structures has increased dramatically, resulting in the need for new designs capable of accommodating even larger crowds (Figure 1). On the other hand, these new designs must also satisfy the architectural and aesthetic considerations such as long cantilevers to provide better lines of sight than typical structures, for instance in stadia, or long-distance spans with rather complicated geometries in footbridges. Being constructed as such and being in service under human excitation with large occupant-structure mass ratios, the structural components might be stressed to their limits as to serviceability and in some critical cases, even safety.

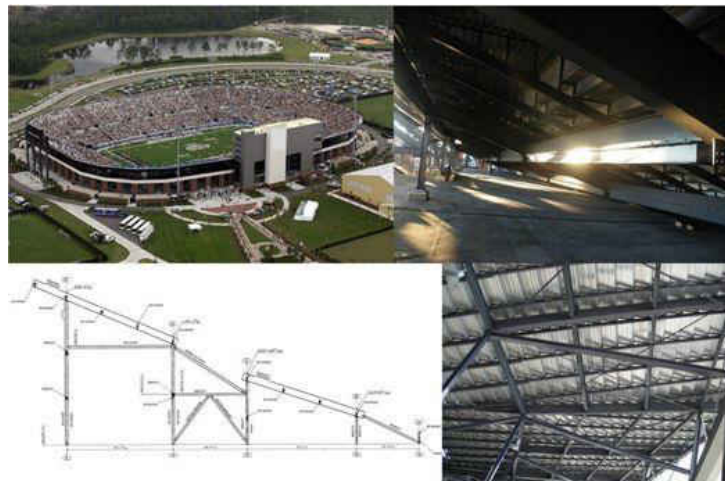


Figure 1 Architectural and structural details of a stadium

## Current Practices

### *Sensing/monitoring of individuals and crowd for load estimation*

Accurate determination of design loads is an important step to create an optimum serviceability design. Almost all different sorts of loads that can be encountered in human structure interaction problems are explained therein [1]. Of all different types of human loading, bouncing and jumping with their variable and long period applicability are viewed to be the most critical cases [2], [3] and are the focus of this dissertation. The dynamic effects of these two loadings on the structures, as it is pointed out by design guidelines[4]–[6], need to be assessed to determine if the vertical resonant frequencies of the structures fall below 8.5 Hz. This limit is based on the observation that higher Fourier harmonics of jumping load between the jumping and bobbing frequencies of 1.5-3.5 Hz can generate critical structural response. Nevertheless, these guidelines lack providing explicit and reliable methods for crowd loading (inter-subject variation). Besides, recreating realistic measured individual force time histories is still an issue due to the variations of motion within a subject's (intra-subject variability) body. The need for clarification of these uncertainties has been the motivation of this research on load quantification and modeling. Recent research is concentrated mainly on the improvement of conventionally recreated force-time history measurements and relatively new image-based techniques.

### *Load-time history measurements*

In general, dynamic force measurements are made by utilizing load cells or force plates that can generate force signals during the 'contact phase' and 'aerial phase' of jumping or bobbing. A unique and novel example of this measurement technique can be seen in a laboratory raked

grandstand model which is used to capture full force time histories via embedded force plates within the structure [7], [8]. The grandstand can accommodate 15 test subjects. The stand is supported by air springs and driven using linear actuators. This setup allows the structure to behave in two different modes namely “rigid” and “floating” which allows the dynamic response to vary between 2.8 - 23Hz. The real-time control techniques allow the researchers to test a variety of structure conditions and understand human-structure interaction, group coordination levels and acceptability limits of vibrations.

However, use of force plates brings some concerns such as (1) having small dimensions (~0.6x0.4m) that require controlled jumping which is quite tough when the subject is to jump at higher frequencies, therefore having distorted ground reaction force (GRF) patterns and (2) giving inaccurate results when mounted on a flexibly moving structure such as grandstand for the reason that additional inertial forces contribute to the measurements [9].

To remedy these problems regarding conventional methods, a preliminary novel load (bouncing/jumping, walking and running) - GRF estimation study based on motion tracking is proposed [10] rendering ‘free field’ measurements possible without the necessity of traditional laboratory restricted tests. The body of a test subject is subdivided into 15 major body segments which are then instrumented with markers at their connection points modeled as spherical hinges. Position of the markers are tracked down by video-based optoelectronic technology at 200Hz and accelerations are derived to be used in the estimation of GRF. Calculated GRFs are then validated by the direct measurements using an instrumented treadmill that is embedded in the ground. The results seem quite promising in capturing three harmonics of jumping records in frequency domain

(up to 15 Hz) especially for extreme loads (bouncing/jumping) commonly encountered in crowd dynamics.

The same method is validated in other studies by the same researchers [9], [11]. The test subjects perform the same test (without force plate measurements) both separately and together at three frequencies: 2, 2.2, 2.5 Hz but with identical conditions on a simply supported floor stripe whose modal characteristics are known from previous modal analysis. Generated force histories via tracking of visual data marker during jumping phase of subjects are input into the computer model and are compared with those acquired through direct acceleration measurements from the floor stripe. The results show a good match between the measured vibration responses and those calculated from the corresponding SDOF model using the recreated forces. The proposed method, is suggested to be applied on many different applications of human induced vibrations such as grandstands, footbridges, etc. to be explored in more depth in terms of practicality and accuracy especially in the existence of a large number of time dependent force records. As shown in the previous study, a database of different loadings can be generated to further create stochastic load models. However, the real-life applications of data markers require the test subjects to stand in a prescribed certain line to fully capture the three dimensional motion. Therefore, for field measurements where exists a high density of crowd, this method does not seem to be really feasible.

This problem is remedied by contactless sensing via the use of computer vision techniques. The earliest works of this kind include tracking the prominent body parts (mainly the face) of people by segmentation and looking at their correlation in consecutive images to estimate the loads applied to grandstands by large crowds. Inspired by some early works on contour detection and Bayesian clustering methods for crowd tracking, researchers use an easier method specifying each

tracked segment with a rectangle for estimating jumping and bobbing pattern on a laboratory grandstand. The results are not quite satisfying for the following reasons: (1) run time for the tracking algorithm being too long since the amount of data is large and (2) method not being sensitive enough to rapid changes in tracking the objects. Similarly, other trials focus on motion measurement of people and the patterns of their behavior in terms of velocity amplitude and frequency through either simulation in a computer controlled environment [12], [13] or utilizing off the shelf regular or thermal imaging cameras on a portion of a real grandstand [14], [15]. A well-known family of algorithms called as digital image correlation (DIC) commonly referred to as particle image velocimetry (PIV) is used in these studies. The application includes dividing the image into different fixed sized rectangular areas called Regions of Interest (ROI) and tracking the displacement of the most similar regions in the consecutive images. Since the elapsed time between consecutive images is known, the displacement and average velocity field as well as acceleration time histories could be acquired. Detailed analyses on some uncertainties regarding the technique such as the size of the ROIs and the resolution of the images are carried out via 2D and 3D image processing. In conclusion, a minimum limit for a successful image based study in terms of acquisition and analysis for grandstands is proposed. Utilization of the technique and recommendations for uncertainties are validated with scaled down images of a real stadium having shaker controlled dummies and a real small crowd jumping [12] in another study. A promising contactless measurements method captures the displacement and acceleration information from a real-life event where a group of people in various sizes demonstrates jumping activities. The novelty of the study lies within the adaptive nature of the algorithm to non-stationary changes as

illumination changes, object deformation. The results are compared with data marker tracking system and wireless accelerometers that can be attached on the human body [16].

After several preliminary trials of DIC algorithm applications, a promising step-up towards the load estimation is achieved relying on the experiments done at a section of an instrumented real life grandstand [17]. The aim is to generate loading functions based on the developed acceleration time histories. Regarding the large number of occupants, poor image resolution and perspective issues, it is chosen to work only on a small portion of the grandstand and with root mean square (RMS) of what values thereby mitigating the noise problem. The application, as before, includes dividing the image into different fixed sized rectangular ROIs and tracking the displacement of the most similar region in the consecutive images. Multiplying the accelerations with the apparent estimated mass of the crowd, force histories are obtained. Generated forcing functions are then used in a FE model of the real stadium with modal space approximation approach. The acquired responses come out much more similar to measured responses than those of calculated by utilizing the forcing functions given in current codes and guidance.

Another vision based approach renders measurement of jumping and bobbing loads on a crowd and on the field by making use of the same family of DIC algorithms [18]. Despite the idea of expanding an individual forcing to the entire crowd, the proposed method uses the motion of the crowd directly for generating forcing functions. The preliminary verifications for the method is performed by comparing the measured DIC data with the data coming from both accelerometers installed on a single test subject and dynamometric platform where the subject is jumping and bobbing within the frequency range of 1.5-3.5 Hz (0.1Hz intervals). The estimation of vertical induced loads is obtained by the sum of acceleration and body mass multiplication of body parts

and they show a reasonable match with high correlation compared to measured quantities. The level of discrepancy is also evaluated based on the difference between the experimental results from the method and the directly measured values by looking at the spectrums. The real-life experiments involve small groups at a stadium, varying in number (1, 4, 8 people) and mass (65, 260 and 600 kg), that are required to jump at frequencies: 2.1, 2.3 and 2.5 Hz. An experimental modal analysis (EMA) is carried out utilizing a moving mass to extract frequency response functions (FRFs) of the system. The structural vibrations are found by multiplying the force spectrum extracted via digital image correlation (DIC) with the frequency response functions (FRFs) acquired from previous experimental modal analysis (EMA) test.

The disadvantages of the computer vision and image processing based approaches are: (1) it generates large amounts of data that are not feasible to be stored and analyzed for the long term, (2) cameras used to capture crowd motion cannot be placed in front of the crowd, (3) the lighting conditions and extraneous camera flashes may affect the results, (4) cameras do not account for extraneous vibrations when recording. These problems are the motivation for further research on generating more efficient algorithms and on classification criteria for data to be stored based on the significance of the event. Creation of algorithms that are capable of counting and tracking multiple subjects through face recognition, might lead to more accurate response estimations and could assist with identification and isolation of passive and active members within the crowd.

The use of image processing and computer vision techniques allow for completely contactless measurement of loads and has the following advantages: it is inexpensive, can track large numbers of people, and can be utilized in virtually every environment. This approach completely removes the need for laboratory measurements and implementation of mathematical

function fittings. It is also suitable for assessing both an individual's induction on a system as well as a crowd's. This is a huge improvement considering the expansion problem of individual load measurements to crowds.

Although it is claimed that the visual marker tracking method can make free field measurements without utilizing force plates, it still has some significant obstacles. Visual tracking methods are quite expensive to instrument large numbers of subjects with data markers in the field and it necessitates that the subjects remain in a prescribed line. This method is currently unable to track the motion of overlapping subjects.

#### *Regeneration of Force Recordings*

The common mathematical function fitting approaches based on the load measurements via force plates or load cells at higher sampling rates either in time or frequency domain have now proven to be inaccurate and deficient for the following reasons: (1) real forcing functions are non-identical and not perfectly periodic, (2) fitting functions or Fourier series are incapable of representing the original forcing signals and (3) it suggests overly conservative designs due to excessive level of vibrations calculated in return. It has been shown by various researchers [19], [20] that walking and jumping loads are not perfectly periodic and are narrow-band phenomenon (intra-subject variation) by evincing the leakage around higher harmonics and frequently varying phase lags.

This knowledge necessitates a more advanced modelling strategy considering the altered morphology, variability of both peak to peak intervals and amplitudes of real jumping records. Although there has been studies towards the solution of the problem by utilizing probability

distributions to model frequency and Fourier coefficients of jumping pulses [21], [22], these are insufficient to reflect the true random nature of the problem. In [2], the consideration of peak to peak timing and amplitude variations are mainly observed through an auto-regression model. Recognizing that the preceding jumps are dependent on each other with an addition of normally distributed error each time, an auto-regression model is constructed upon two statistics namely mean delay (between the beat and the corresponding jump) and phase scatter (deviation about the mean). However, measured and generated force recordings do not closely match along the full frequency band except for the first two dominant harmonics. This is due to the reason that cosine-squared functions could only fit smooth shaped jumping pulses which are not always the case for different jumping frequencies. It should be noted that the consecutive pulses belonging to the same jumping frequency also change their shape.

In a series of recent studies by the same researchers, all these variations in peak to peak timing and amplitude and inadequate modelling issues seem to be mostly resolved with a novel approach [23]–[25]. Through stochastic processes, researchers can create a model that considers the lack of symmetry of the single peaked shapes by fitting Gaussian functions. They also achieve in representing local irregularities by increasing the number of Gaussians in the sum covering high frequency content of Fourier amplitude spectra. They expand their findings by developing a stochastic jumping load database. 825 measured force signals for the rates between 1.7 and 2.5 Hz are synthetically regenerated utilizing the new method. Considering that each synthetic recording is unity scaled, a vast majority of amplitudes for each recording can be acquired simply incorporating mass distributions for any human population of concern. This novel method seems

to reflect the true nature of jumping loading more closely than any other proposed method as well as showing promising indices for the expansion to crowds.

The stochastic load modeling approach is superior to the conventional half sine or Fourier series fitting methods because of its abilities to replicate intra-personal variations and to reproduce force-time histories of variable length. Acquisition of every harmonics as in the original recordings with their spread over the spectral energy are factors that would prevent overestimations of responses. Stochastic load modeling has not been expanded from individual load modeling to crowd modeling. The next step is to generate synthetic histories by using data from a large variety of jumpers, boppers at varying frequencies. These histories could then be condensed into a database that would later on let these excitations to be treated as a spectrum as in earthquake resistant design. Such a spectrum might easily be adopted in current guidance and used by designers.

### *Structural Identification*

There are several studies that address the performance of conventional identification methods for in-service data [26]–[28]. In these studies, different powerful operational modal analysis methods, such as Enhanced Frequency Domain Decomposition (EFDD), Least Square Complex Exponential (LSCE), Stochastic Subspace Identification (SSI-CVA, SSI-UPC, SSI-PC), Natural Excitation Technique (NExT) and Eigensystem Realization Algorithm (ERA) are used to analyze the data from common stadium conditions observed during a football game [27], [28]. The different conditions observed are, empty, crowd entering in, crowd seated, half-time, crowd leaving and celebration due to a successful play. Two notable observations from the study are that

dominant changes occur in the frequency and damping values, and that the magnitude of the changes depend on the crowd configuration. The first observation is consistent with the findings from other literature. The study also reveals that the estimated parameters for each method are different although the same data is used to estimate them. Based on the results from the study, it is suggested to use all possible different methods for creating reliable intervals and to complete a comprehensive identification study.

While it is suggested to use all possible methods to study a structure, not all methods may be applicable for flexible structures. For instance, an OMA method may only be applied if several requirements are met, such as the whole frequency band must be excited, the structural system must be linear and time invariant, and most importantly, the excitation must be in the form of Gaussian random white noise. These requirements can be prohibitive for the analysis of flexible structures, since individual or crowd motion can introduce dominant harmonic components into the system which transform the excitation into colored noise. Additionally, the dynamic response parameters of the structure are not time invariant. In a finite element modeling and updating study, it is observed that structural systems are possibly non-linear systems because of the large variability in measured damping values [29].

OMA identification techniques that have been used so far give fairly approximate results but it a huge question remains whether the existing OMA methods are suitable to use for flexible structures under human motion. The efficiency of the numerous identification methods still needs to be assessed. Newly developed methods should be introduced.

In future research, possible nonlinearities of slender nature of flexible structures, time-variant characteristics of the excitation and existence of possible harmonics need serious investigation.

### *Human Comfort*

In light of research from 2008, it has been proven difficult to assess the extreme vibration levels on humans with the prescribed methods, current standards and guidance for several reasons: (1) vibration levels are perceived differently from person to person and also from one location to another in the same structure, (2) spectators react differently depending on the type of the event, even though the same discomfort parameters are found for each event and (3) each structure responds uniquely to group/crowd excitation. The current well known and widely used assessment methodologies for vibration level measurements are [30]–[32]. These standards were originally developed to evaluate human exposure to vibrations caused by operation of machinery and vehicles, but the same procedures were thought to be applicable to flexible structures as well. The assessment measures used in these standards, such as root mean square (RMS), running RMS, maximum transient vibration value (MTVV), fourth power vibration dose value (VDV) or root mean quad (RMQ), have slight differences in their calculations of measurement directions, subjects' posture, application of frequency weightings, etc. Detailed information on the application of these measures have already been given in the review study by [1] mentioned above.

The research in the last decade has mainly focused on the application of health, perception, motion sickness and comfort classification measures for sporting events [33], [33]–[35], concerts [36], [37] or a combination of both; and for a long term monitoring [38]–[41]. The following

section intends to discuss some of the significant findings of this recent research and to indicate all critical research areas with somewhat consistent findings related to grandstands.

A psychophysical experimental method, called subjective scaling, was used to study an occupants' comfort and perception levels, while either sitting or standing [42]. [43] studied the often-confused relationship between human vibration-perception and comfort levels through the use of a controlled occupied grandstand. Subjects were asked to stay on the grandstand as it was gradually excited with different RMS powered sine wave vibrations from 2-6 Hz. The subjects were then asked to choose their subjective vibration-perception and comfort levels from a bank of provided text descriptors. Their responses were compared with frequency weighted acceleration of two particular standards namely [32], [44]. Extreme perception levels seemed to be occurring before the actual discomfort was felt, thus making perception levels more important in serviceability assessments. Also, the serviceability data for grandstands are found to be below the limits given for transportation structures (BS6841) but significantly above the limits for buildings (BS 6472).

Following the same experimental psychophysical methodology, [42] proposed a new approach for perception assessment that considered the relation between human comfort and either the root mean square (RMS) of the normalized ground reaction forces (GRF) time history, or the normalized foot point acceleration time history [45]. The study was originally motivated by the idea that the GRFs obtained with stationary measurements are different from those of a perceptibly moving structure [3]. The study consisted of ten subjects of varying weight, who were asked to stand on force plates that were mounted on a grandstand's floor while it was being excited. Then their subjective responses were recorded. For frequencies of excitation lower than 2 Hz, GRF

oscillations displayed the same characteristics as the grandstand oscillations. However, for frequencies greater than 2 Hz, GRF wave forms became inconsistent and almost nonlinear in trend. This pattern indicates that the subjects were trying to adapt themselves to the new state of motion. At a frequency of 4 Hz, the subjects began to experience acute levels of discomfort. The study concluded with normalizing the GRF histories by gravity (meaning foot point acceleration), which revealed that the RMS values of normalized GRFs are more reliable for the assessment of human discomfort levels. GRF and RMS values were found to increase proportionally, but were not necessarily proportional with increasing RMS values of the grandstand vibrations.

Although the weighting of acceleration record seemed to favor the calculation of primary assessment measure (RMS), the method's outcomes are not drastically different from those of other methods. Reported RMS values are likely to vary within the time window that they are calculated; unfortunately, it is still unknown how long the duration should be. Although the evaluation via MTVV (derived from running RMS) is independent from duration and is mostly the case for grandstands considering the excessive vibration exceeding crest factor (CF) threshold, the information on the event causing the extreme values cannot be extracted. VDV and RMQ calculations experience the same problems. These alternative measures have not been given specific limits in the standards. However, VDV measures of perception can be made referring to a scale given in previous studies, which has proven to be the most reliable method among the others so far. In most cases, measures of perception or human discomfort levels from the measurement scale do not match with the actual, observed behavior of the occupants; raising questions of its appropriateness for application on flexible structures.

Of all the preceding research, the main point of discussion is on the applicability and compatibility of the operating machinery based standards for the grandstand serviceability problem; as the excitation type have different inherence compared to machinery based vibrations.

The idea of forming new type vibration serviceability limits, or the revision of existing ones to include human induced excitation and building characteristics, is widely agreed upon, since the ones currently in use are incapable of accurately reflecting the true state. In the future, incorporation of more structure or event based case studies can assist with the creation of a database and of more robust limit state measures.

Another possible area for investigation is the generation of a new assessment measure based on displacements of the structure that consider that vibration based measures vary from person to person, are event dependent and they are equally likely to create panic by visual inspection of the audience

### Objective and Scope

A widely accepted procedure for vibration serviceability problem is to evaluate the system as a three-step framework (input/excitation/source – system/path/structure – output/response/receiver) [1], [5]. The problems that are addressed along this dissertation are being handled with a similar analogy but with a different approach (Figure 2).

The first objective of the study is to introduce alternative load time history measurement techniques for singular individuals and crowds using advanced computer vision algorithms along with their applications in both laboratory and real life. The algorithms are briefly explained, and their applications are presented starting from singular individuals on a simple beam going up to

groups in different sizes on a modular grandstand simulator that is instrumented with different types of conventional sensors. The results of a sample field study at a stadium hosting a fairly large crowd is provided. The study makes a valuable contribution in terms of providing contactless vision based load measurement techniques that are verified with both direct and indirect comparisons between estimated results and conventional sensor measurements. Additionally, applying the method on a real crowd, building a simulator that can be adjusted to flexible and stiff configurations thereby accommodating experiments for groups of different sizes are other contributions. In this sense, the study is taking one more step in support of creating a database for crowd loading that is strongly needed as it is pointed out by other researchers dealing with the same problem.

The second objective is to investigate the applicability of an alternative method that can track instantaneous changes of the dynamic behavior and possible nonlinearities over time for human-structure interaction problem. In addition, the identification is also conducted by making use of so called intrinsic mode functions (IMFs). In this regard, the study aims to contribute to the understanding of such structures' (especially stadiums [46]) behavior under operational effects with more informative and enriched findings so that better design guidelines could be prepared or possible serviceability issues could be remedied. The method is based on noise assisted and adaptively transformed multivariate empirical mode decomposition. First, the improved version of multivariate empirical mode decomposition and its expansion to operational modal analysis are introduced. Second, the proposed algorithm is applied on the response measurements of a flexible laboratory grandstand simulator, a stadium subjected to group jumping and a footbridge under pedestrian walking. In this regard, to the best of the authors' knowledge, the study also

demonstrates the first application of the method on real-life examples. Finally, the results and interpretations are presented.

The last objective delves into finding an alternative measurement and monitoring technique for human comfort levels on flexible structures. Flexible structures are generally prone to excessive vibration levels. Therefore, structural elements as well as crowd monitoring may become essential to prevent tragic events. However, current monitoring and surveillance techniques can be tedious to apply. In response to this, a novel, easy and useful method that can be adopted for the monitoring of such structures as well as spectators by making use of computer vision discipline is proposed. First, the current comfort measures are briefly described and then their computation by tracking structural elements and audience occupying the structure is carried out.

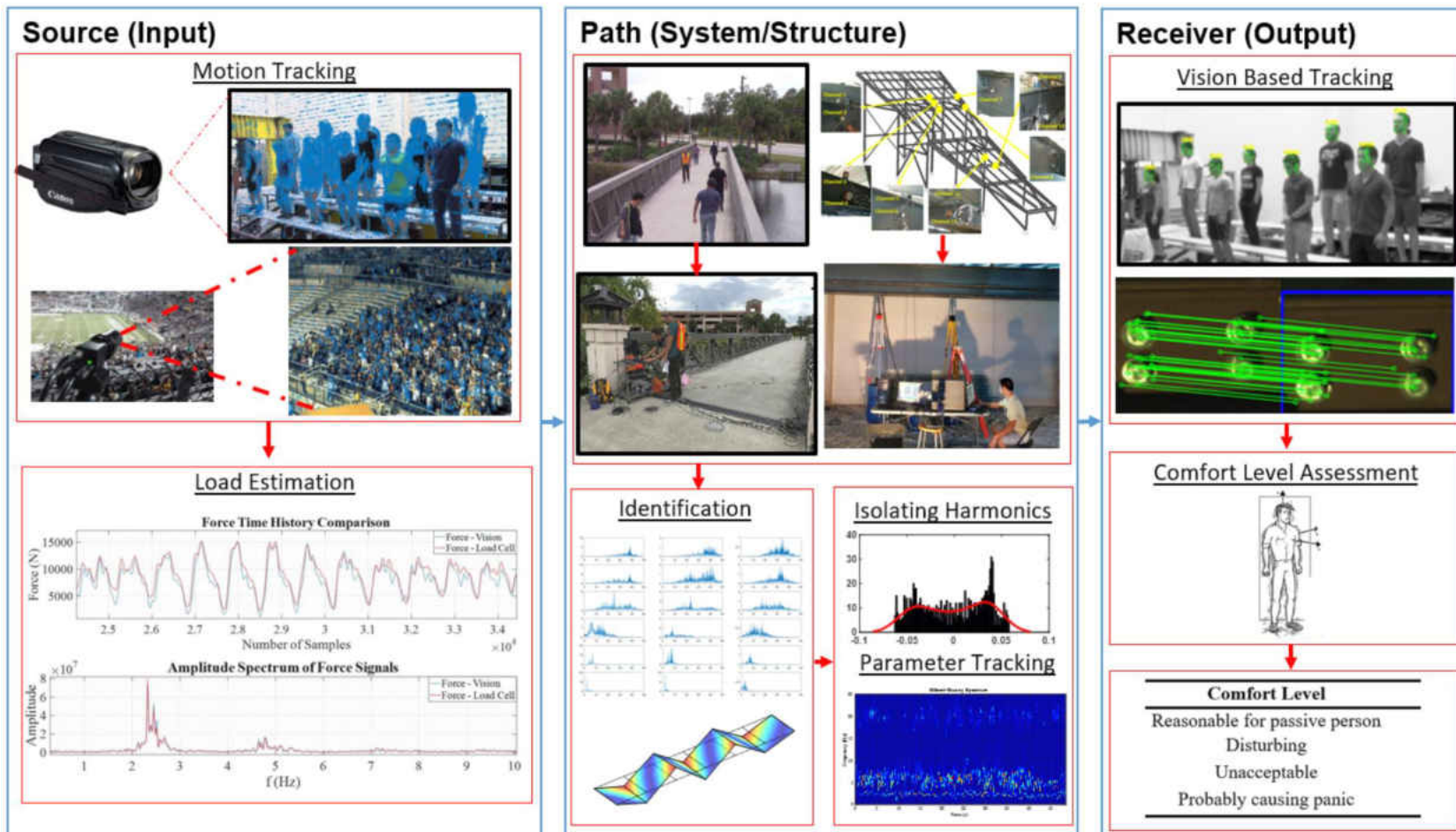


Figure 2 Objective and scope of the dissertation

## Organization of the Dissertation

The organization of the dissertation is as follows.

In *Chapter 2*, a computer vision based human motion tracking system is proposed to estimate human induced loadings of lively individuals and crowds. The well-established computer vision algorithms based on optical flow are presented and their integration into load time history estimation are explained. The findings from the tests conducted on a unique laboratory grandstand simulator and on a real-life stadium are presented along with discussions.

*Chapter 3* presents a hybrid, data-driven and adaptive signal processing algorithm and how it is incorporated into operational modal analysis. The differences and shortcomings of conventional methods compared to the proposed method are explained and the theory behind the proposed method is explained. Some of the tests conducted for Chapter 2 are processed to validate the efficiency of the method. Then, two different field studies when in service are presented.

*Chapter 4* is dedicated to the assessment of comfort levels in flexible structures. The motion tracking algorithms explained in Chapter 2 are used to monitor both structural members and occupants as an alternative way of measuring displacement and acceleration levels.

Finally, *Chapter 5* provides the summary and presents the conclusions after theoretical and applied studies are given in the dissertation. General comments about the methodologies described in this study are reviewed along with recommendations and possible directions for future research.

## **CHAPTER TWO: A COMPUTER VISION APPROACH FOR THE LOAD TIME HISTORY MEASUREMENT OF LIVELY INDIVIDUALS AND CROWDS**

### General Remarks

A widely accepted vibration serviceability criterion is to evaluate the system as a three-step framework namely excitation, path and response [1], [47], [48]. The excitation, which is the focus of this study, requires correct characterization of loads caused by humans. A great deal of research that has been done on human induced load measurement and modeling in civil engineering indicates that the estimation of jumping type loads (jumping/bouncing/bobbing/etc.) of both individuals and crowds are critical since these may create extreme vibration responses [2], [3], [49]. In case these loads are acted upon flexible structures such as stadiums, concert venues, dance floors, which have low frequency behavior by design requirements, vibration and displacement levels could be exacerbated to the point where catastrophic damages may occur [1]. On the other hand, when the motion of the crowd is in question, the severity of loading may vary significantly and may not be as strong depending on the level of synchronization between individuals. Some guidelines adopt conservative approaches in which individuals are thought to be generating the same type of force and crowds are simulated as a combination whereas other guidelines take the variability of force pulses and their expansion to crowd with a slightly probabilistic approach. The consensus is that the assumptions so far are still simplistic, and they ignore the sophisticated nature of the actual behavior, such as time lags between each loading sequences or peak to peak variations. As a result, an accurate expansion of these simplified models to crowd motion has not been achieved yet. Either for singular subjects or crowds, there are two widely applied methods for representing human induced loads.

A common method is the direct mathematical representation which makes use of trigonometric functions and their Fourier series representations. Early attempts of this kind are now known to be incorrect for they assume the loading being perfectly periodic and ignore the non-stationary variations. In return, they engender overly conservative designs due to excessive vibration and displacement responses. More reliable techniques take the jumping pulse variability of real jumping records into consideration and use the probability of their periodicity and amplitude changes for the reconstruction of force records [21], [22]. A similar probabilistic information on mean delay and phase scatter may also be fed into an auto-regression model [2] for improved results. However, measured, and generated force recordings do not closely match along the full frequency band due to the reason that cosine-squared functions could only fit smooth shaped jumping pulses. In the last decade, some promising research has been done to advance this approach with stochastic process based load generators in which sum of Gaussian functions are fitted to the measurements from real subjects to reconstruct accurate mathematical models [10], [23]–[25], [50].

Unfortunately, such applications are still limited to individual subjects and similar measurements or load generation models for crowds almost do not exist except a few [7], [8]. Besides, whether the case is utilizing the reconstructed simulations or directly using the measured forcing functions, accurate measurements for both individuals and crowds especially when on flexible structures are necessary. The conventional apparatus for dynamic force measurements of singular subjects are force plates. However, use of force plates brings some concerns such as (1) having small dimensions ( $\sim 0.6 \times 0.4$ m) that require controlled jumping which is quite tough when the subject is to jump at higher frequencies, therefore having distorted ground reaction force (GRF)

patterns and (2) giving inaccurate results when mounted on a flexibly moving structure such as grandstand for the reason that additional inertial forces contribute to the measurements. In search of solutions to such problems, some novel techniques are proposed.

A GRF estimation study, in which the body of a test subject is subdivided into fifteen major body segments and then instrumented with physical markers and tracked with video-based optoelectronic technology [9], [11], shows good alignment when compared with direct or indirect load measurements. The proposed method seems applicable in the field for sparsely distributed groups that remain in sight. As to the field measurements where exists a high density of crowd, this method does not seem to be feasible as the tracking device requires the subject to be visible at all times.

Some other alternatives exploit digital image processing and computer vision techniques. Several applications of computer vision based health monitoring studies may be found therein [51], [52]. The earliest works of this kind are carried out mostly using a well-known family of algorithms called digital image correlation (DIC). One study includes tracking the prominent body parts of people by segmentation and looking at their correlation in consecutive images to estimate the loads applied to grandstands by large crowds. Inspired by some early works on contour detection and Bayesian clustering methods for crowd tracking, researchers use an easier method specifying each tracked segment with a rectangle for estimating jumping and bobbing pattern on a laboratory grandstand. Similarly, other trials focus on motion measurement of people and the patterns of their behavior in terms of velocity amplitude and frequency through either simulation in a computer controlled environment [12], [13] or utilizing off the shelf regular or thermal imaging cameras on a portion of a real grandstand [14], [15]. Particle image velocimetry (PIV) is used in these studies.

The application includes tracking the displacement of the most similar regions in the consecutive images and eventually acquiring acceleration time histories [12], [53]. Another study estimates the load generated by a crowd at a section of an actively monitored real-life grandstand [17]. The aim is to generate loading functions based on the developed acceleration time histories. Another vision based approach renders measurement of jumping and bobbing loads on a crowd and on the field by making use of DIC algorithms [18]. The efficiency of the proposed method is verified in the laboratory and at the field with a small group of people. The aforementioned methods require improvements for the fact that they assume the motion of the crowd in the same direction and may perform poorly under changing environmental conditions.

Apart from DIC based studies, couple of more advanced methods capture the displacement and acceleration information where a group of people in various sizes demonstrates jumping activities. The novelty of these studies lie within the adaptive nature of the algorithm to non-stationary changes as illumination changes, object deformation. The results are compared with data marker tracking system and wireless accelerometers that can be attached on the human body and on a flexible laboratory slab floor with indirect acceleration responses [16], [54].

### Force Measurement Using Computer Vision

Utilization of computer vision allows the body motion of individuals or crowds to be measured with a camera from a long distance, without any contact and on any structure regardless of their flexibility. In case each body part is tracked individually, according to Newton's second law of motion the ground reaction force is estimated as follows:

$$F_{GR} = \sum_{i=1}^n m_i (a_i - g) \quad (1)$$

where  $m_i$  and  $a_i$  are mass and acceleration of the center of the mass of the  $i$ -th body segment,  $g$  is the standard gravity and  $n$  is the total number of body segments. The first step for force estimation is to find the displacement of the body. Once the displacement time history is known, acceleration record can be determined by taking either the second numerical derivative or the numerical gradient of the record. For the measurement of ground reaction forces, the mass is assumed to be concentrated at the head of a subject since this is a realistic assumption for the head is almost only visible part of the body regarding especially densely populated crowds. Besides, the motion of the head is more stable and it is easier to avoid abrupt mechanical motions when compared to other limbs of the body. Two algorithms based on the well-known optical flow estimation called sparse flow (Lucas-Kanade) and dense flow are explained along with their mathematical background to find the subject displacement.

### *Sparse Flow*

Optical flow is an image registration technique where the surface motion in three-dimensional environment is approximated onto approximate two-dimensional motion field by making use of spatiotemporal patterns of image intensity [55], [56]. The optical flow measurement along with its improved different versions have been accepted as a reasonable and fairly accurate estimation of displacement and velocity and has had numerous applications such as recognition, tracking, motion modeling, segmentation, etc. in different engineering fields. In the scope of this study, two well-established variations proposed by [57] and [58], [59] for sparse and dense motion estimation respectively are applied.

Determining optical flow requires the assumption of constant brightness in spatial and temporal space of consecutive frames by

$$f(x, y, t) = f(x + dx, y + dy, t + dt) \quad (2)$$

where  $f$  represents the image frame with the parameters  $x$ ,  $y$  and  $t$  indicating pixel locations and time respectively. Expanding Equation (2) into Taylor series gives

$$f(x, y, t) = f(x, y, t) + \frac{\partial f}{\partial x}(x + dx - x) + \frac{\partial f}{\partial y}(y + dy - y) + \frac{\partial f}{\partial t}(t + dt - t) \quad (3)$$

Canceling the same terms on both sides and simplifying Equation (3) result in

$$f_x u + f_y v = -f_t \quad (4)$$

Equation (4) is the so called optical flow equation indicating a line having a slope of  $-f_x / f_y$  with the two unknowns  $u$  and  $v$  corresponding to motion in  $x$  and  $y$ . The solution of Equation (4) necessitates one more assumption which eventually gives name to different variations on the computation of optical flow. Lucas-Kanade method assumes that the motion within the small neighborhood of the pixel of interest is the same and small thereby generating more equations than unknowns:

$$\begin{bmatrix} f_{x_1} & f_{y_1} \\ f_{x_2} & f_{y_2} \\ \vdots & \vdots \\ f_{x_n} & f_{y_n} \end{bmatrix} \begin{Bmatrix} u \\ v \end{Bmatrix} = \begin{Bmatrix} -f_{t_1} \\ -f_{t_2} \\ \vdots \\ -f_{t_n} \end{Bmatrix} \quad (5)$$

Equation (5) can be written in matrix form as follows:

$$\mathbf{A}\mathbf{u} = \mathbf{f}_t \quad (6)$$

Since the matrix  $\mathbf{A}$  is not a square matrix and the system is overdetermined, the solution is found utilizing the least squares method:

$$\min \sum_i (f_{x_i} u + f_{y_i} v + f_t)^2 \quad (7)$$

which leads to:

$$\frac{\partial}{\partial u} \sum_i (f_{x_i} u + f_{y_i} v + f_t)^2 = \sum_i (f_{x_i} u + f_{y_i} v + f_t) f_{x_i} = 0 \quad (8)$$

$$\frac{\partial}{\partial v} \sum_i (f_{x_i} u + f_{y_i} v + f_t)^2 = \sum_i (f_{x_i} u + f_{y_i} v + f_t) f_{y_i} = 0 \quad (9)$$

It is now possible to solve this system of two equations with the two unknowns. By rearranging Equation (8) and (9) the solution is found:

$$\begin{Bmatrix} u \\ v \end{Bmatrix} = \frac{1}{\sum f_{x_i}^2 \sum f_{y_i}^2 - (\sum f_{x_i} f_{y_i})^2} \begin{bmatrix} \sum f_{y_i}^2 & -\sum f_{x_i} f_{y_i} \\ -\sum f_{x_i} f_{y_i} & \sum f_{x_i}^2 \end{bmatrix} \begin{Bmatrix} -\sum f_{x_i} f_t \\ -\sum f_{y_i} f_t \end{Bmatrix} \quad (10)$$

Equation (10) constitutes a useful specialty. The second term on the right-hand side of the equation corresponds to what is known as a corner detector in image processing. This simply means that the locations of points to be tracked can be selected from good features [60]–[67] which are more reliable for tracking and then optical flow computation can be executed around that neighborhood. Once a reliable feature is extracted and their flow is computed, a translation model is introduced to link the estimated locations and build up their trajectory:

$$W(\mathbf{x}; \mathbf{p}) = (x + b_1, y + b_2) \quad (11)$$

where  $W$  is the spatially varying motion model (translation here) or correspondence map with  $b_1$  and  $b_2$  coefficients to be determined and parametrized by a low dimensional vector  $\mathbf{p}$ .

The parametric incremental motion update now boils down to the minimization of the following residual function implementing iteratively reweighted least squares technique:

$$\sum_{\mathbf{x}} [f(W(\mathbf{x}; \mathbf{p} + \Delta \mathbf{p})) - T(\mathbf{x})]^2 \quad (12)$$

where  $T(\mathbf{x})$  is the template image. Expanding Equation (12) to Taylor series, differentiating with respect to  $\Delta \mathbf{p}$  and rearranging gives the update term for:

$$\Delta \mathbf{p} = H^{-1} \sum_{\mathbf{x}} \left[ \nabla f \frac{\partial W}{\partial \mathbf{p}} \right] [T(\mathbf{x}) - f(W(\mathbf{x}; \mathbf{p}))] \quad (13)$$

where

$$H = \sum_{\mathbf{x}} \left[ \nabla f \frac{\partial W}{\partial \mathbf{p}} \right]^T \left[ \nabla f \frac{\partial W}{\partial \mathbf{p}} \right] \quad (14)$$

Equation (14) is what is known as Hessian matrix. An iterative updating of  $\mathbf{p} \rightarrow \mathbf{p} + \Delta \mathbf{p}$  leads to the translation alignment of tracked features and this last step concludes the tracking procedure.

The accuracy of the displacement measurement can further be increased by two additional methods. The first method is to fine tune the residual errors caused by large motions that violate the Lucas-Kanade assumption. The resolution of the original image is subsampled by a factor of two as to create a multi-layer image pyramid. The iterative tracking starts at the lowest resolution and ends until a reasonable convergence is achieved. Consecutive layers take the previous result as their first estimation propagating the same procedure towards the final layer. The latter method is to compensate for the unreliable features that may be lost during tracking. The optical flow is computed forward and backward expecting the return of the same location. However, this is not always the case as it is seen at point **B** in Figure 3-B. This difference is named as the bidirectional error and removed by imposing a threshold leaving only the reliable and features to track within that acceptable threshold.

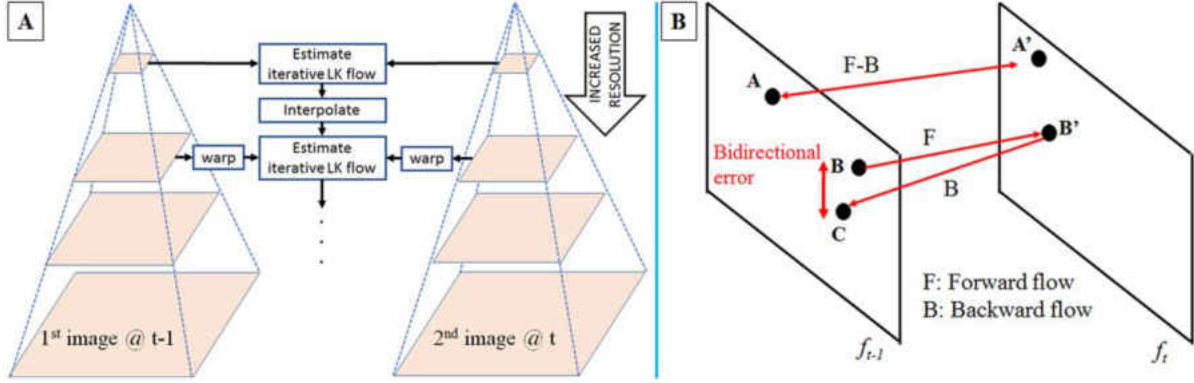


Figure 3 A: Gaussian Image pyramid; B: Bidirectional error

### Dense Flow

Implementing Lucas-Kanade tracking is fast and accurate as it only focuses on the tracking of the small neighborhood of extracted reliable features. On the other hand, as to dense motion estimation, which in our case is the motion of a lively crowd, the processing of the entire frame is required. Towards the solution of this problem, a second algorithm widely known as dense is introduced [58], [59], [68]. In brief, the idea is to approximate each small neighborhood of the frame by quadratic polynomials and observing the translation of that polynomial in consecutive frames. The polynomial model can be described as:

$$f(\mathbf{x}) \sim \mathbf{x}^T \mathbf{A} \mathbf{x} + \mathbf{b}^T \mathbf{x} + c \quad (15)$$

Where  $\mathbf{A}$  is a symmetric matrix,  $\mathbf{b}$  a vector and  $c$  a scalar that are determined by weighted least squares fitting. Considering that the neighborhood undergoes into a global translation  $\mathbf{d}$ , a new signal can be constructed as:

$$f_2(\mathbf{x}) = f_1(\mathbf{x} - \mathbf{d}) = \mathbf{x}^T \mathbf{A}_2 \mathbf{x} + \mathbf{b}_2^T \mathbf{x} + c_2 \quad (16)$$

where  $\mathbf{A}_2 = \mathbf{A}_1$ ,  $\mathbf{b}_2 = \mathbf{b}_1 - 2\mathbf{A}_1 \mathbf{d}$ ,  $c_2 = \mathbf{d}^T \mathbf{A}_1 \mathbf{d} - \mathbf{b}_1^T \mathbf{d} + c_1$ . As long as the condition of  $\mathbf{A}_1$  being non-singular holds, the displacement vector can be found as follows:

$$\mathbf{d} = -\frac{1}{2} \mathbf{A}_1^{-1} (\mathbf{b}_2 - \mathbf{b}_1) \quad (17)$$

In practice, the accuracy of the results can be increased by introducing several improvements. First, with the assumption of motion slowly varying, integration can be made within the same small neighborhood and the errors in results can be minimized. Then finding  $\mathbf{d}$  of Equation (17) comes down to minimizing the following expression:

$$\sum_{\Delta \mathbf{x} \in I} w(\Delta \mathbf{x}) \|\mathbf{A}(\mathbf{x} + \Delta \mathbf{x}) \mathbf{d}(\mathbf{x}) - \Delta \mathbf{b}(\mathbf{x} + \Delta \mathbf{x})\|^2 \quad (18)$$

where  $I$  is the neighborhood of interest and  $w(\Delta \mathbf{x})$  is a weight function for the points in  $I$ . Finally, the displacement vector is found as:

$$\mathbf{d}(\mathbf{x}) = \left( \sum w \mathbf{A}^T \mathbf{A} \right)^{-1} \sum w \mathbf{A}^T \Delta \mathbf{b} \quad (19)$$

Secondly, a further improvement can be achieved implementing the same iterative and multiscale approach in Figure 3-A so as to handle larger displacements.

#### *Conversion of displacement units from image space to real world*

Vision based estimation of displacements returns pixel units. To get the real-world displacement values in SI units requires a conversion by using a scale ratio which is acquired by calibrating the camera:

$$r_1 = \frac{Z}{f} = \frac{D}{d} \quad (20)$$

Where  $Z$  is the distance from the lens to the object motion plane,  $f$  is the focal length,  $D$  is the physical length of the object on the motion plane and  $d$  is the length in pixel of its corresponding image part. Figure 4 shows the scheme for scale ratio calibration. In most practical applications, it

is difficult to accurately estimate the  $f$  for zoom lens. In this case, it makes more sense to use the physical length of the object  $D$  and the length in pixels  $d$  to calculate the scale ratio  $r_1$ .  $D$  is found by following a procedure as shown in Figure 4-A. If the distances between points A, B and C ( $l_1$  and  $l_2$  in Figure 4-A), are measured utilizing a laser distance measurer and the angle  $\alpha$  using a protractor, then  $D$  is calculated as follows:

$$D = \sqrt{l_1^2 + l_2^2 - 2l_1l_2 \cos \alpha} \quad (21)$$

The actual displacement  $V$  is then:

$$V = r_1 v \quad (22)$$

where  $v$  is the displacement in pixels of the image.

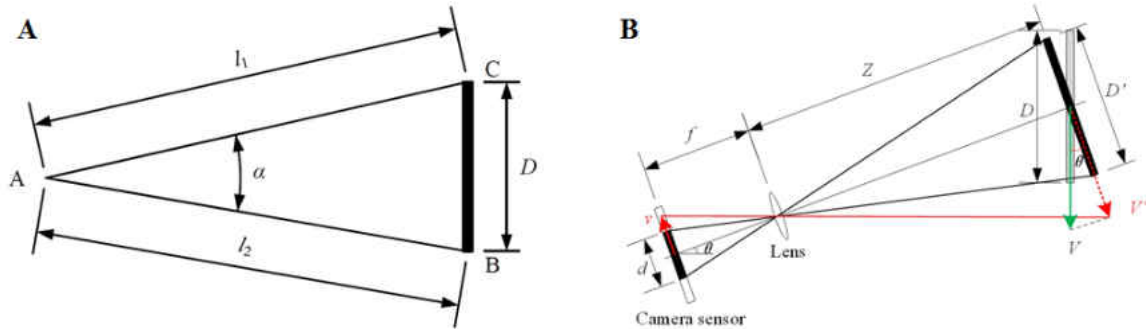


Figure 4 A: Scheme showing the measurements to acquire scale ratio; B: Scheme for scale ratio calibration in case of inclined camera

In many field applications, site-specific constraints prevent the optical axis from being oriented perpendicular to the plane of motion of the object. As shown in Figure 4-B, the measurement point moves in the direction of  $V$  (vertically) and there is an angle  $\theta$  between the optical axis and the horizontal plane. The corresponding motion direction  $v$  in the image is parallel to  $V'$ , which is the projection of  $V$  in the image plane. The scale ratio will then be:

$$r_2 = \frac{D'}{d} \quad (23)$$

where  $D'$  is the projection of the  $D$ . Usually it is easier to take a physical measurement of  $D'$  than  $D$  in practical application. In this case, the displacement is:

$$V = \frac{r_2 v}{\cos \theta} \quad (24)$$

### Laboratory Verification

The idea behind the controlled experiments conducted is to first assess the efficiency of explained tracking algorithms and to create a database of jumping type load time histories starting from the singular individuals going up to groups of different sizes. As it is very well stated in the literature, jumping and other loads of similar nature (bobbing, bouncing, etc.) may vary approximately between 1-3 Hz in their frequency band. For this reason, the subjects are asked to jump synchronously with the metronome beat corresponding to the same range. Subjects are also asked to accompany a certain song that is played during the football games at the real-life stadium within their campus so as to make a comparison between the findings from the laboratory studies and the real-life stadium which is also subjected to research within the context of this study.

### *Experimental Setup*

The first set of tests are conducted on a force platform which is put together as an alternative to a force plate and to accommodate more than only one person. Two thick plates are placed on the ground in a way to completely prevent their movement and four load cells are fixed on the plates (Figure 5-A). A steel beam of U channel type (Figure 5-C) that is 4 feet long with welded plates (Figure 5-B) at four ends are placed on the load cells by making sure a full contact surface is provided.



Figure 5 Force platform and its constituents

Free vibration tests of the force platform show that the first fundamental frequency falls around 80 Hz range which makes it a rigid-like structure that would not be heavily influenced by jumping type loads.

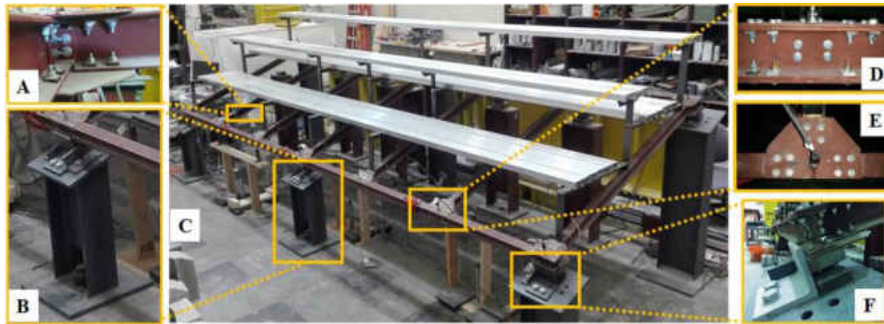


Figure 6 The grandstand simulator along with the details of its elements

The upper and lower end of the structure are tilted with a  $20^\circ$  angle and placed on inclined columns. The tilted structure is stabilized with 5X5X2" angles that are bolted to the columns. 2X2X3/16" angles are welded on the cross braces and aluminum bleacher planks are attached on these angles with bolts and washers to provide seating and footing for the spectators

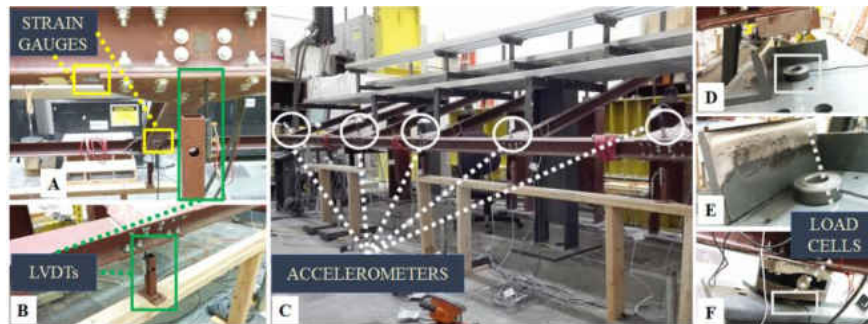


Figure 7 The sensors installed on the simulator

A grandstand simulator is constructed and used for further series of tests Figure 6-C. The simulator is the modified version of the test grid which has served as a multipurpose specimen for researchers to try different technologies, sensors, algorithms prior to real life implementations. The grandstand Figure 6-B can be adjusted to have one or two clear spans with continuous beams across the middle supports. It has two 18 ft girders (S3x5.7 steel section) in the longitudinal direction. The 3 ft transverse beam members are used for lateral stability (Figure 6-A). The simulator can be modified to reveal different structural stiffness and damage cases by altering specially designed intermediate and boundary conditions (e.g., pin supports, rollers, fixed support, and semi-fixed support) (Figure 6-D, E, F)

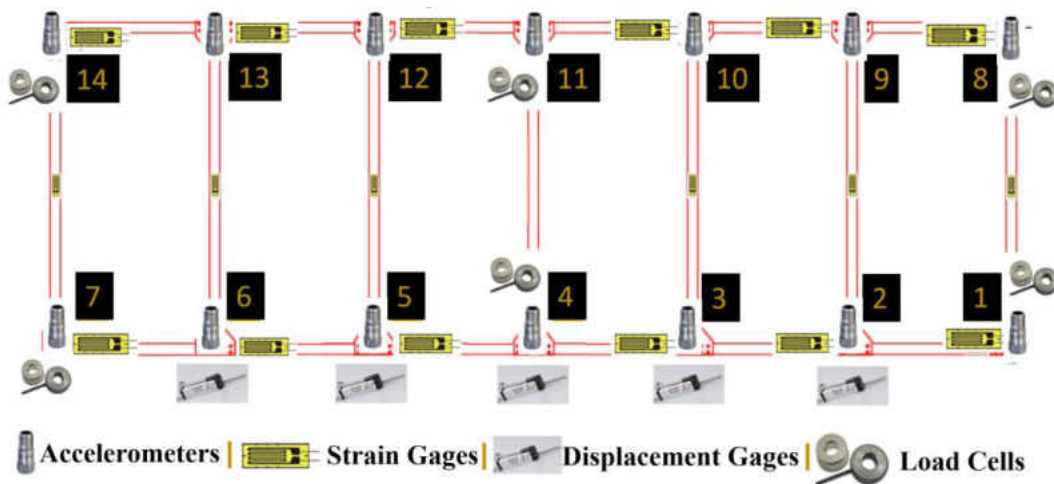
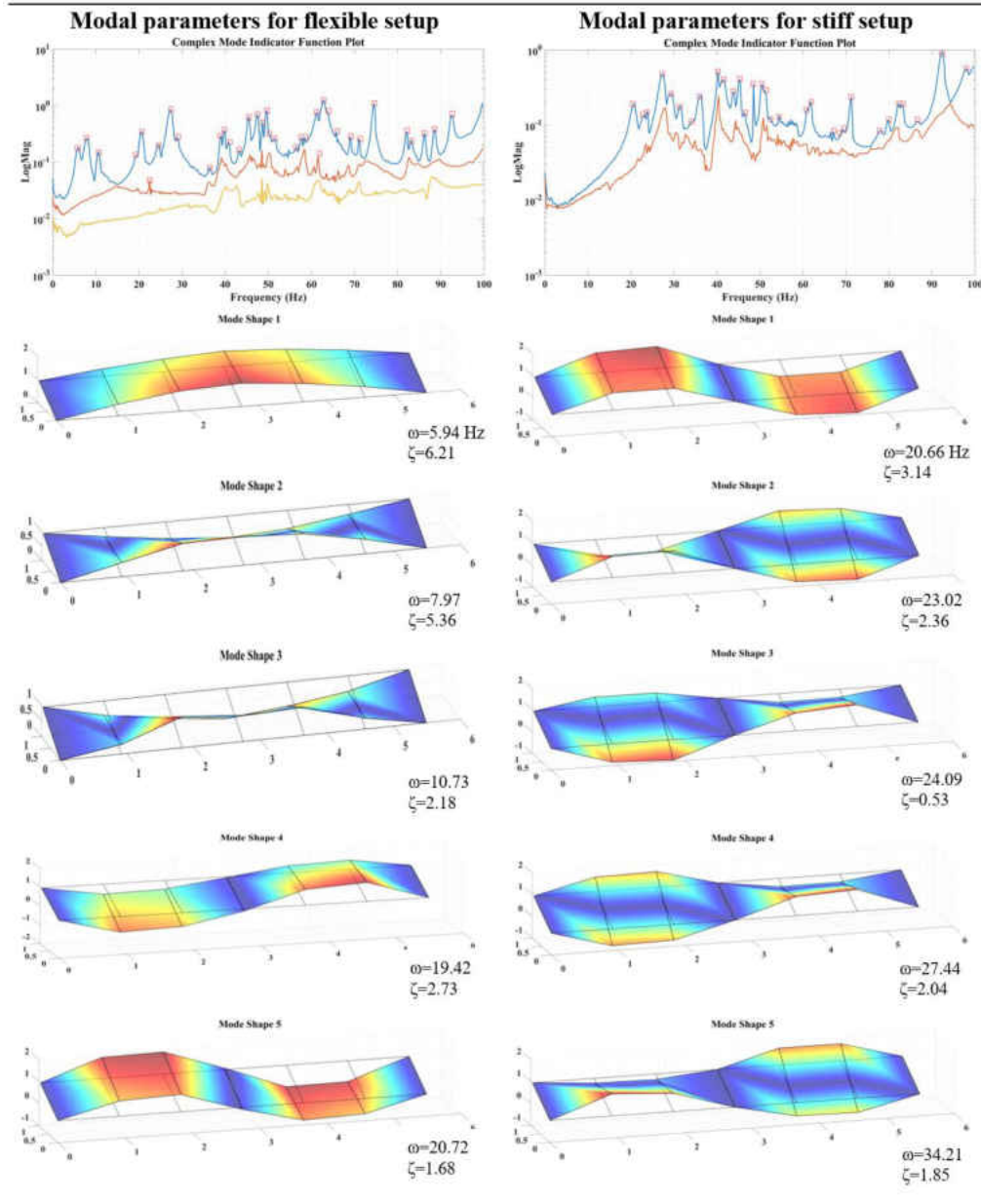


Figure 8 Plan view showing the locations of sensors placed on the structure

Figure 7 shows the type of sensors that are used in the experiments. High sensitivity piezoelectric accelerometers are placed on beam-beam connection nodes to ensure the required low and high frequency ranges are covered (Figure 7-C; Figure 8). An off the shelf camera that can capture 60 frames per second is used to record the entire tests series focusing specifically on human subjects and crowd and structural motion.

## Dynamic Characterization of The Grandstand Simulator

Table 1 Modal parameters of the grandstand simulator within 0-100 Hz frequency band



The grandstand simulator is designed to provide two different stiffness conditions by placing/removing the intermediate columns seen in Figure 6-B. The columns are fixed to the strong ground and two different conditions could be simulated being single/ two-span simple/semi-

fixed/fixed supported for observing lower and higher frequency behavior respectively. Table 1 shows the results of experimental modal analysis conducted on the structure. Modal parameters that belong to the two different setups are extracted using Complex Mode Indicator Function (CMIF) and Enhanced Frequency And Spatial Domain Decomposition (EFDD) [69]–[71]. The setup without intermediate columns is a reasonable approximation of a real-life flexible grandstand resembling of their behavior that stems from long cantilevers which are mostly the concern for vibration serviceability. The first two frequencies found are around the second and third harmonics of jumping type loads. The structure resembles of a simple beam but the mode shapes are not as simply observed. The geometry of the structure and the boundary conditions cause the structure to have intermediate global and local like modes between the main sinusoidal expected mode shapes. Also, the inclined shape of the structure results in forward – backward swaying modes coupled with torsion. Only the first five modes are provided in Table 1

### *Finite Element Model*

The finite element model (FEM) of the structure is created as a supportive indirect comparison tool as seen in Figure 9.

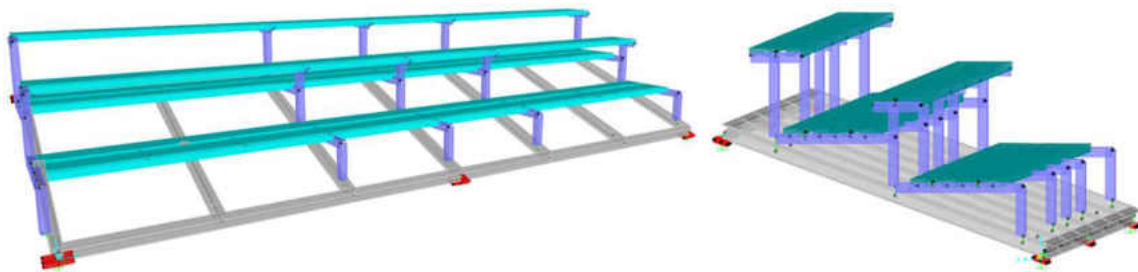


Figure 9 Frontal and side view of the grandstand finite element model

The supports are made of ASTM36 steel and modeled as thick shell plate members. The beams are connected to the supports by means of bolts (A307 –  $\phi 1/4''$ ) which are modeled as links in the FEM. Beams and cross members are of the same kind (AISC S3X5.7; ASTM36) and are picked out from AISC section library with the original specifications. The beam-beam connections are assumed to be transferring moment and are simulated with appropriate connections. The connection between the seating-footing planks and the beams are made by using several different sizes of L beams. They are selected from SAP2000 AISC section library. The connections from angle to angle and angle to cross beams are assumed to be rigid and the connection with cross braces are simulated as rigid links since they are welded. The planks are made of aluminum and of prefabricated unique shapes and modeled as area sections. The bolts between the angles and the aluminum planks are simulated as links as well.

Table 2 Comparison of dynamic properties of the one-span simply supported structure with EMA parameters

<b>Mode</b>	<b>FEM - f (Hz)</b>	<b>EMA - f (Hz)</b>	<b>MAC</b>
1	5.25	5.94	0.98
2	7.61	7.97	0.94
3	13.02	10.73	0.78
4	17.7	19.42	0.84
5	19.05	20.72	0.92

Table 2 and Table 3 show the relation between the experimental results (Table 1) and the characteristics of the finite element model that is going to be used as an indirect comparison tool. Tabulated results confirm that the correlation is at a reasonable level to make that comparison.

Table 3 Comparison of dynamic properties of the two-span simply supported structure with EMA parameters

Mode	FEM - f (Hz)	EMA - f (Hz)	MAC
1	20.14	20.66	0.92
2	23.03	23.02	0.89
3	26.06	24.09	0.81
4	29.70	27.44	0.72
5	33.68	29.35	0.64

### *Tests Conducted*

The motivation behind the construction of the grandstand simulator is to build a model that can serve for the solution of various vibration serviceability problems alongside with the scope of this work. Footbridges, floor vibrations, narrowband non-stationary disturbances can all be tested. In scope of this study, laboratory tests can be summarized into three groups. The first tests involve one and two subjects jumping on the force platform shown in Figure 10-A,B. This set is designed to show the applicability and efficiency of the Lucas-Kanade method in tracking the subjects and on an almost rigid platform as an alternative to force plates.

The second group of tests is an expansion of the first group with more subjects and on the flexible grandstand (Figure 10-C). These tests are designed to further investigate the Lucas-Kanade algorithm and to show the performance on flexible structures that may influence the balance of subjects and alter jumping histories recorded by force plates mounted on structures. This comparison is valuable since the load cells are installed under the supports of the simulator and are expected to experience the effects of the structural flexibility.

The last group of tests are carried out on the stiff setup of the grandstand to prove the feasibility on larger groups (Figure 10-D). Unfortunately, the flexible setup must be switched to stiff due to the structure not being able to accommodate such a large group and the overall integrity

that might be risked. On this last group, the computer vision algorithm is changed to dense flow for it is a more appropriate way of tracking larger crowds (Figure 10-E). For each test, subjects are asked to accompany the metronome beats of 1, 2 and 3 Hz which is the common way of controlled jumping tests in the literature. In addition to that, subjects also jump to a commonly played song that they are familiar with especially from the football games that are hosted in local games. This study is focused mainly on this last specific beat to compliment the field implementation in section 4 and for the general consistency.

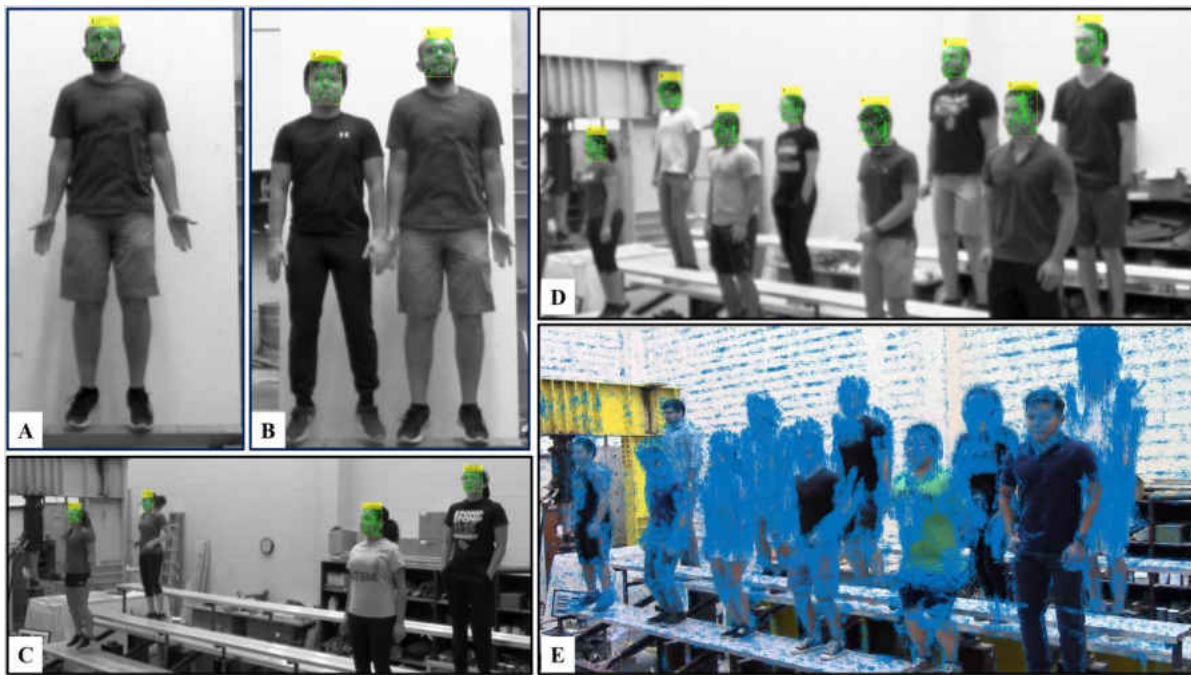


Figure 10 A: Single subject on the rigid beam (Lucas-Kanade method); B: Two subjects on the rigid beam (Lucas-Kanade method); C: Four subjects on the flexible grandstand simulator (Lucas-Kanade method); D: Eight subjects on the stiff grandstand simulator (Lucas-Kanade method); E: Eleven subjects on the stiff grandstand simulator (Dense flow method)

### *Results and Discussion*

Figure 11 shows the results of a single jumper on the rigid beam. The dominant beat frequency of the song played is known to be around 2.3 Hz that can clearly be observed looking

at the frequency domain representations of the force records. Figure 11-A is the displacement time history after post processing. The raw data before processing is in the unit of pixels which is then converted to unit of meters as described earlier. The second step is taking the gradient of the displacement to find the acceleration record as in Figure 11-B.

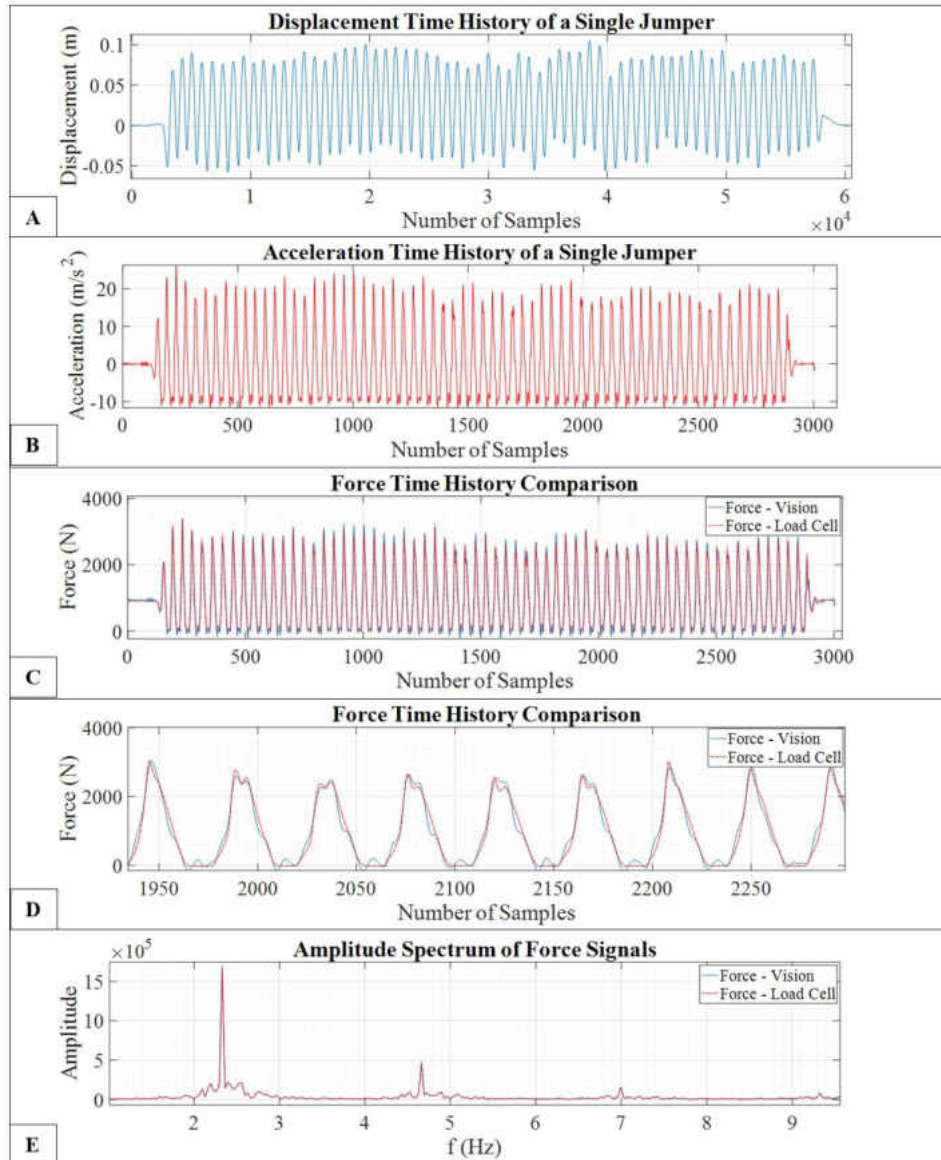


Figure 11 A: Displacement history of a single subject on the rigid beam; B: Acceleration time history; C: Comparison of estimated and measured forces; D: Close-up view of the comparison; E: Comparison of estimated and measured forces in the frequency domain

It is evident that the acceleration results have a base at around  $10 \text{ m/s}^2$  that indicate the gravitational acceleration at the time the jumper starts falling freely. The next step is to find the GRF according to Newton's law of motion. The sampling frequency of the camera is 60 Hz whereas all data from other sensors are sampled at 2000 Hz. The target frequency to compare force measurement is chosen to be 100 Hz which results in the measurements from camera to be up sampled using cubic spline interpolation and the load cell to be smoothed with a fifth order Butterworth low pass filter.

The signals from the camera are already synchronized since they are coming from once single source. When total force records from load cells and camera are to be synchronized, their cross correlation is calculated first:

$$\hat{R}_{xy}(m) = \begin{cases} \sum_{n=0}^{N-m-1} u_{n+m}^1 u_n^{2*}, & m \geq 0, \\ \hat{R}_{yx}^*(-m), & m < 0, \end{cases} \quad m = 1, 2, \dots, 2N - 1 \quad (25)$$

Where  $u_n^1$  and  $u_n^2$  are two signals from different sources,  $N$  is the number of samples and  $\hat{R}_{xy}$  is their cross correlation. The asterisk stands for the complex conjugation. The cross-correlation of the two measurements is maximum at a lag equal to the delay. Based on the delay information in terms of number of samples, two signals are aligned. In this manner, correlation is used for both as a way of synchronization and as a measure of similarity.

Figure 11-C, D compare the estimated and measured forces with an overall and then a close-up view. Morphology of the force time histories almost perfectly match with an accurate representation of peak to peak as well as subtle period differences in jumping pulses. Their cross-correlation is 99.1%. Figure 11-E shows the amplitude spectrum of this comparison. The main

beating frequency of the song along with its first and second harmonics are observed in both histories with a reasonable match.

The second and all the other subsequent test results follow the same exact procedure. Vision based displacement records of multiple subjects are captured via multi-point tracking. Although the subjects are asked to jump to a certain beat, the inherent nature of the human body does not always allow to keep up with it. As a result, the phase differences between subjects which are often referred as the inter subject variability in the literature reveals itself as an alteration in amplitude and pulse timing. This phenomenon is easily observed at the beginning of the test results in Figure 12-A that belong to the two subjects. One of the subjects has difficulty to keep up with the beat at the beginning that reveals itself as an amplitude reduction.

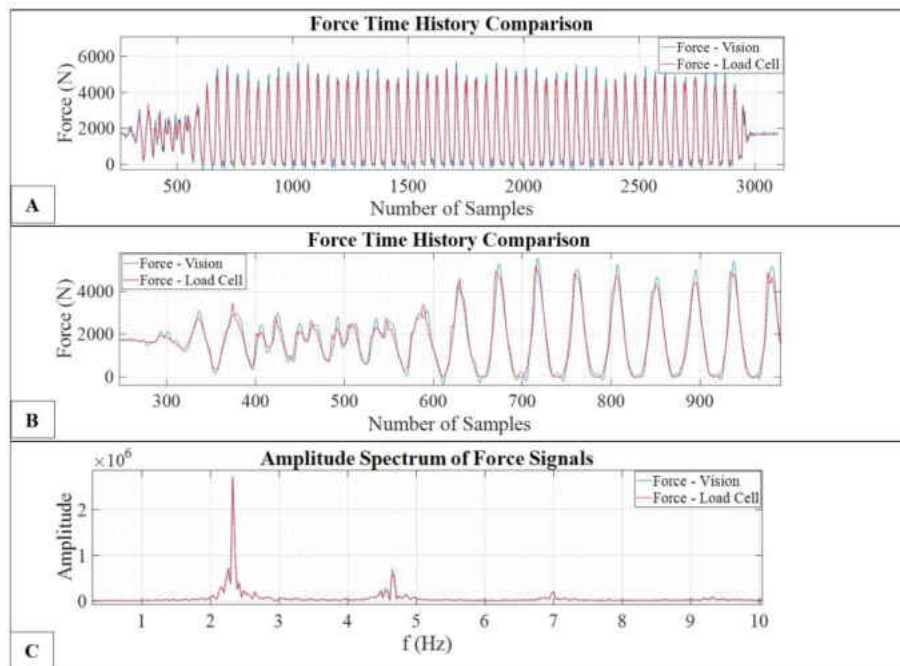


Figure 12 A: Comparison of estimated and measured forces of the two subjects on the rigid beam; B: Close-up view of the comparison; C: Comparison of estimated and measured forces in the frequency domain

Figure 12-B is the close-up view of that specific segment. It is clearly seen that the pulse peaks show a distorted trend due to different time of their arrival. This result is quite good for the fact that the estimation method works almost as precisely as the conventional sensors. Figure 12-C again shows the main beating frequency of the song along with its first and second harmonics are observed in both histories with a reasonable match having 98.8% correlation.

After rigid beam tests, the subjects jumping on the flexible grandstand are monitored with the same routine. Figure 13-A shows the force time history of each individual breaking down the time of arrival differences of each pulse along with their sum. The second harmonic of the force pattern is close to the first fundamental frequency of the simulator which creates extreme deflections that sometimes cause the subject to lose balance and even stop. The time frames that the jumpers are in and out of phase because of this imbalance are seen in Figure 13-B and are captured by the proposed method. The general morphology is almost an exact match with except for the amplitudes. The cross correlation is 92.3%. Total force history captured by the sensors are higher in amplitudes than the vision based methods (Figure 13-C). This observation is only made when the structure is in flexible setup with visible deflections. This difference stems from two sources. The first is the magnification of the dynamic displacements as the jumping harmonics are close to the resonant frequencies of the structure. The second is that when the subjects jump off of the structure and when in phase, an uplift force is sometimes generated. Both sources thereby cause the inertial forces of the structure to be involved and measured by the load cells. Figure 13-B shows that this effect is severe when the jumpers are in phase but ceases to be so as the subjects lose coordination. The frequency domain representation in Figure 13-D smears over the other bands indicating the imbalance and out-of-phase jumping trend.

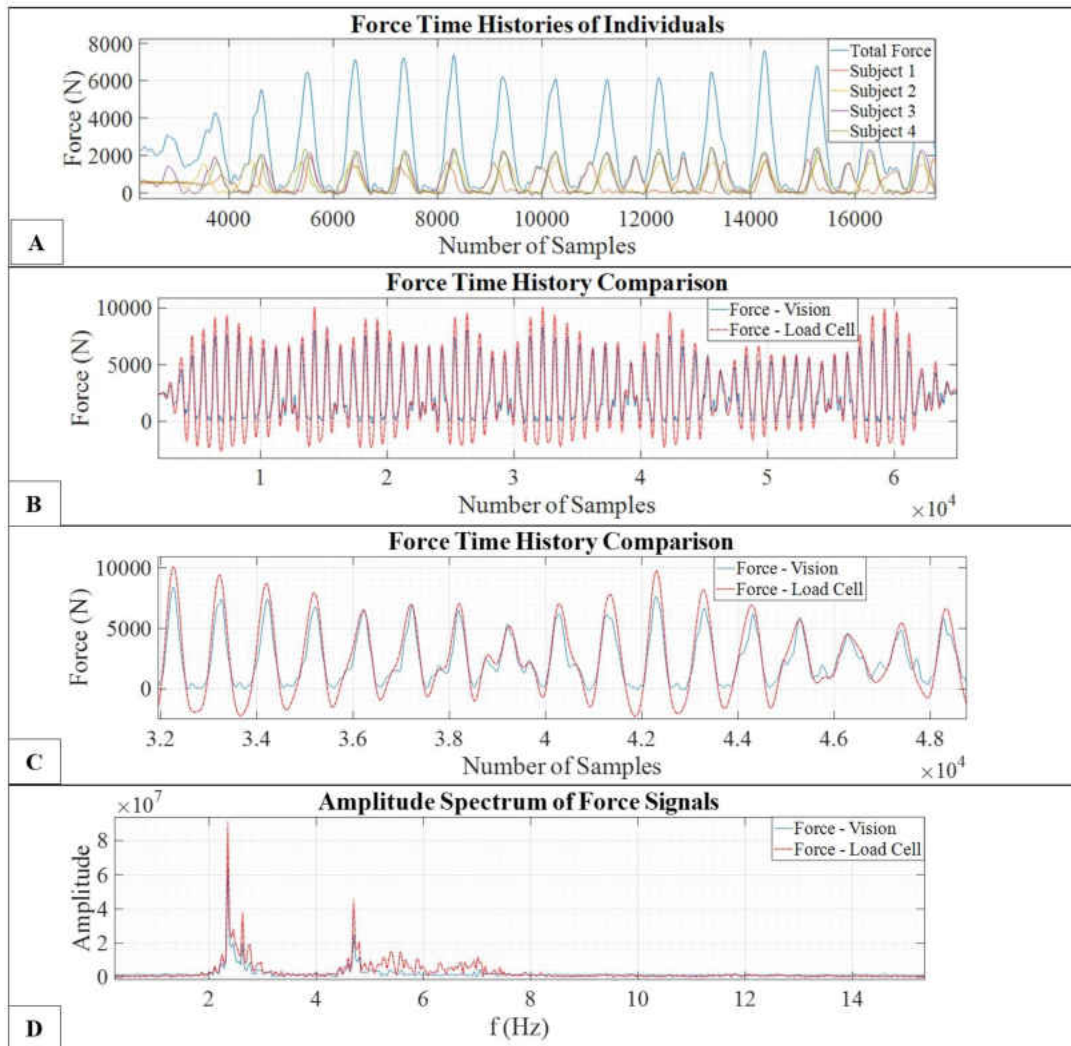


Figure 13 A: Force time histories of each individual (four subjects) and their sum B: Comparison of estimated and measured forces of the four subjects on the flexible grandstand; C: Close-up view of the comparison; D: Comparison of estimated and measured forces in the frequency domain.

The estimated individual forces using computer vision from Figure 13-A are exerted upon the FE model with respect to their exact locations so as to compare the responses with that of the conventional sensors. Figure 14-A compares the displacement at node 4 seen in Figure 8. As it is indicated earlier, the flexible structure shows visible large deflections that is also observed here. The results overlap well with each other. Alike displacement measurements, accelerations seem to

relate at an acceptable level. For a clearer observation, the acceleration values from the sensors are sketched as an envelope. Figure 14-B indicates that there are instances that the acceleration reaches 1g which feels as if floating in the air with zero gravity in case the subjects that are intact with the structure. These time periods concur with where the sensor measured force records are higher than vision based measurements.

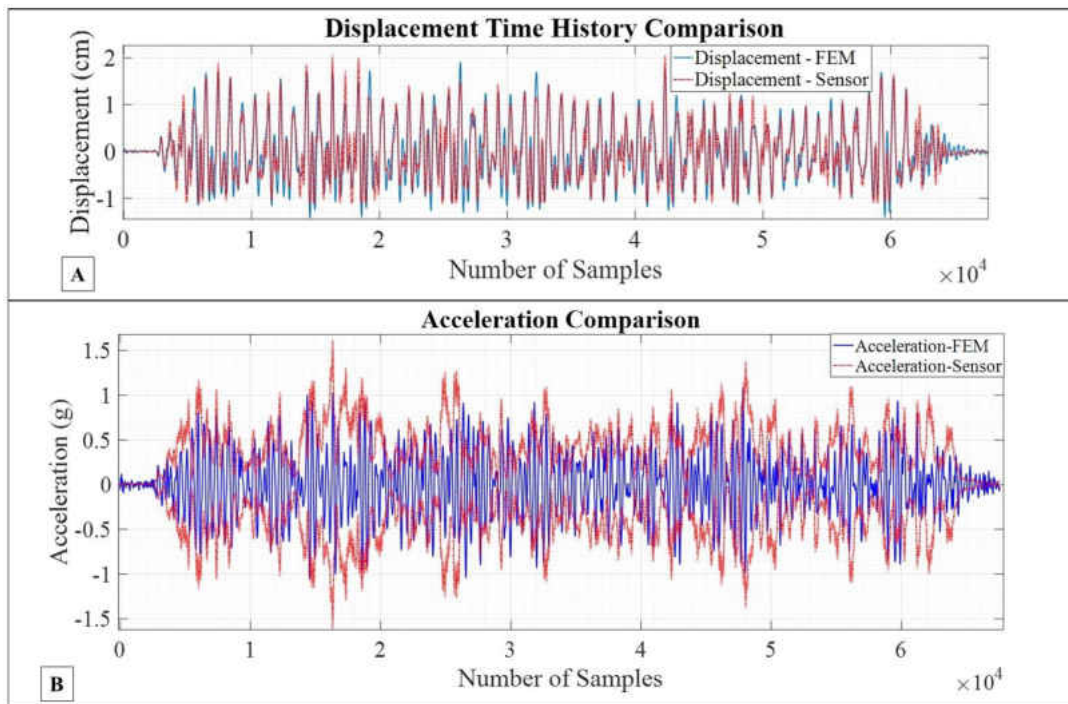


Figure 14 A: Comparison of displacements between FEM and LVDT generated by four subjects on the flexible grandstand; B: Comparison of acceleration for the same case

The flexible grandstand tests can allow up to four subjects. The setup is switched to stiff mode to observe the feasibility of the method on more subjects. Since the resonant frequencies lie in a higher band, the response is nearly static and dynamic magnification seems to be not a problem anymore. Consequently, force recordings are not affected by inertial effects. Figure 15-A shows the force time history of each individual breaking down the time of arrival differences of each pulse along with their sum. In Figure 15-B, C comparison of the total force is shown. Unlike the

previous flexible setup, both histories match well with a correlation of 98.6%. It can also be inferred that the eight subjects jump at a reasonable synchronization. Figure 15-D again shows a good match in the frequency domain.

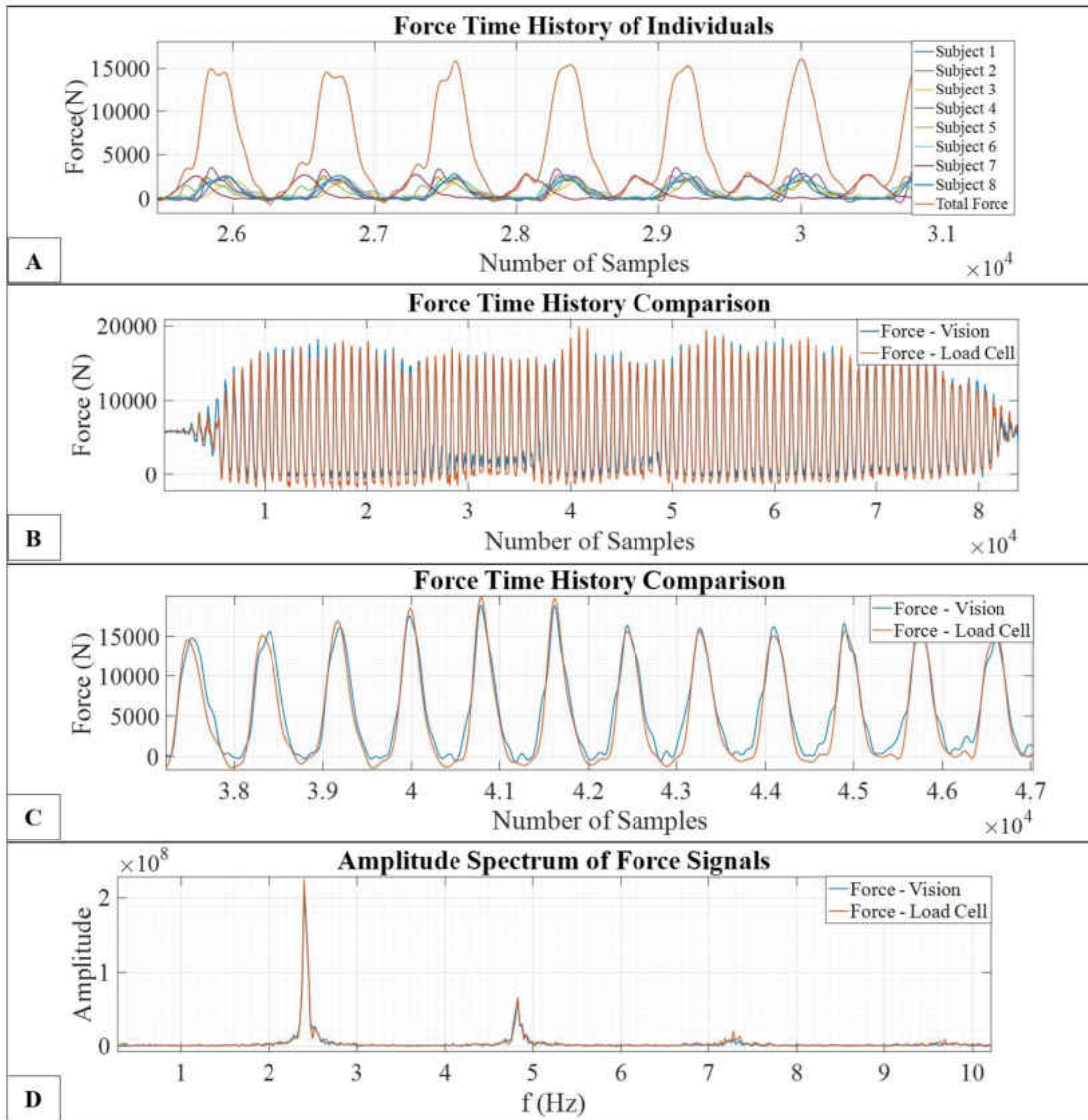


Figure 15 A: Force time histories of each individual and their sum B: Comparison of estimated and measured forces of the eight subjects on the stiff grandstand; C: Close-up view of the comparison; D: Comparison of estimated and measured forces in the frequency domain.

Once again, the responses from FE model with loading from computer vision are compared with that of the conventional sensors. Figure 16-A compares the accelerations at node 2 seen in Figure 8. The envelope seen in Figure 16-B is the close-up view of a certain time frame in the acceleration record. The results seem to correlate well with each other. In the stiff simulator setup, comparison of displacement measurements is replaced with strain measurements at node 2. Figure 16-C shows that the correlation between two responses are at an acceptable range.

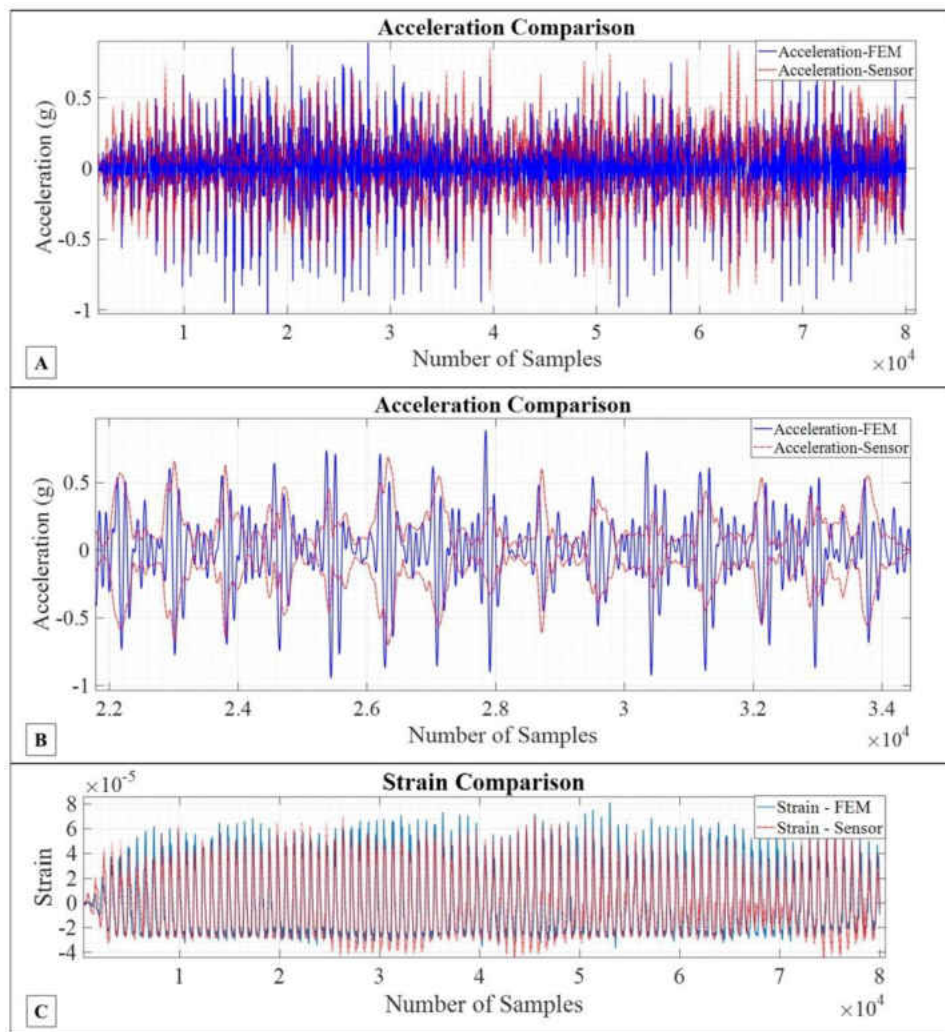


Figure 16 A: Comparison of accelerations generated by eight subjects on the stiff grandstand between FEM result and accelerometer; B: Close-up view of the same comparison, C: Comparison of strain values between FEM and strain gage

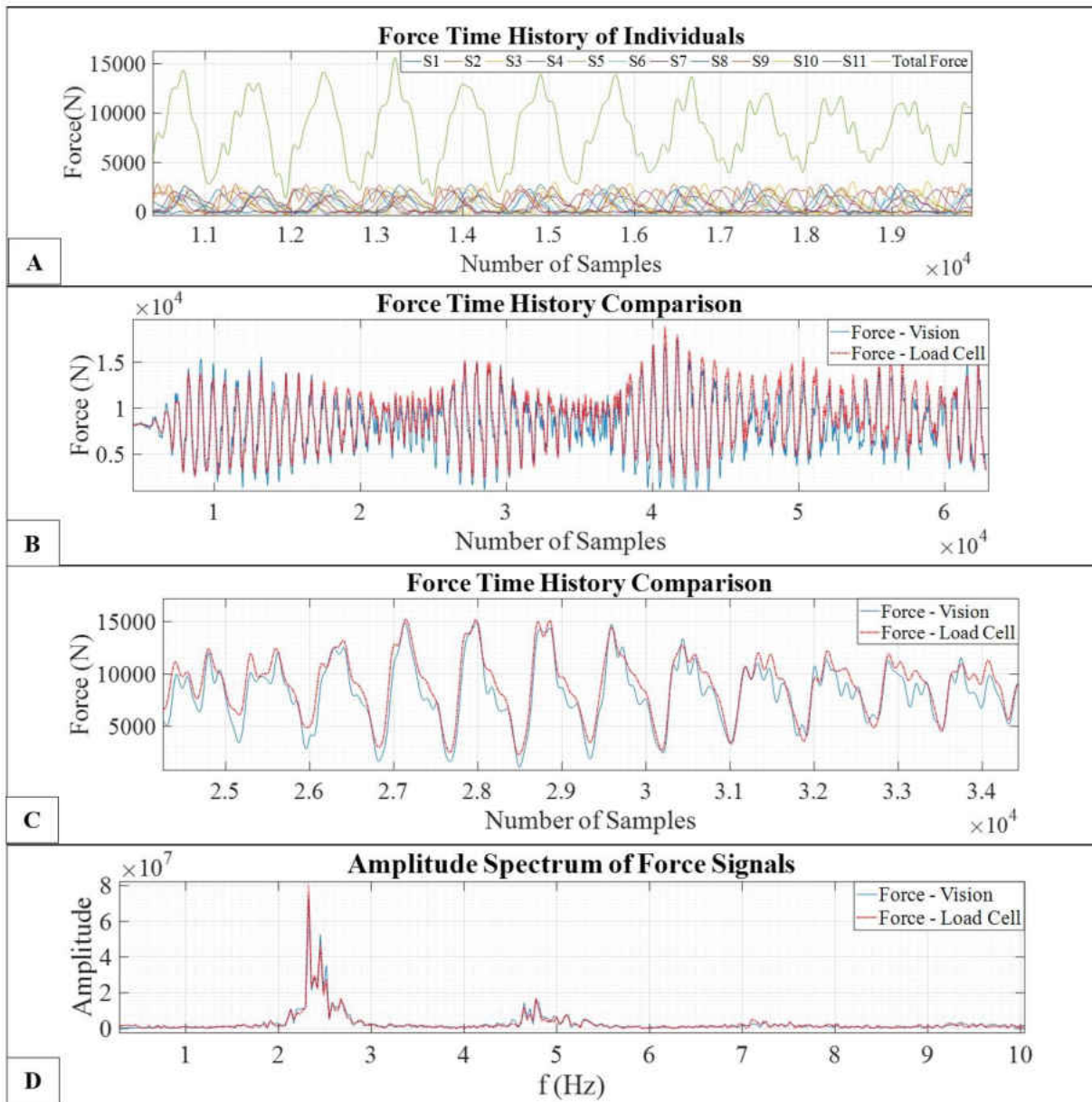


Figure 17 A: Force time histories of each individual and their sum B: Comparison of estimated and measured forces of the eleven subjects on the stiff grandstand with dense flow; C: Close-up view of the comparison; D: Comparison of estimated and measured forces in the frequency domain

The last set of tests are conducted using eleven subjects on the stiff grandstand (Figure 10-E). These tests are the closest approximation to the real-life events in terms of number of participants. Post processing of this data is done by using dense flow algorithm instead of sparse

flow to track the motion of every small neighborhood of a pixel. (Figure 10-E) shows the directions of vector flow around the subjects. The areas with small or no motion have short length vectors indicating low magnitude whereas the areas with larger motion have long vectors corresponding to higher magnitudes. Several recordings are taken but the results shown in Figure 17 are specifically selected as they show how much the real force histories generated by a crowd may differ from a purely mathematically defined pulse functions. Figure 17-A shows the force time history of each individual, their different times of arrival and sum. The estimated and measured forces are in a reasonable alignment with a cross correlation of 98%. However, the subjects are out of phase at almost every time step and there is always more than one individual interacting with the structure along the entire record. The time frames that the subjects are at different phases are seen better in Figure 17-C in time domain and also in Figure 17-D and they are correctly estimated by the proposed method.

### Real Life Implementation

A real-life experimental study is conducted to investigate the efficiency of the approach. The second algorithm, dense flow, is applied as it is more convenient to track large groups and crowds. Unfortunately, the constraints such as the scale of the structure, infeasibility of placing force sensors beneath audience because of the size of the crowd necessitate an indirect comparison approach for the field study. The approach applied here is to estimate the crowd force exerted upon the structure followed by creating a computer model. The estimated loads are applied on the model and the generated responses are compared with the acceleration recordings captured during the real event.

## Monitoring and Modeling of the Structure



Figure 18 A: Overlook of the stadium showing the monitored section and the location of the camera; B: Experiment setup; C: The computer controlled industrial camera; D: One sample frame from the camera record

The stadium is constructed as a steel structure which has a typical inclined architecture to provide the best line of sight for the audience. It hosts football games with the capacity of 45,000 seating for spectators on 25 acres of land since 2007. In scope of this study, a small portion of the stadium is investigated as seen in Figure 18-A. The reason for this choice is that this certain section is allocated to the audience who are known to create the highest excitation, hence the vibration values, in response to any event during the game. Additionally, the official marching band for the motivation of the crowd is also located close to the monitored section. Monitoring is carried out during the entire game with accelerometers and a camera during the time sequences when spectators jump to the same song in laboratory experiments. The number of accelerometers used in the study are twenty-five, two of which are placed in horizontal direction, whereas others are in vertical. Figure 19 gives a detailed overview of the accelerometer locations along with their pictures.

Simultaneously with the accelerometers, the crowd over the monitored section is recorded using a frequency controlled (~60Hz max.) industrial camera that is connected to a computer (Figure 18-B,C,D). The time stamps that correspond to the same song that was played during the laboratory studies are specifically targeted and extracted from both video and acceleration time histories so as to make a reasonable comparison. The plan view distance between the measurement location and the monitored section is approximately 120 meters.

An FEM is constructed using the blueprints and on-site inspections (Figure 20). The structure is purely made of well-known AISC steel frame sections, which are modeled as such, with complexly detailed connections. The structure comprises eight different grandstands that might work independently if not connected with aluminum seatings, footings and concrete decking. They may partly restrain the independent motion and add rigidity to the structure and are found to have considerable effect on the general behavior as it is pointed out in several studies in the literature. These members are modeled with links, springs and constraints to the point that they are thought to fit best to the dynamic results. Cross members for stability act as truss members and are modeled accordingly.

Structural identification is conducted under ambient conditions as an alternative to shaker testing as this method excites mostly the local modes in case of large structures. Complex nature of the structure such as steel connections, seatings, footings, their connections with rakers and the overall size also contribute to many local modes to occur. Due to the limited instrumentation means, several monitoring surveys on two specific locations of the upper and lower portion of the whole section are carried out at separate times and are combined to capture the global motion of the

structure. The CMIF function shown in Figure 21 indicates only the first five singular lines that the modes are picked out from.

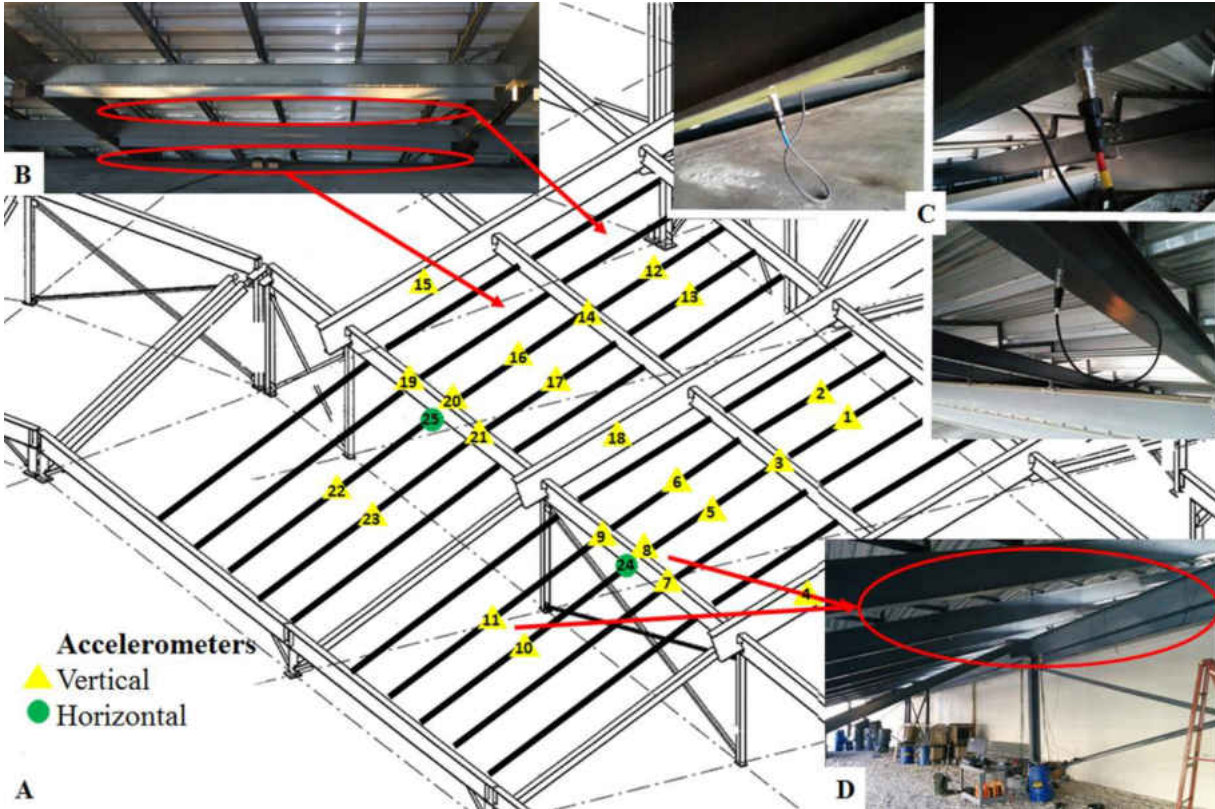


Figure 19 A: Accelerometer locations marked on the structure plan; B,D: Picture from the stadium corresponding to accelerometer locations; C: Sample detailed views of sensor-element attachments

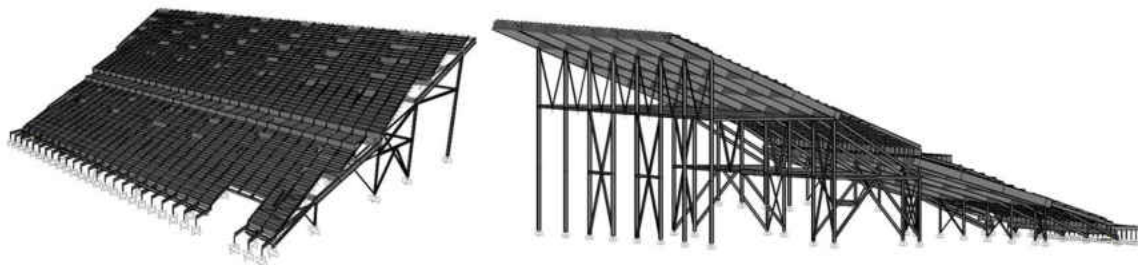


Figure 20 Finite element model of the monitored section

FE model update is done manually by a systematic procedure. First, global modes and frequencies are made sure to be in the same order as in experimental results by altering the

boundary and continuity conditions. After acquiring a reasonable proximity between analysis and experiments, a further calibration is carried out in the modal and flexibility space by changing the stiffness levels and connection details of individual members. As the next step, the correlation between the measurement points and their counterparts in the computer model are calculated and differences are fine tuned. It is always possible to carry out a more comprehensive model calibration by exploiting sensitivity analysis and probabilistic models, however, this procedure is not within the scope of this work. The model is assumed to be fairly close as long as it reflects the common global dynamic characteristic of the actual behavior.

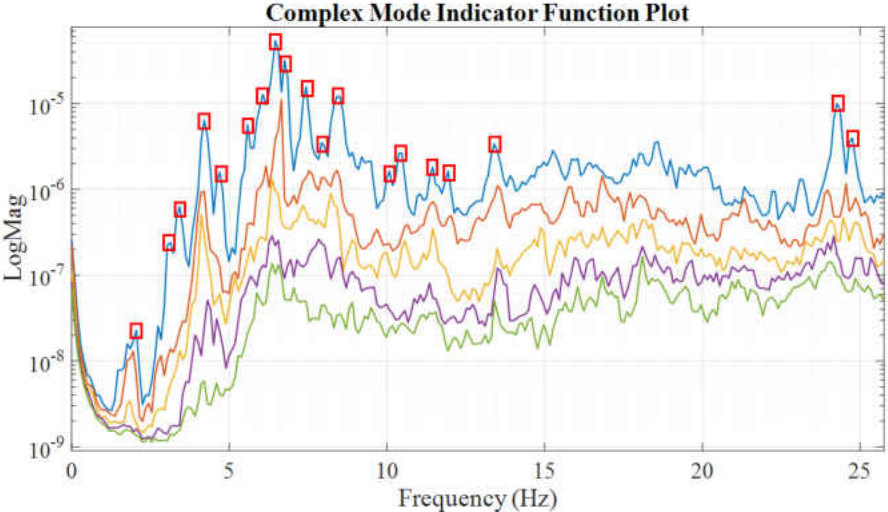


Figure 21 CMIF plot of a sample data taken from stadium under ambient vibration

Unlike many examples in the literature, the structure does not have cantilever tiers with low vertical vibration modes. When cantilever sections are of question, it is more convenient to make a calibration as they behave as an isolated component. As to the structure in this study, it is rather difficult to do so due to the lack of full scale information and the motion being more complex. That’s why, the modes that are included in the calibration process and presented here are those which are thought to represent the global motion the best (Figure 22).

The low resonant frequencies concentrated under 15 Hz frequency band belong to the vicinity of the edge of the upper section in form of swaying with a slight bending in two different directions. The first vertical motion observed underneath the lower portion where the monitored crowd resides is seen after 20 Hz range. This means that the monitored section does not considerably magnify the effects caused by the crowd in the lower monitored section. Although it would have been more desirable to work on a flexible structure to reflect the reality as close as possible, this does not necessarily pose a restriction to the experimental work.

Unlike controlled laboratory conditions, field studies constitute uncertainties that may be hard to predict and incorporate. Some known uncertainties are the number of people in the monitored section, their mass, the distance between the camera and the spectators to make the pixel-to-meter unit conversion, the ratio of the active/passive spectators and their exact locations. In addition, more uncertainties regarding video processing such as alteration of illumination, occlusion in densely crowded scene may introduce additional errors to the results.

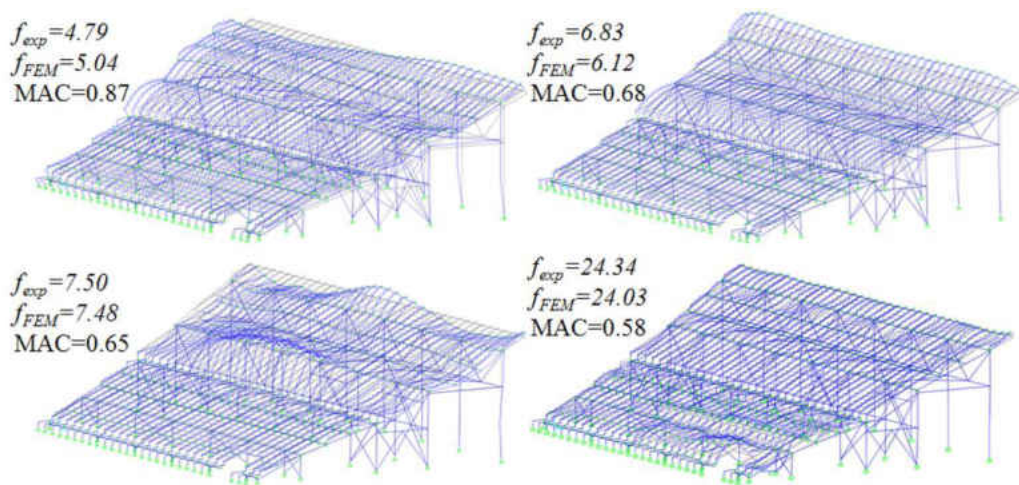


Figure 22 Mode shapes of the monitored grandstand

## Analysis and Results

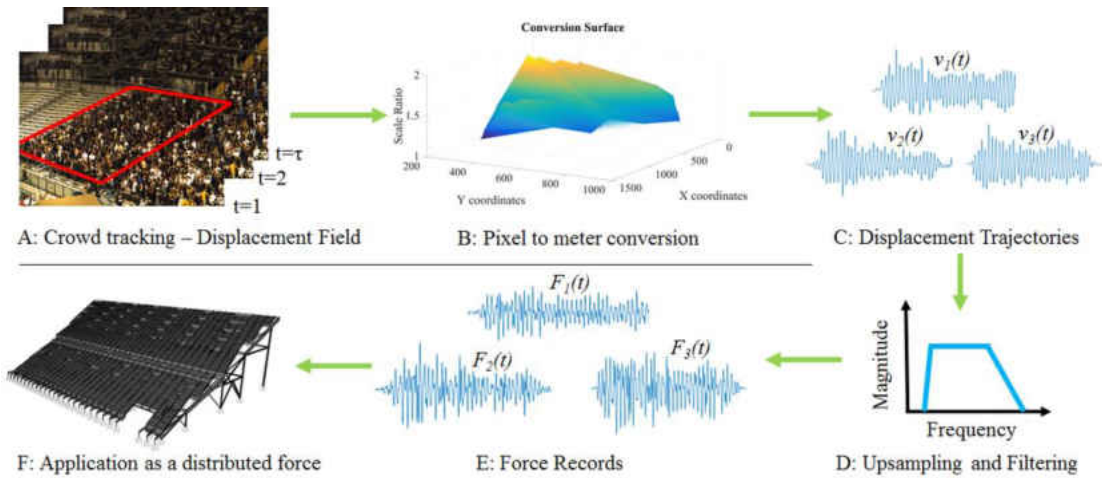


Figure 23 Overview of force estimation approach for the field study

An automated people counting algorithm and an average mass may be applied to estimate the number of people and their total mass. However, for this study, the use of such an algorithm is avoided as this is not the objective and is the scope of a future work. People are manually counted since the section is small enough and the number of people is within a countable range Figure 23-A. The distance problem between the camera and the audience is solved by building a surface of calibration ratios. As it is described before, one practical way of finding the calibration ratio is to divide the actual dimension of the elements in the field to their pixel values in the image frame. Some structural members that stand out such as walkway posts, seating planks, etc. covering the region occupied by the crowd are measured in the field and their scale ratios are computed. A three-dimensional surface is then constructed via surface interpolation for the entire image frame (Figure 23-B). Once the dense flow vector field is multiplied with the calibration surface, approximate real displacements are found followed by finding acceleration time histories (Figure 23-C).

Before deriving acceleration time histories, displacement signals are up sampled to 200 Hz with cubic spline interpolation to match the sampling rate of the accelerometers. Since the spectators' GRF frequency response to the song played is known a priori, a fifth order Butterworth filter that falls within [1,16] Hz is applied on the signals. The quality of displacement trajectories is not always of high quality. Because of the uncertainties regarding video processing mentioned earlier, some trajectories may show erratic behavior. One solution is to eliminate the low-quality displacement records by a rejection threshold which is obtained based on the distribution of the areas of each trajectory. The loss of the eliminated trajectories can be compensated by replacing them with another in the closest neighborhood of their location in the frame. Another option is to apply a principal component analysis (PCA) to the entire family of trajectories. By selecting the first two principal components and projecting the position time series onto corresponding eigenvectors, one dimensional position signals can be found.

As to application of the load, the best way is to apply each load time history with respect to their exact locations similar to distributed mass-spring elements. However, this needs a further integration between a counting algorithm and the model, thus, is not utilized at this stage. As an alternative, the total force is converted into a distributed load and applied on the area surfaces of FEM. The passive members show a flatline in their time histories and taken as a static load. Since the magnitude of the load is unknown, an incremental average mass multiplied by the number of people is considered.

Figure 24 shows the comparison of acceleration responses between accelerometer at location 17 in Figure 19 and the corresponding node in FEM. This result is generated under 435 people counted with an average mass of 70kg. Acceleration response of the sensor is sketched as

an envelope for a better visualization. An exact overlap of acceleration records is not expected between the field and computer simulation as too many uncertainties are involved. However, general morphology and amplitude values fall within an acceptable range. Peak accelerations reached in sensor readings are almost always higher than of FEM responses. Figure 25 makes the same comparison in the frequency domain. For the first beat pulse, there seems to be a good match. Unfortunately, the second and the third harmonics are lost for the vision based approach.

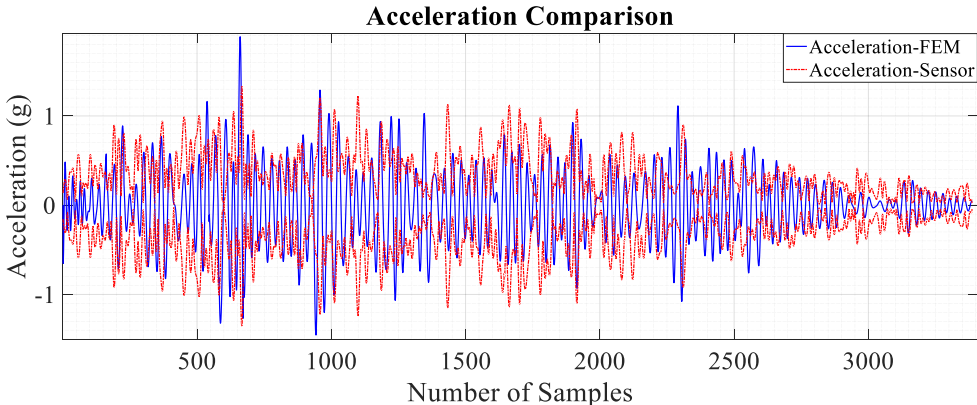


Figure 24 Comparison of accelerations generated by the crowd on the monitored portion of the stadium between FEM result and accelerometer at 17 in Figure 19.

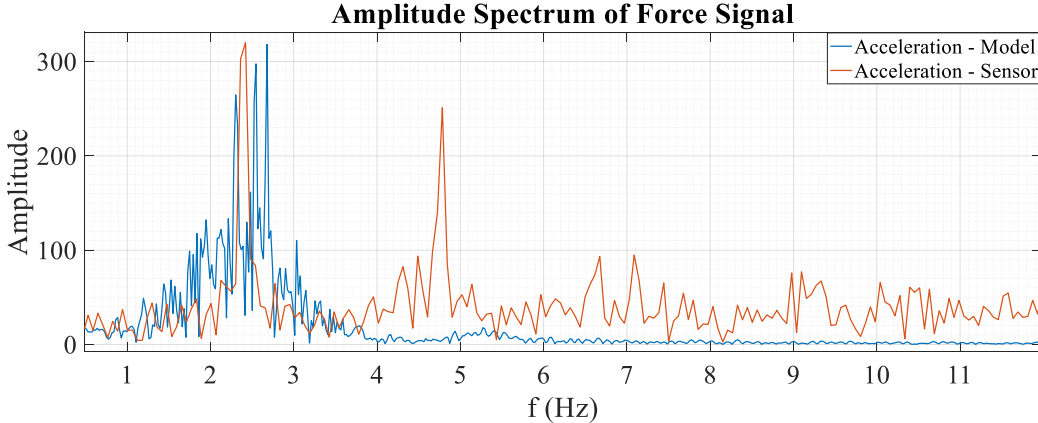


Figure 25 Frequency comparison of accelerations generated by the crowd on the monitored portion of the stadium between FEM result and accelerometer at 17 in Figure 19.

The difference in results generally stem from the uncertainties involved in computer vision approach. The first thing to consider is the sensitivity of the equipment. For large distance measurements, the accuracy is expected to decline. A higher resolution camera with a long fixed focal length can increase the measurement sensitivity at subpixel levels. However, with today's technology, there is generally an indirect proportion between the increased sensitivity and speed. That's why there needs to be a reasonable balance between the two. Another problem is the occlusion of the densely crowded scene. Displacement trajectories often get affected by the subjects blocking each other's visible and trackable features. The spectators waving their hands, the interference of the image frame with the natural or artificial effects such as smoke, rain, confetti, etc. may cause erratic trajectories to occur. When several of these uncertainties are involved in the real-life measurements, the efficiency of the methods may decrease such in the case herein.

### Concluding Remarks

A computer vision approach for the load time history measurement of individuals and crowds when jumping, bobbing and its feasibility are investigated. The method comprises of tracking the displacement trajectories of individuals and crowds using optical flow based algorithms followed by generating force time histories. Laboratory experiments, in which individuals and groups perform jumping at regular beats and songs on a force platform and on a grandstand simulator, are conducted. The estimated trajectories are compared directly with conventional sensors as well as indirectly with responses acquired from finite element models and results are presented. The method is further validated via a field demonstration. Limitations of the method and future work for improvement are discussed. The proposed methods along with their

applications on a real crowd, building a grandstand simulator that can be adjusted to flexible and stiff configurations thereby accommodating experiments for groups of different sizes are some of the contributions. In this sense, the study is taking an important step in support of creating a database for crowd loading that is needed as it is pointed out by other researchers dealing with the same problem.

# **CHAPTER THREE: MODAL ANALYSIS UNDER HUMAN INDUCED EXCITATIONS USING NOISE ASSISTED AND ADAPTIVELY TRANSFORMED MULTIVARIATE EMPIRICAL MODE DECOMPOSITION**

## Introduction

Structural identification under human induced excitations is a special case that constitutes several challenges in one place. The nature of human excitation may be in the form of walking, jumping, dancing, etc. which are non-stationary and they contain most of their energy at low-narrow bands and as consecutive harmonics in their frequency spectrum. Traditional methods to identify such systems work under the assumption that the disturbance is Gaussian white noise assuring that the output spectrum constitutes poles belonging only to the structure. In spite, when the external excitation is in the form of non-stationary human induced loads, white noise assumption does not hold anymore, and a desirable flat excitation spectrum ceases to exist. This may cause the output response spectrum to be significantly different than normal and to not show some of the fundamental modes as they are weakly excited or do not fall in the high-power excitation range. In addition, harmonic narrowband excitations are possibly mixed into the output spectrum as operational modes and may be confused with structural modes. The problem becomes more complicated considering the fact that the structures that are subjected to human interaction such as stadiums and footbridges are almost always of flexible nature and their fundamental frequencies are also condensed within low frequency bands. This phenomenon increases the probability of having ambiguous mixtures of closely spaced operational-structural modes and undermines the estimation of frequency and damping parameters. Therefore, the identification of flexible structures under human-structure interaction necessitates more specific approaches.

As it is indicated in [46], [72]–[74], structural health monitoring and identification of flexible structures -especially stadiums- are vastly untouched. They need improved approaches that consider the intrinsic changes of the system over time and indicate possible nonlinearities, yet the number of studies are scarce. The existing studies [75]–[81] hover around the application of traditional algorithms on the data taken from certain portions of structures. Obviously, operational modal analysis (OMA) is the most effective way that is used in these studies [82]–[84]. The procedure is convenient because large structures as stadiums can be tested without the need of artificial excitation devices and under operating/in-service conditions. There are now many well-established OMA algorithms in time [85]–[90], frequency [91]–[95] and frequency-spatial [96]–[99] domains. In brief, time domain methods exploit the correlation or covariance of the response time histories or auto-regression moving average vector (ARMAV) models. Frequency and spatial domain algorithms follow a similar technique but in frequency space. In the end, modal parameters are extracted by feeding the information to estimators such as orthogonal triangular (QR) decomposition, singular value decomposition (SVD) or least squares. There are also relatively new methods that have been applied to identification, fault detection and denoising by adopting blind source separation and/or wavelet analysis. The first provides a practical solution by representing the entire structural system in the form of non-parametric linear system of algebraic equations [100]. The solution of the equation system results in a sequence of single degree of freedom components from which the dynamic parameters are extracted. The latter is superior when the response is non-stationary that vary in both amplitude and frequency over long periods of time. The procedure follows as finding the correlation between a wave (packet) of a certain period and finite extent by sliding over the response output and generating new projected time series. As the

scale (width) of the wave packet is changed, different simpler oscillatory time series are generated and parameter extraction is carried out from there [84], [101]–[104]. These algorithms may outperform one another and may or may not be ideal or provide the same results when implemented for the same case due to several issues that are often common in almost all of them. Lately, the methods that make use of wavelet packet decompositions and their hybrid versions with BSS have been the most suitable candidates to handle these issues. Some other recent examples implement blind source separation [105], [106] under sparsely distributed sensors with decentralized deployment whereas others make use of wavelet decomposition techniques [107], [108]. Overall, the need for improvement on mitigating the user intervention such as model order selection, peak picking, distinguishing of structural operational and spurious modes, selection of appropriate wavelets still stands.

The implementation of previously mentioned traditional methods on the problem of stadium structures do not go further than a collective statistical comparison of findings. General inference derived from the results is that the dynamic parameters are significantly affected based on the occupancy ratio of the structure. In that, resonant frequencies tend to decrease and damping ratios to increase as the mass ratio of crowd to structure increases. However, since the dynamic parameters are altered because of the non-stationary narrowband excitations and occupant-structure mass ratios, their instantaneous change needs to be realized over time to see the real nature of the behavior and possible nonlinearities. As to footbridges, the studies in the literature are more focused on the improvements of vibration serviceability design [109]–[115]. Some of these studies take advantage of performance assessment of real bridges and incorporate the findings into the design.

To sum up, the human excitation effects on the dynamic response of flexible structures and the realization of those changes on the system over time still need to be understood better yet the number of studies focusing on the issue is limited.

### Empirical Mode Decomposition (EMD) Algorithm and Its Improved Variations

The empirical mode decomposition (EMD) is a non-parametric signal processing technique which breaks down a signal into its simple oscillatory components named as intrinsic mode functions (IMFs) [116].

$$x(t) = \sum_{m=1}^M c_m(t) + r(t) = \sum_m a_m(t) \psi_m(t) + r(t) \quad (26)$$

where  $c_m(t)$  is the IMF,  $a_m(t)$  is the amplitude,  $\psi_m(t)$  is the oscillation and  $r(t)$  is the residual term. The method is powerful as to handling non-stationary data by representing riding complex waves and uneven amplitudes through mono-component intrinsic temporal modes. To get the IMFs from a given time series  $x(t)$ , local minimum and maximum points of the entire signal are found and interpolated using cubic spline interpolation. This interpolation provides the upper  $e_{\max}(t)$  and lower envelopes  $e_{\min}(t)$  of the signal and their local mean:

$$m(t) = (e_{\min}(t) + e_{\max}(t)) / 2 \quad (27)$$

By subtracting the local mean from the original signal, the modulated oscillation [117] is found:

$$d(t) = x(t) - m(t) \quad (28)$$

At this stage  $d(t)$  is expected to show two properties. The first is to have zero mean with both upper and lower envelopes to be symmetric and the second is to have either same number of

zero crossings and extrema or to differ with only one [116], [118], [119]. These criteria are two mandatory conditions for a signal to be classified as an IMF. In case the stopping criteria are not met, the same procedure is applied to  $d(t)$  until the first IMF is acquired. Once the first IMF is found then the same procedure is repeated for the residual:

$$r(t) = x(t) - IMF_m, \quad IMF_m = d(t) \quad (29)$$

This iterative routine is named after sifting process and it stops when the residual  $r(t)$  has no more meaningful component.

Following its first proposal and early applications, EMD is found to suffer from either mode mixing where an IMF may have more than one oscillatory mode or mode splitting where a single mode may appear in multiple IMFs. In some cases, aliasing may also occur due to the sampling of extrema. These problems are realized when cubic spline interpolation ceases to fit ideally to the signal that is intermittent; has relatively flat spectrum or when it doesn't have proper extrema at the ends (end effect artefacts). This issue is remedied by an improved version called ensemble empirical mode decomposition (EEMD) [120]. The procedure includes creating an ensemble of the same signal with the addition of independent Gaussian white noise realizations:

$$\{s_n(t)\}_{n=1}^N = x(t) + \{w_n(t)\}_{n=1}^N, \quad \{w_n(t)\}_{n=1}^N \sim N(0, \sigma^2) \quad (30)$$

Each noise contaminated signal is passed through the same sifting algorithm and the resultant IMF is obtained by taking the ensemble average of the multiple IMFs with the same index:

$$\bar{c}_m(t) = (1/N) \sum_{n=1}^N c_m^n(t) \quad (31)$$

The ensemble EMD significantly reduces the effect of mode mixing. However, the conditions for IMF is violated resulting in the estimation of only the modes instead of the local means. Independent processing of each realization may create additional spurious modes due to the noise on different ensembles being added to the signal when they are to be averaged. Besides, the final extracted modes may contain high-power noise which may cause the weak modes to be buried in. To overcome these problems, and to incorporate into this study a method called complete EMD with adaptive noise (CEEMDAN) is utilized. The following steps need to be taken for the application [121], [122];

- i. Calculate the local means of  $l$  realizations  $x^{(i)} = x + \beta_0 E_1(w^{(i)})$  for the first residue  $r_1 = \langle M(x^{(i)}) \rangle$  where  $E(\cdot)$  and  $M(\cdot)$  are the operators that produce the  $k$ th mode of EMD and produce the local mean;  $w^{(i)}$  is the white noise
- ii. Calculate the first mode  $\tilde{d}_1 = x - r_1$  at the first stage ( $k=1$ )
- iii. Obtain the second residue as the average of local means of the realizations  $r_1 + \beta_1 E_2(w^i)$
- iv. Determine the second mode  $\tilde{d}_2 = r_1 - r_2 = r_1 - \langle M(r_1 + \beta_1 E_2(w^{(i)})) \rangle$
- v. For  $k=3, \dots, K$  calculate the  $k$ th residue  $r_k - \langle M(r_{k-1} + \beta_{k-1} E_k(w^{(i)})) \rangle$
- vi. Find the  $k$ th mode  $d_k = r_{k-1} - r_k$

CEEMDAN is incorporated as a complementary method in the identification process incase modal mixing occurs even after the application of the main algorithm that is explained in the next sub-section.

### *Multivariate Empirical Mode Decomposition (MEMD)*

When multiple data channels are of concern, channel-by-channel application of EMD algorithms could result in issues such as having different number of IMFs per channel. Also, mode misalignment where IMFs with same index have different mode information may occur. In general,

multivariate signal analyses require the simultaneous processing of the entire channel sequence so that mode alignment and uniqueness of findings could be preserved. In this case, the previous computation method of local mean and thus single component IMFs need to change to account for the multiple joint oscillations. The early works on the extension of EMD cover the processing of bivariate [123]–[125] and trivariate [126] signals that eventually pave way for the extension to multivariate empirical decomposition [127].

The MEMD application starts with forming an  $(n-1)$ -dimensional unit sphere which comprises  $K$  Hammersely sequence points (quasi-Monte Carlo sampling) [117], [127], [128]. Each generated Hammersely point is the direction of a unit vector given by angels  $\theta^k = \{\theta_1^k, \theta_2^k, \dots, \theta_{(n-1)}^k\}$  and form the entire set of projection vectors:

$$\mathbf{x}^{\theta^k}(t) = \{x_1^k, x_2^k, \dots, x_n^k\}, \quad k = 1, 2, \dots, K \quad (32)$$

Projecting multivariate signal  $\mathbf{s}(t) = \{s_1(t), s_2(t), \dots, s_n(t)\}$  on the direction vectors, set of projected signals are acquired.

$$\{p^{\theta^k}(t)\}_{k=1}^K \quad (33)$$

The time instants  $\{t_i^{\theta^k}\}$  that correspond to the local minima and maxima of the projected signals are connected via cubic spline interpolation and the multivariate envelope curves

$\{\mathbf{e}^{\theta^k}(t)\}_{k=1}^K$  are obtained. Then the  $k$ -dimensional mean is found:

$$\mathbf{m}(t) = \frac{1}{K} \sum_{k=1}^K \mathbf{e}^{\theta^k}(t) \quad (34)$$

As in the original EMD algorithm, the mean is extracted from the original signal set:

$$\mathbf{d}(t) = \mathbf{s}(t) - \mathbf{m}(t) \quad (35)$$

Based on whether  $\mathbf{d}(t)$  satisfies the stoppage criteria, the sifting is either applied to  $\mathbf{s}(t) - \mathbf{d}(t)$  or repeated for  $\mathbf{d}(t)$ . In its last shape, the MEMD becomes a method to separate joint rotational modes in  $k$ -dimensional space instead of separating oscillations as in basic EMD algorithm. Thus, the previous definition of EMD is extended to its vector form:

$$\mathbf{s}(t) = \sum_{m=1}^M \mathbf{c}_m(t) + \mathbf{r}(t), \quad \mathbf{s}, \mathbf{c}_m, \mathbf{r} \in \mathbb{R}^k \quad (36)$$

where  $\{\mathbf{c}_m\}_{m=1}^M$  are  $k$ -variate IMFs and  $\mathbf{r}$  is the residual. The extracted IMFs are aligned, and they indicate the same modes.

*Noise Assisted Adaptive Projection Intrinsically Transformed Multivariate Empirical Mode Decomposition (NA-APIT-MEMD)*

The MEMD is an important improvement as to processing of multichannel signals with sufficient alignment between same index IMFs and it can be used to conduct intrinsic multiscale analysis such as entropy, correlation and intra or inter component dependencies [129]. On the other hand, research shows that the method can be further improved by mitigating several weak points. The first point to be improved is the existence of mode mixing and mode splitting as encountered in standard EMD. It is shown that the MEMD algorithms have a quasi-dyadic filterbank structure for broadband noise [130]. When the initial algorithm is modified by adding extra uncorrelated Gaussian white noise realizations to the original set of signals, the broadband filterbank acts a series of bandpass filters so that the IMFs with the same frequency content could align themselves (Figure 26). It should be noted that unlike the EEMD, the noise channels are not added directly onto the signal but added as separate noise channels and the resultant set of channels are fed into MEMD algorithm.

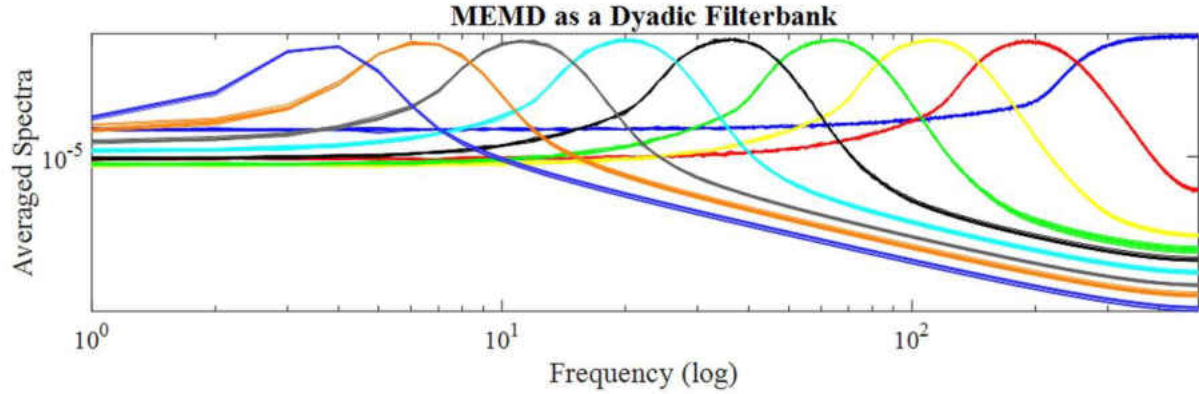


Figure 26 Illustration of dyadic filterbank property of MEMD after averaging the IMF spectra of multiple channel 500 Gaussian white noise realizations

In many practical applications including modal analysis, multichannel signals contain intrinsic inter-channel correlations from which useful information is obtained. However, the MEMD may suffer from loss of this information unless a considerably high number of projection vectors is used. The use of such high number of vectors drastically increases the computation time. Additionally, power inequalities between the channels may make the recognition of these similarities even more difficult. Therefore, in addition to noise assisted version of the MEMD, another improvement with an adaptive method that relocates the randomly distributed projection directions on hyper dimensional sphere is used [131]. The method is based on finding the first principal component of the covariance matrix of the input signal pointing in the direction of the highest power inequality.

$$\mathbf{C} = E \{ \mathbf{s}^T(t) \mathbf{s}(t) \} = \mathbf{V} \mathbf{\Lambda} \mathbf{V}^T \quad (37)$$

where  $\mathbf{V} = [\mathbf{v}_1, \mathbf{v}_2, \dots, \mathbf{v}_n]$  is the eigenvector and  $\mathbf{\Lambda} = \text{diag} \{ \lambda_1, \lambda_2, \dots, \lambda_n \}$  eigenvalue matrix.

Once the direction of the highest power inequality is known, another vector in the opposite pole

$\mathbf{v}_{o1} = -\mathbf{v}_1$  is generated. The previously generated points are reorganized concentrated around the new directions based on their Euclidian distance:

$$\hat{\mathbf{x}}_{\mathbf{v}_1}^{\theta_k} = \frac{\mathbf{x}_{\mathbf{v}_1}^{\theta_k} + \alpha \mathbf{v}_1}{|\mathbf{x}_{\mathbf{v}_1}^{\theta_k} + \alpha \mathbf{v}_1|}, \quad \hat{\mathbf{x}}_{\mathbf{v}_{o1}}^{\theta_k} = \frac{\mathbf{x}_{\mathbf{v}_{o1}}^{\theta_k} + \alpha \mathbf{v}_{o1}}{|\mathbf{x}_{\mathbf{v}_{o1}}^{\theta_k} + \alpha \mathbf{v}_{o1}|} \quad (38)$$

where  $\alpha$  is a factor to arrange the condensation of these points around the new directions.

The last step is to obtain the local mean as in original MEMD algorithm. The relocation of projection vectors lets intrinsic inter-channel correlations be captured much easier and with less computational effort.

#### *Time-Frequency Representation via Hilbert-Huang Transform*

The most exceptional aspect of working with EMD based methods is to track the intrinsic changes of the mono-component IMFs. Since IMFs are represented based on an amplitude-phase modulation  $c_m \approx a_m(t)\cos(\theta_m(t))$ , time varying nature of both amplitude and phase can be observed. If an IMF is represented with its analytic representation:

$$\mathbf{s}(t) = \sum_{m=1}^M (\mathbf{c}_m(t) + jH[\mathbf{c}_m(t)]) = \sum_{m=1}^M a_m(t) e^{j\theta_m(t)} \quad (39)$$

where the so called Hilbert transform is defined as

$$H[c_m(t)] = \frac{1}{\pi} \mathbf{p} \cdot \mathbf{v} \cdot \int_{-\infty}^{\infty} \frac{c_m(\tau)}{t - \tau} d\tau \quad (40)$$

then the instantaneous frequency is  $\omega_m(t) = d\theta_m(t)/dt$ . Thus, when time varying frequency is to be plotted with respect to time, Hilbert-Huang spectrum (HHS) is achieved from the related IMFs. HHS is powerful as it shows intra-wave modulations or drifts of the signal which is a sign of nonlinearity. It will be used as a tool to keep track on the changes of dynamic parameters.

### *Adaptation to Operational Modal Analysis (OMA)*

The first known study on the application of multivariate empirical mode decomposition to operational modal analysis is carried out by [132] in which the modal parameters of a simulated system and a laboratory frame are successfully identified. Following up the first successful implementation, the new noise assisted adaptive approach is adopted with a specific interest on the response of structures exposed to human induced vibrations. In its most fundamental form, a multi degree of freedom (MDOF) system under the assumption of discretized lumped mass and proportional damping may be represented as follows:

$$\mathbf{M}\ddot{\mathbf{x}}(t) + \mathbf{C}\dot{\mathbf{x}}(t) + \mathbf{K}\mathbf{x}(t) = \mathbf{F}(t) \quad (41)$$

where  $\mathbf{M}$ ,  $\mathbf{C}$ ,  $\mathbf{K}$  are the mass, damping, stiffness matrices respectively.  $\mathbf{x}(t)$  and  $\mathbf{F}(t)$  are the nodal displacement and input force vectors. Due to the unique orthogonality properties of the modal vectors Eq. 41 can be rephrased as follows:

$$\mathbf{x} = \boldsymbol{\psi}\mathbf{q} \quad (42)$$

where  $\boldsymbol{\psi}$  is the transformation matrix whose columns are the modal vectors of the original system and  $\mathbf{q}$  represents the modal coordinates. Considering the relation between the nodal displacement vector in Eq. 41 and the IMFs of Eq. 36, modal vector representation of Eq. 41 can be written in the form of:

$$x_i(t) = \sum_{j=1}^n c_{ij}(t) = \sum_{j=1}^n \theta_{ij} q_j(t), \quad i = 1, 2, \dots, m \quad (43)$$

where  $i$  indicates the measurement location whereas  $j$  is the relevant IMF index or the corresponding modal response. If the index  $i$  is switched to  $p$  and  $r$  to represent two different

simultaneous response/measurement locations, partially normalized mode shape coefficients are obtained:

$$\frac{\mathbf{c}_{pj}}{\mathbf{c}_{rj}} = \frac{\theta_{pj}q_j}{\theta_{rj}q_j} = \frac{\theta_{pj}}{\theta_{rj}} = \bar{\theta}_{pr} \quad (44)$$

If the expected value of Eq. (44) is taken after reorganizing and pre-multiplying with  $\mathbf{c}_{pj}^T$ , the following expression is acquired:

$$E[\mathbf{c}_{pj}^T \mathbf{c}_{pj}] = E[\mathbf{c}_{pj}^T \bar{\theta}_{pr} \mathbf{c}_{rj}] \quad (45)$$

Eq. 45 leads to the expression of mode shape coefficients by the standard deviations of IMFs:

$$|\bar{\theta}_{pr}| = \frac{\sigma_p}{\sigma_r} \quad (46)$$

Eq. 46 is incorporated into the computation of cross correlation coefficient between  $\mathbf{c}_{pj}$  and  $\mathbf{c}_{rj}$ .

$$\rho_{pr} = \frac{E[\mathbf{c}_{pj} \cdot \mathbf{c}_{rj}^T]}{\sigma_p \times \sigma_r} = \frac{\bar{\theta}_{pr} \cdot \sigma_r^2}{|\bar{\theta}_{pr}| \sigma_r \cdot \sigma_r} \quad (47)$$

and is an indicator of both having mono-component content and the sign of a modal displacement. Therefore, the partial modal coefficient can be described with its final shape:

$$\theta_{pr} = \frac{|\rho_{pr}| \sigma_p}{\rho_{pr} \sigma_r} \quad (48)$$

### *Separation of operational modes and applications steps*

As previously mentioned, the harmonic nature of excitation that is generated by humans yield to several challenges such as mixed identification of harmonics as structural modes, poor

damping estimation due to structural modes being affected by closely located harmonics and harmonics inhibiting the identification of structural modes. In scope of this study, the issue is remedied by applying statistics driven techniques [105], [133]. The first method is to utilize probability density function (PDF) over IMFs. It is known that when sufficient signal to noise ratio (SNR) values are achieved, the shape of the PDF of a harmonic has two peaks allowing it to be isolated from the structural modes. Another measure to complement the use of PDF is kurtosis:

$$\kappa(x|\mu, \sigma) = \frac{E[(x - \mu)^4]}{\sigma^4} \quad (49)$$

The kurtosis is the fourth central moment of  $x$ , a stochastic variable normalized with respect to the standard deviation  $\sigma$  and it is used as a measure to indicate the sharpness of the PDF peak and its severity. The kurtosis values that are close to 3 is an indicator for structural modes whereas the lower values are the signs for harmonic excitation modes. Once these two measures are applied on the mono-component signals, operational modes are easily determined.

As a finally step, the implementation of the method is summarized below:

- i. Select a suitable set of output channels  $\mathbf{s}(t) = \{s_1(t), s_2(t), \dots, s_n(t)\}$  for identification
- ii. Perform intrinsically adaptive ensemble NA-MEMD algorithm by setting a proper value for  $\alpha$  condensation factor and extract mono-component IMFs  $\{\mathbf{c}_m\}_{m=1}^M$
- iii. If mode mixing is present or a closely spaced mode is failed to be separated, perform CEEMDAN algorithm and finalize the IMF extraction process
- iv. Compute probability density function and kurtosis to isolate operational modes from structural modes
- v. Estimate the modal frequencies and damping ratios from the mono-component IMFs
- vi. Find modal matrix  $\Psi = [\psi_1 \ \psi_2 \ \psi_3 \dots \psi_n]$

## Experimental Studies

### *Laboratory structure and tests conducted*

The performance of the method is assessed through a controlled experiment on a grandstand simulator (Figure 27-A). The grandstand simulator is constructed as a multipurpose structure for researchers to investigate different SHM related technologies and algorithms such as sensors, parametric or non-parametric damage detection or identification methods prior to real life implementations. The structure is simply a steel grid that resembles of a simple supported beam with a 20° angle inclination. It is placed on columns where connections in between are made with supports that may be adjusted to represent a variety of support conditions (Figure 27-E). The grandstand can also be adjusted to have one or two clear spans with continuous beams across the middle supports. In this sense, the simulator can be modified to reveal different structural stiffness and damage cases by altering specially designed intermediate and boundary conditions. Dynamic response of the simulator is captured utilizing high sensitivity piezoelectric accelerometers that are placed on beam-beam connection nodes located at the front and at the back of the structure to ensure that the sufficient spatial resolution is achieved (Figure 27-A, B). PCB 054114 force washers are installed beneath the supports to record force time-histories generated under human excitation (Figure 27-C, D, E).

In scope of this study, the flexible grandstand is tested within a specific scenario in which four subjects exert synchronous jumping loads upon. During the test, the subjects are asked to accompany the popular song called ‘Zombie Nation’ that is played during the state Football gamers (Figure 28). Before the test, the subjects are put through a training phase in which they get familiar with the song and adjust themselves to the main beat accordingly.

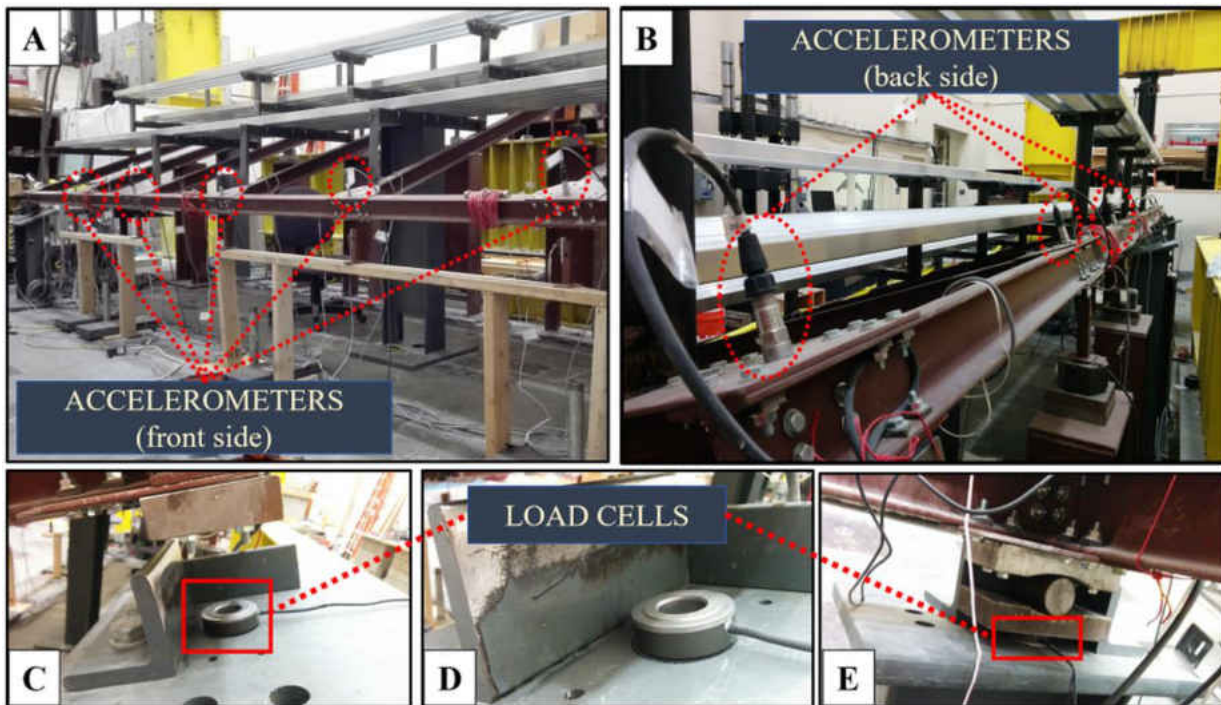


Figure 27 A, B: The grandstand simulator with accelerometers mounted at the front and at the back side of the structure; C, D: The placement of force washers between the steel grid and the support columns; E: The view of connections after the placement

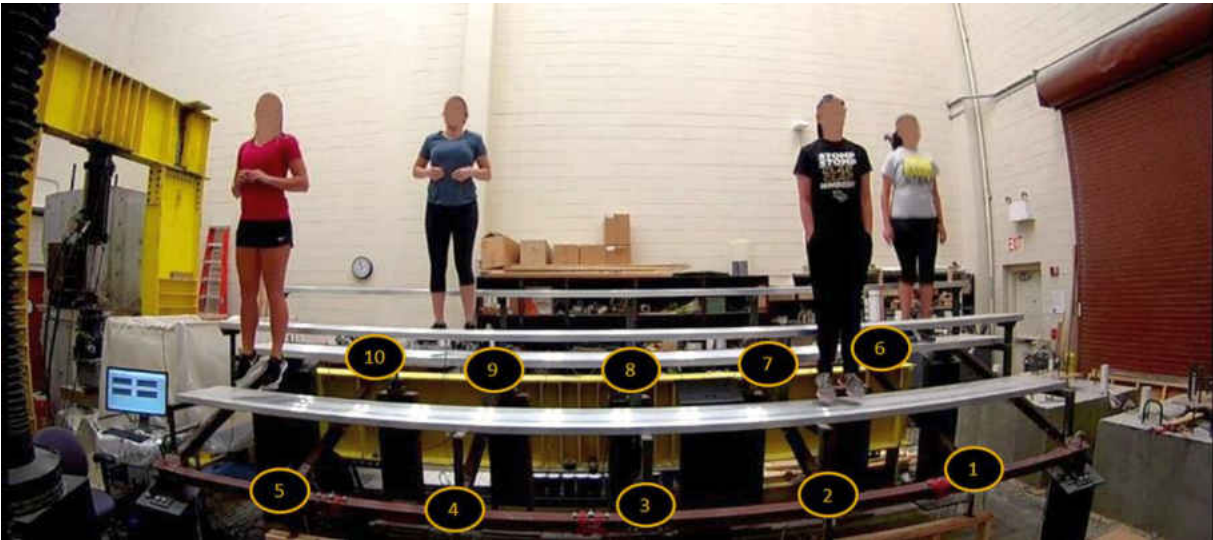


Figure 28 An instant from the test as the subjects jump to the song on play and the locations of sensors

### *Results and Discussion*

In Figure 29, the blue line shows the amplitude spectrum of the total force record that is captured by the load cells placed beneath the supports. From the previous sound wave analysis, it is known that the main beat frequency of the song is 2.34Hz which is clearly observed in the jumping record. The following peaks are the second and the third harmonics of the main beat. The power of the signal is concentrated heavily around the first harmonic and slowly attenuated over higher frequency band. The second flat line is the frequency response of the Gaussian white noise having the same variance as the recorded force time history.

The visualization of the two different excitation levels is important as to what to expect from the structural response. The flat spectral response is very well suited to satisfy the general assumption of all the linear time invariant system theory and is expected to stimulate all the resonant frequencies. On the other hand, a non-stationary narrowband excitation is expected to have a similar performance in the narrowband where its energy is concentrated but also to introduce new information that may easily be mixed with the actual modal response especially when there are modes residing in the same range. The higher frequency modal information is not possible to observe as the excitation energy quickly drops out after the third harmonic. This is not a serious problem due to the fact that civil engineering structures that are exposed to narrowband excitations preserve their highly participated modes within the first several modes.

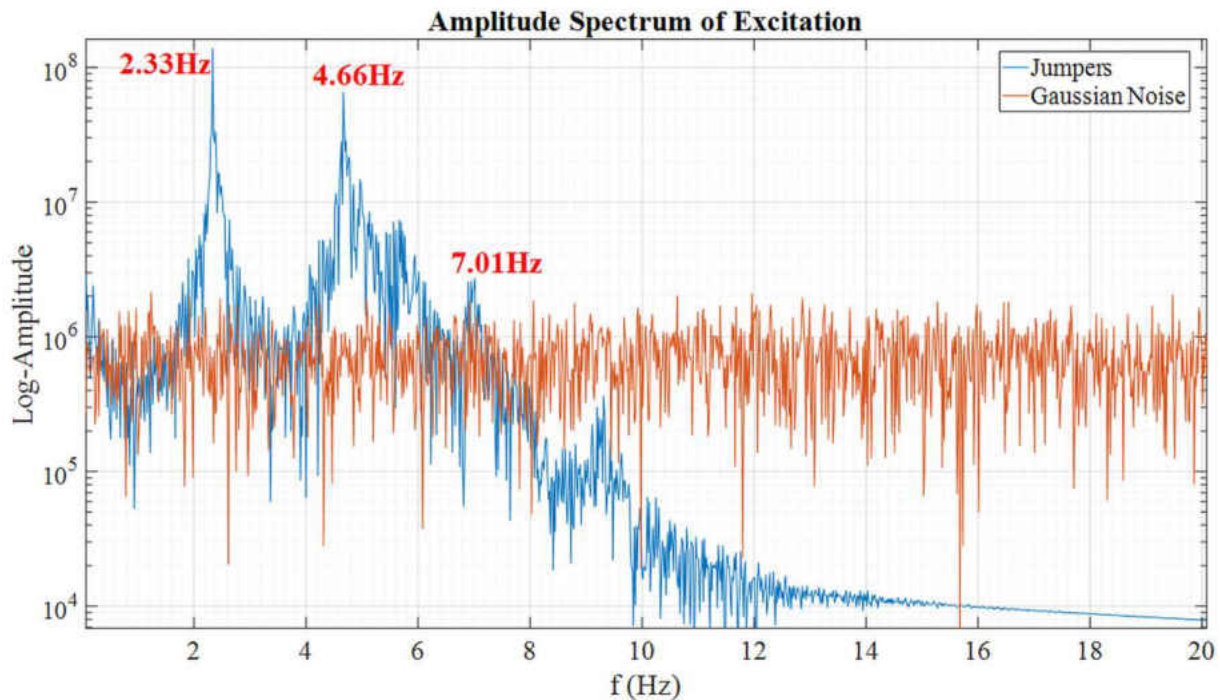


Figure 29 Amplitude spectrum of the recorded force and the white Gaussian noise of the same variance

Figure 30 shows the CMIF plot of two tests regarding the excitations in Figure 29. The first line corresponds to the first singular value line extracted from the impact hammer test where several nodes are excited and a relatively flat input spectrum covering a wide frequency band is achieved. The second singular value line corresponds to the jumping test previously introduced. There are significant differences between the two response spectrums. It is evident that the excitation effects completely leak into the response altering the output spectrum within the low 0-10Hz frequency band. Compared to the response spectrum of the impact test, there are now operational modes that are hard to distinguish from the structural modes. In some cases, peaks become distorted and some modes can even be lost when averaging of the record which is a preprocessing routine. Due to the reasons that the structure is flexible and the jumping excitation can create very high levels of vibration (especially when it is close to being coupled with the

structure resonant frequency), the amplitudes are much higher compared to the impact test. This scale difference prevents the amplitudes of the impact test from being clearly seen in Figure 30. There also seems to exist several peaks in 10-20 Hz band that are not normally present on the impact test spectrum.

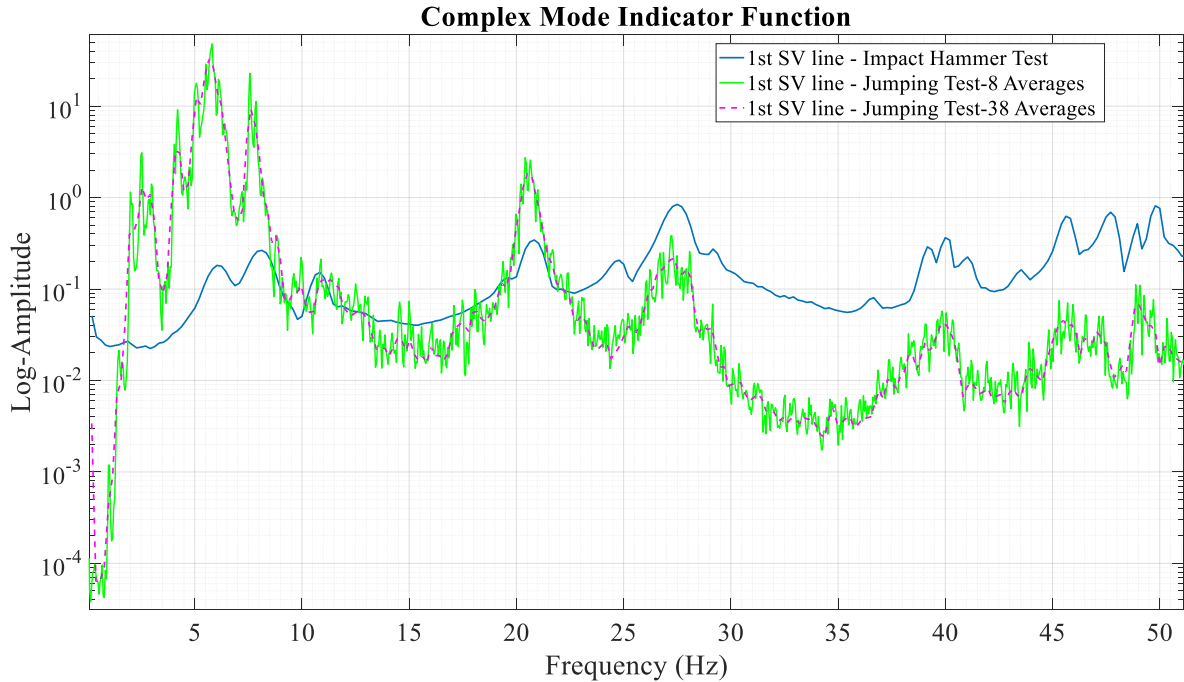


Figure 30 The CMIF plot of the first singular value line under ambient testing and jumping excitation

As another example, Figure 32 shows the stability diagram of extracted parameters from SSI-COV [134], [135] for the grandstand under an ambient excitation. In SSI-COV, based on the prescribed time lags during the formation of the covariance matrix, model order can be increased or decreased. As it is quite difficult to initially estimate the real order of the modal model, general application is over-modeling and then select the proper order from there. In Figure 32 the system poles are drawn with respect to the model order and the identification is carried out from a clear stability diagram.

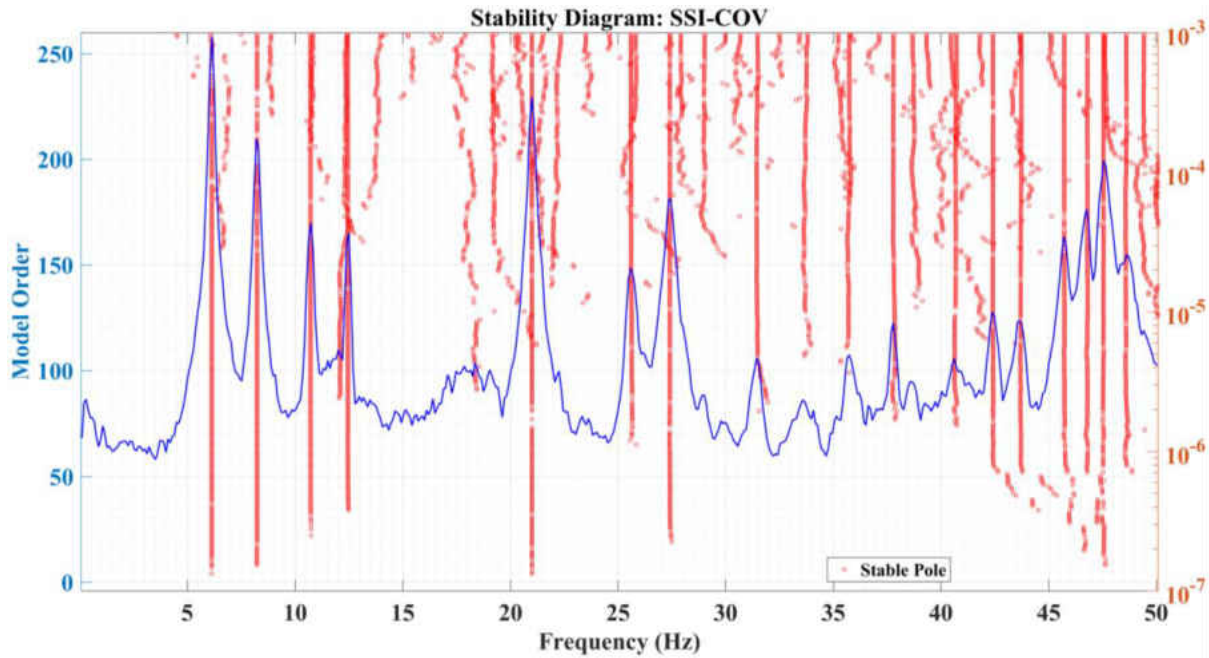


Figure 31 SSI-COV stability diagram for the grandstand under ambient excitation

Conversely, Figure 32 shows a significantly altered diagram. Several studies in literature state that the subspace methods can handle non-stationary excitations as long as the data is long enough and a higher model order is used. However, over modeling may also create spurious modes that are not physically meaningful. Although certain thresholds are applied on the extracted parameters based on the difference of frequency, damping and modal assurance criterion (MAC) values, when non-stationary excitation and its harmonics are involved the stability diagram may get corrupted. From Figure 32, it can be concurred that both the structural and operational frequencies are successfully extracted but it is hard to distinguish whether they are operational, spurious or real structural modes.

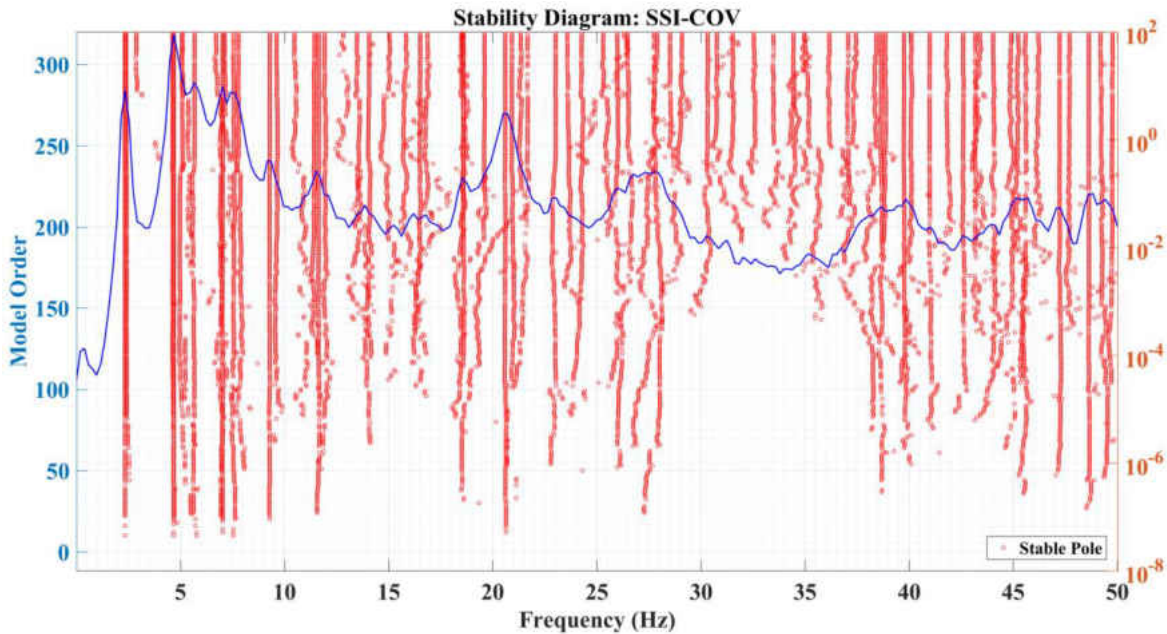


Figure 32 SSI-COV stability diagram for in-service data.

For a typical operational modal analysis study, the quality of the data is in direct proportion with the time window selected. Generally, longer data sequences are required to mitigate the excessive noise through averaging. Short data sequences may result in poor estimation of system poles, a lower frequency resolution and loss of temporal information. This is one of the drawbacks of Fourier spectrum based approaches. From this point of view, the time for the grandstand test data is quite short as being approximately 30 seconds. Thanks to the adaptive property of the EMD based methods, data length is not an issue to extract meaningful information from IMFs but it should be noted that it is better to apply some sort of filtering to mitigate the noise content as several studies show susceptibility of EMD to input noise. Before the application of the NA-MEMD, the data is decimated from the original 2kHz sampling rate down to 200Hz. A low pass Butterworth filter with a 50 Hz cutoff frequency is applied to get rid of the high frequency noise content and then the data is passed onto the algorithm. The condensation factor  $\alpha$  is chosen as

0.5 and the same number of independent noise channels varying 2-5% of the processed signal are added as additional channels. Figure 33 shows the successfully extracted IMFs after the method is applied on the sensors that are attached to node 1, 2, 4 and 5 (Figure 28). Each row in the group corresponds to the IMFs that are of the same index whereas each column indicates the IMF sequence that belongs to the same sensor location. From the shape of the time varying signals, it is evident that the noise assisted MEMD with adaptive transformation can align the same scale modes across multiple channels.

This property is observed much clearly in the frequency representation in Figure 34 and is quite important for the processing of multiple channel data as it might get difficult to visualize and reorder the same index IMFs when the number of channels increases. Also, when the same IMFs are aligned across different channels, it is more convenient to apply CEEMDAN in case mode mixing is present.

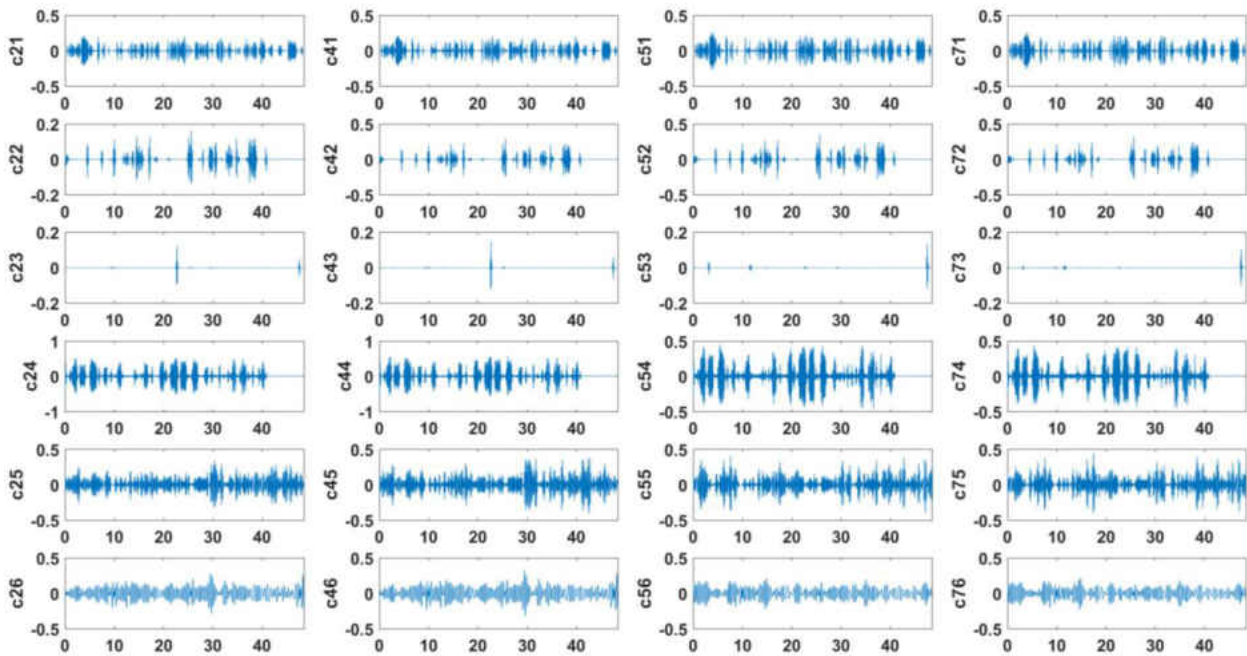


Figure 33 IMFs that belong to the grandstand jumping test

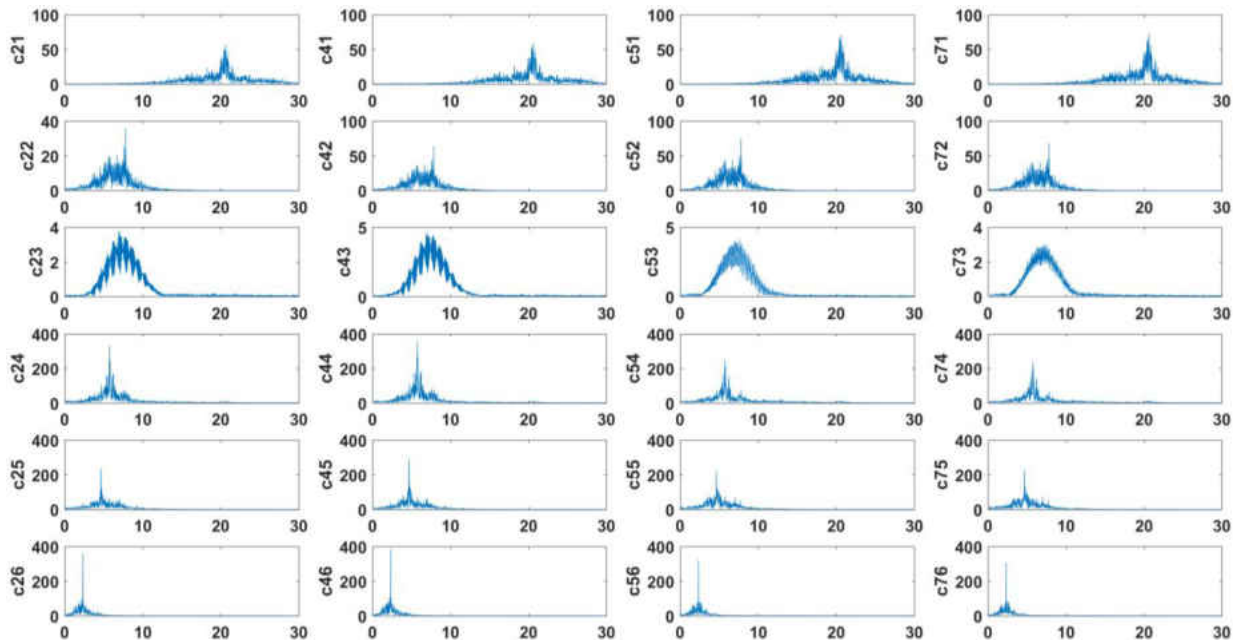
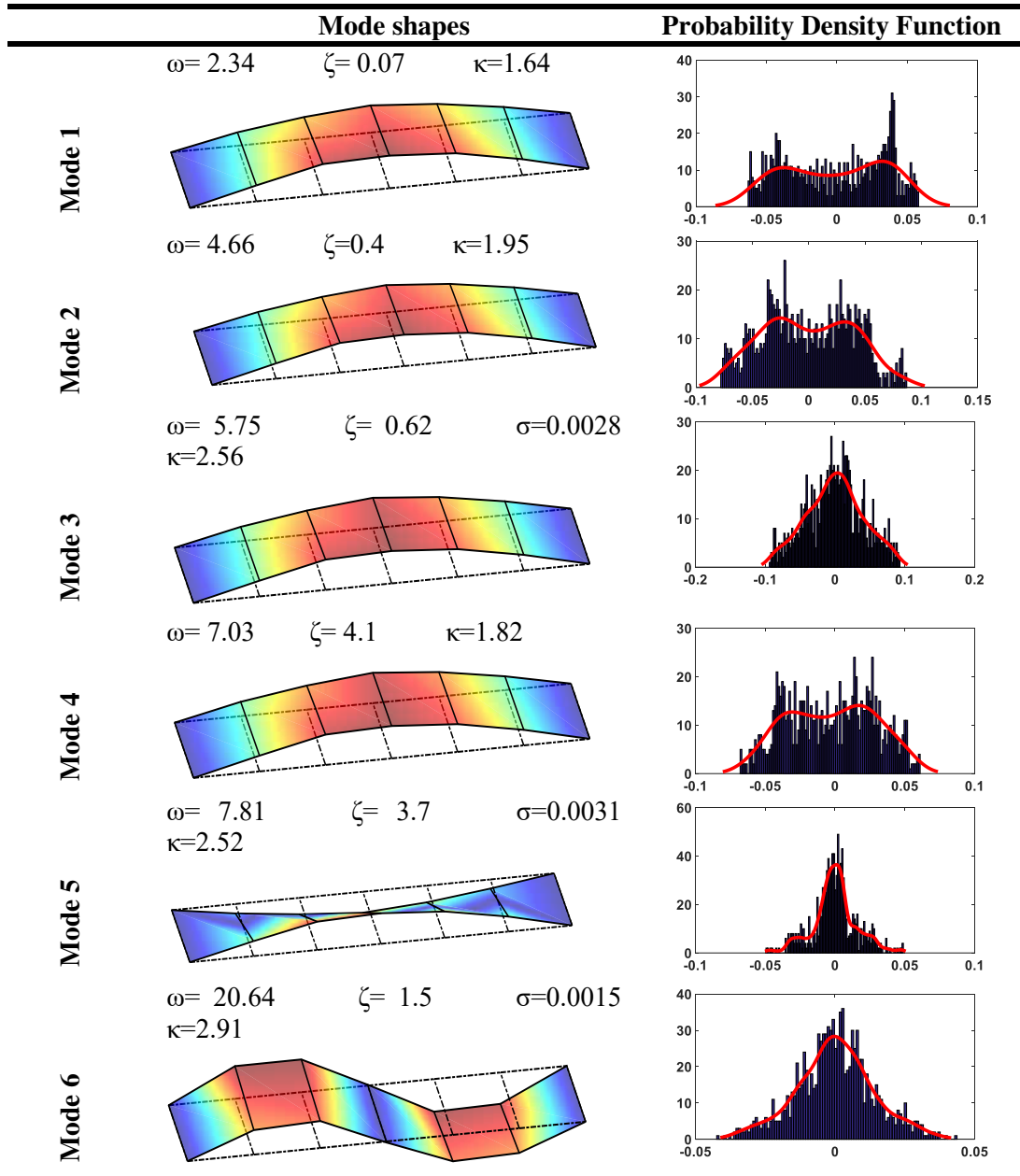


Figure 34 Power spectra of each IMF from four different locations on the grandstand

During the processing of the grandstand data, several observations have been made. Although the noise content in the processed signal may initially reduce the performance of the MEMD, the noise assisted version significantly increases the performance especially mitigating mode mixing and providing scale alignment. The power of the added noise channels has a direct influence on the extracted IMFs. As the power of the noise increases, the concentrated Fourier amplitudes indicating the signal power are also increased and the mixing is either reduced or eliminated. However, as the power of additional noise channels go higher, leakages in the IMF spectrum are observed bringing about unnecessary mode mixing. As a rule of thumb, the power of noise channels is selected between the %2-5 of the variance of the input signal. Number of noise channels doesn't seem to have a drastic effect on the results [117], [136].

Table 4 A summary of the identification results for the laboratory grandstand simulator



As the next step, the PDF and kurtosis of the extracted IMFs are obtained. The PDFs of Mode 1 and Mode 2 fit to that of harmonic excitation with their two-peaked bath-tub shape. Additionally, the Kurtosis values are also quite low for a structural mode. Also, it is known that

the mode shape vectors that belong to the operational modes have high correlation. By using the partial cross correlation coefficients of the mono-component IMFs, the modal matrix and hence the mode shapes are determined as in Table 4. The similarity between the first three is another indicator for a mode to be determined as operational mode. Therefore, mode 1 (2.34 Hz) and mode 2 (4.67) Hz are marked as the operational modes. From the excitation spectrum of the grandstand simulator test, it is evident these same frequencies overlap with each other and are deemed to be harmonics.

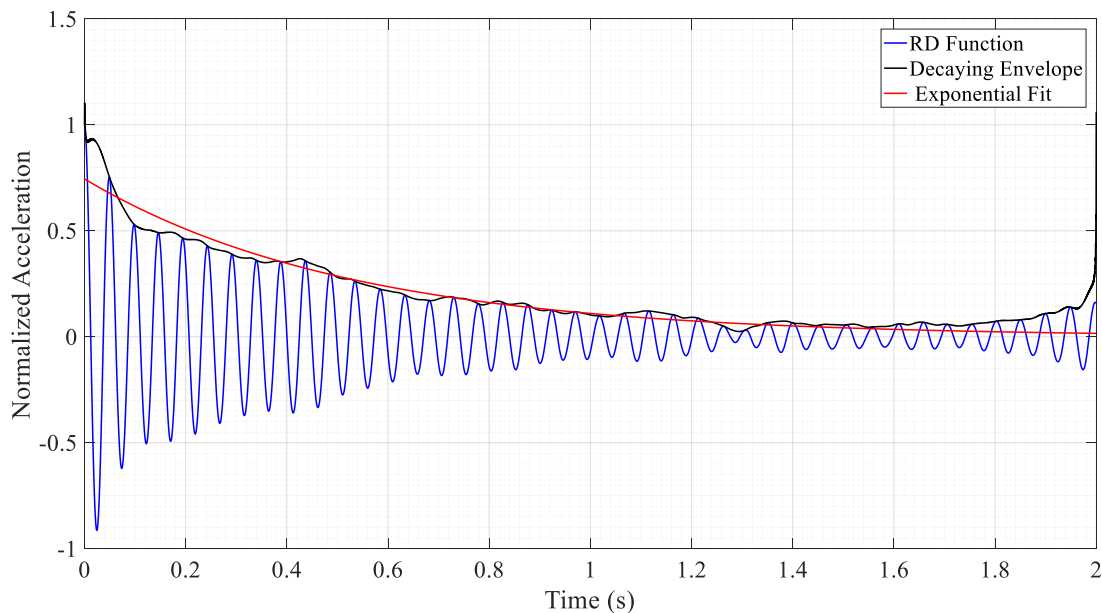


Figure 35 Estimation of damping from the auto correlation function of IMFs

Figure 35 shows the calculation of damping using IMFs. As it is explained before, damping estimation under non-stationary excitations are unreliable and sometimes not possible especially when frequency domain curve fitting methods are used. IMFs present a convenient way of solving this issue. Once the IMF of a certain mode is extracted, the auto-correlation of that IMF can be computed. The resultant function reveals itself as a typical decaying vibration signal. An envelope

over the local maxima of the function is extracted and an exponential decaying window is fitted over the entire envelope. After this point, the logarithmic decrement method can easily be applied to find the damping ratio corresponding to that mode.

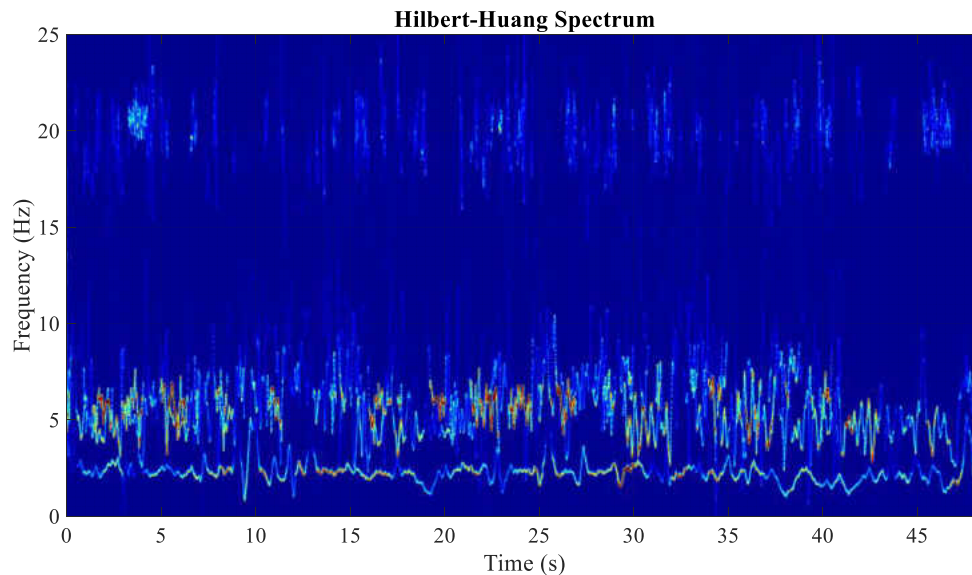


Figure 36 Hilbert-Huang spectrum showing the variation of frequency over time

Figure 36 is the illustration of the Hilbert-Huang transform out of extracted IMFs. The information derived from the computation and visualization of HHT is superior to the information derived from the Fourier transform. The first couple of average frequencies 2.34, 4.66 Hz extracted and identified are the instances of this phenomenon and they preserve the highest power. Their duration also continues until the end whereas the structural frequencies that lie above this range tend to have a transient trend that are likely to die out. Another observation is that the third harmonic in Figure 29 (7.03 Hz) is not seen in the Fourier spectrum of extracted  $c_{i_2}$  IMFs. On the other hand, HHT realization shows a large drift around the fourth mode of the structure. These large drifts stem from several reasons that need attention when a signal is observed with HHT. When there are drastic amplitude changes within an IMF as can be seen in  $c_{22}$   $c_{23}$ , the Fourier

spectrum for the envelope and carrier are not separable violating the Bedrosian theorem. Because of this problem, the signal through Hilbert transform doesn't give the phase function of the carrier alone without the influence of the variation from the envelope [137], [138]. Since vibration data is strongly intermittent by nature, extreme spikes in the HHT are more likely to be observed.

### Real Life Applications

#### *Monitoring of a stadium during a football event*

A small portion of a football stadium is also investigated as seen in Figure 37. The whole stadium is constructed as a steel structure which has a typical inclined architecture to provide the best line of sight for the audience. The reason as to the choice of the monitored section is that this certain section is allocated to students who are expected to create the highest excitation, hence the vibration values, in response to the events that take place within the game. Additionally, the marching band for the motivation of the crowd is also located close to the monitored section. In light of this information, the instrumentation plan is prepared. 12 accelerometers are installed at mainly two portions from the top to the bottom, namely upper and lower deck and in different positions where vibration level is observed to be higher than other sections of the stadium.

Figure 38 is an illustration of the sensor locations at the upper and lower deck of the section. As it is seen, motion of the main girder, floor beam, and stringer are measured in both vertical and horizontal direction. For the upper and lower stringers, channels 3, 4, 11 and 12 are placed in the middle. Upper and lower floor beam, together with the upper main frame girder are monitored through channels 1, 2, 5, 6, 9, 10. Finally, channels 7 and 8 are installed at the connections of main beams and stringers of upper deck Figure 38.

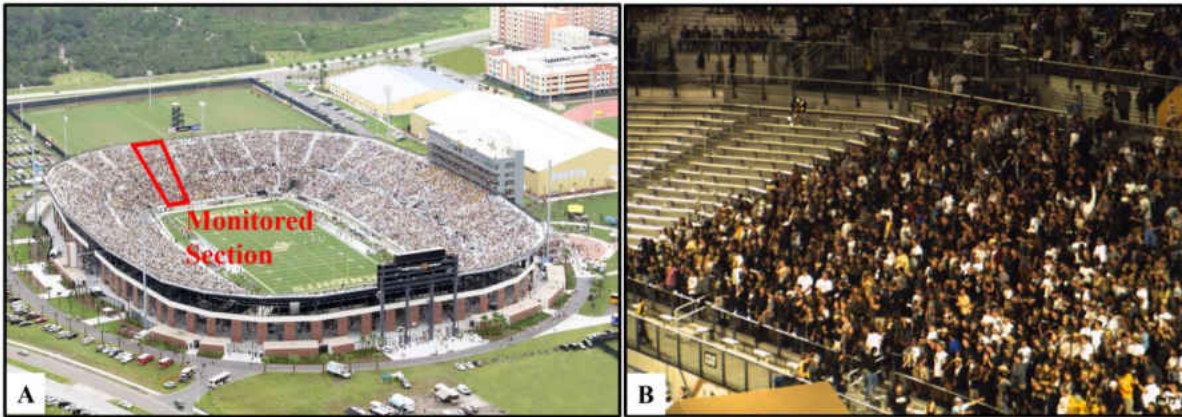


Figure 37 A: Monitored portion of the stadium; B: An overview of the crowd over the section

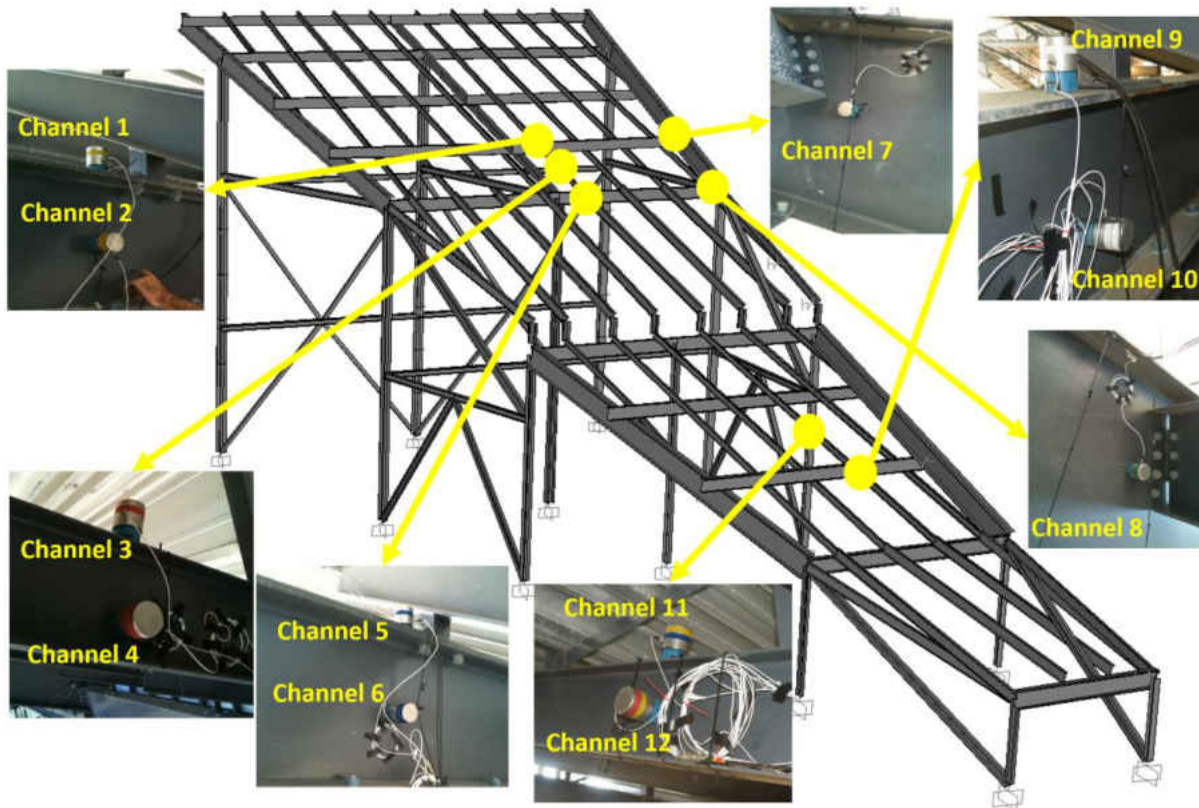


Figure 38 The high sensitivity seismic sensors along with their locations on the structure

The transducers used in this monitoring study are PCB 393C general purpose seismic type accelerometers with the sensitivity of 1000mV/g. VXI data acquisition system with Agilent Technologies module is used to record the vibration data. The sampling frequency is chosen to be 100 Hz and for each game recording is taken for 10 minutes and several recordings are saved throughout the game. As the recording is put in progress, notes and video footages are taken to make sure none of the significant movements are missed.

### Findings

For the separation of the modes, the same number of independent noise channel as the number of the output signal are added. The power of the noise, the condensation factor  $\alpha$  and the number of projection vectors are all consecutively changed to see their effects on the final result. Since the objective of the study is not to demonstrate a statistical study on the performance of the extraction, illustrations in regards to those different results are not given here. As a brief explanation, when the real-life signals are to be processed, the consecutive IMFs almost always present some sort of mode mixing but the alignment is never lost. When the signal is exposed to some sort of preprocessing so as to increase SNR or to get rid of high frequency noise, the performance seems to be increased. It is hard to estimate an optimum power level for the extra noise channels because even with the same noise, the same results may not be achieved. On the other hand, it is a fact that the results get corrupted with excessive noise once the noise power goes over 15-20% range of the output signal. In scope of this study, for the mixed modes, previously told CEEMDAN is utilized with a sufficient accuracy. However, considering the fact that the modes preserve their alignment, NA-MEMD method can also be iteratively applied for the mixed

channels instead of focusing on individual IMFs. Figure 39 shows the extracted IMFs for the channels 3, 4, 7 and 8. The monitored portion of the stadium is a retrofitted version of its original design. The lower seating section behaves almost as static whereas upper seating section has several low frequency swaying motions. Although the mono-component rotational modes are extracted, the results are hard to see from the Fourier representation as the added noise induce some amount of leakage which Fourier approach is susceptible to.

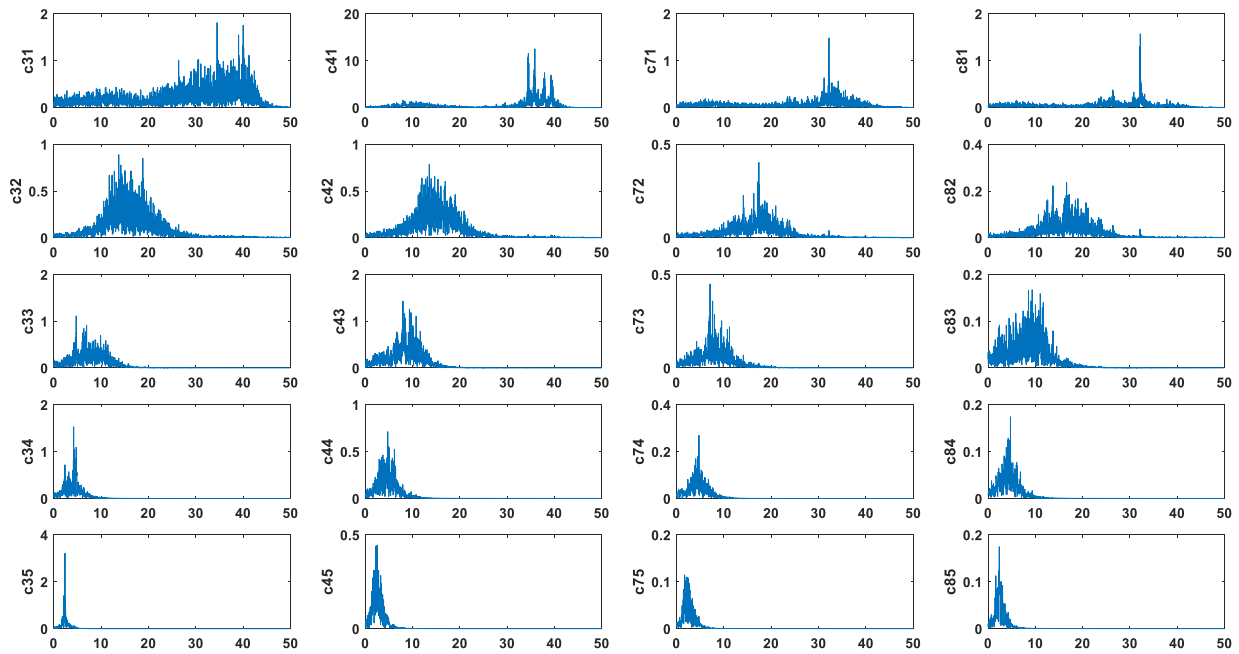
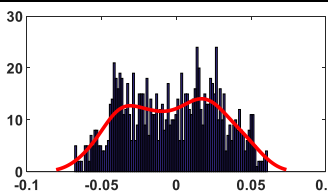
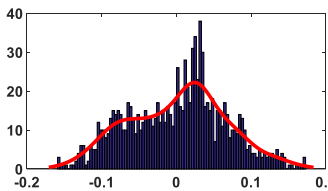
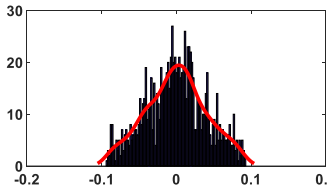
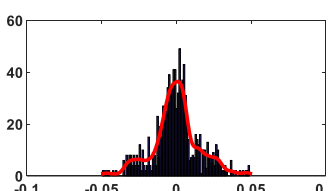
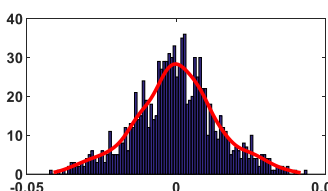


Figure 39 Extracted IMFs from the stadium field implementation

Table 5 is a summary of the findings from the stadium test. The data set that belong to this identification study is captured when the audience jump accompanying the same song played in the laboratory experiments. Because of that same disturbance on the system as in grandstand simulator case, the first three modes are identified as excitation harmonics. This observation is confirmed also by looking at the PDF and kurtosis realization of the IMFs. After the third harmonic excitation.

Table 5 A summary of the identification results for the stadium structure

	Mode shapes	Probability Density Function
Mode 1		 $\omega = 2.37$ $\zeta = 1.88$ $\sigma = 0.00$ $\kappa = 1.96$
Mode 2		 $\omega = 4.78$ $\zeta = 3.02$ $\sigma = 0.007$ $\kappa = 2.06$
Mode 3		 $\omega = 6.69$ $\zeta = 6.36$ $\sigma = 0.0032$ $\kappa = 2.76$
Mode 4		 $\omega = 12.81$ $\zeta = 0.01$ $\sigma = 0.0012$ $\kappa = 3.85$
Mode 5		 $\omega = 34.72$ $\zeta = 0.01$ $\sigma = 0.0011$ $\kappa = 3.19$

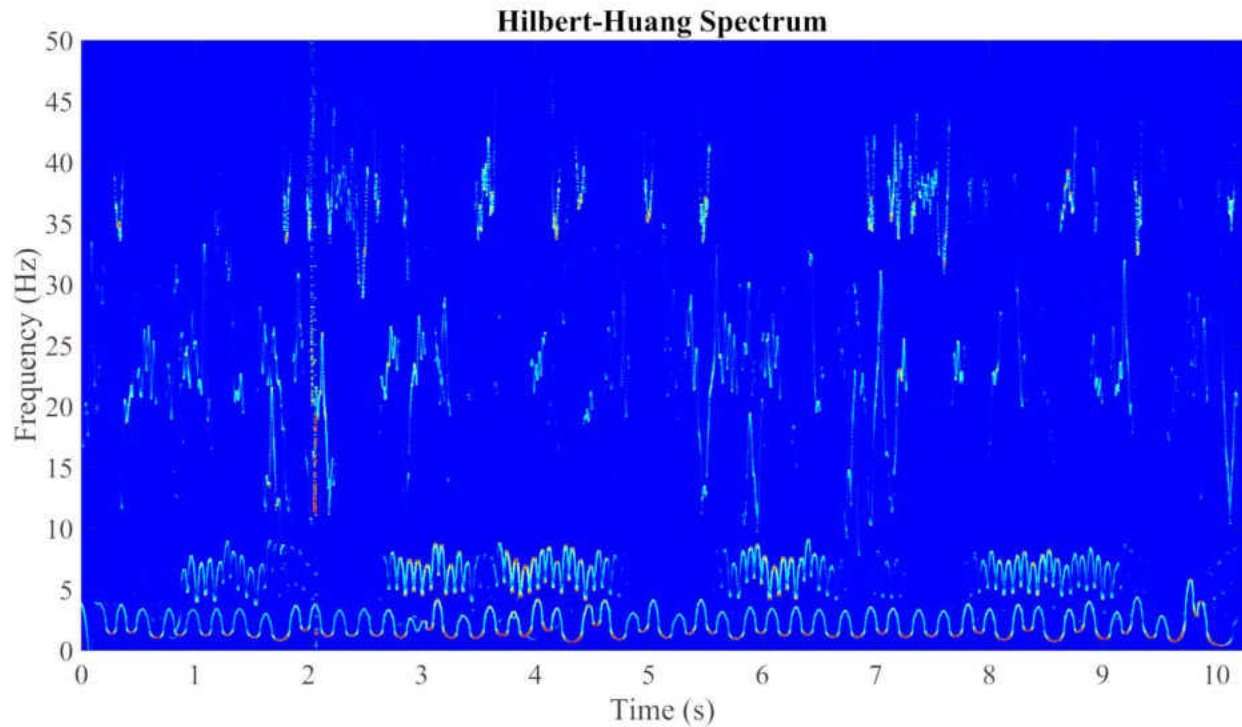


Figure 40 Hilbert-Huang spectrum showing the variation of frequency over time

Figure 40 shows the dynamically changing fashion of frequencies over the entire time through HHS. The power of the signal is concentrated mainly in the low frequency range and they are constantly drifting which is known as the intra-wave modulation in the literature. Intra-wave modulations are the distorted harmonic vibrations of systems with nonlinearities in response to harmonic excitations [139], [140]. Such systems are mono-component, however they have an intra-wave element that may cause sudden amplitude changes. This observation is also the proof that humans have intra and inter changes as they are imposing jumping, walking etc. loads on the structures. They cannot keep the phase/frequency of the motion as the same throughout the entire duration of excitation. Based on the same amplitude intermittency of the signal and violation of Bedrosian theorem in Figure 36, frequency looks scattered over the spectrum. However, human induced excitations can clearly be seen and in this condition, the spectrum can be used as a

complimentary tool to delineate the operational modes in support of the statistic measures described previously.

### *Monitoring of a Footbridge*

Another real-life implementation is conducted on a footbridge where non-stationary human induced loads are prominent (Figure 41). The bridge comprises of 19.5m long vertical truss frames that are connected via post-tensioning in the middle and spans an entire length of 39m over a pond. The vertical truss members on the left and the right side are made of C type vertical and F type diagonal steel members. The lateral stability is provided by another truss frame that is 3.65m wide which is constructed with G type diagonal cross braces, H type lateral box members and F type longitudinal members. This frame holds the entire thin layered aluminum-concrete composite deck. The bridge is located at a university campus and is under a light pedestrian traffic.



Figure 41 A: The side view of the footbridge and locations of accelerometers; B: Name tags for accelerometers on both sides of the bridge

The dynamic response of the study is captured via ten high sensitivity piezoelectric accelerometers mounted in vertical directions (Figure 41-A). The sensor locations are shown in Figure 41-B where A1-A5 are installed on one side and A6-A10 on the other. Several experiments are conducted with a sampling rate of 200Hz as this range is suitable to observe the sufficient number of modes within the expected narrowband low frequency range and as the amount of data, which needs to be as long as possible in case of OMA, is reasonable to store (Figure 42-A). The bridge is tested under operational conditions where a group of people walk over with a certain pace of their preference. This way, multiple harmonics are introduced to the system within the same band.



Figure 42 A: A perspective view from the footbridge and the data collection setup; B: The footbridge under the uncoordinated walking excitation of a group

### Findings

In Figure 43, the decomposition of signal for the channels 1, 5, 6 and 9 are given. As in the stadium example, the first extraction presents two mode mixing issues. Application of CEEMDAN eliminates this problem and provides mono-component signals. It is observed that, even though

the required mode is extracted successfully, sometimes it may still have the remaining artefacts of the signal that it is separated from. For instance,  $c_{16}$  set of IMFs has small peaks around the main lobe of the frequency signal which has not been efficiently separated by any means. However, intrinsic correlation relation between channels is at an acceptable level which makes it a mono-component source. Taking both the laboratory and field applications into consideration, from all the experiments, it can be said that the separation gets harder in the high frequency band. Especially when the power of the signal is low in the high frequency band, or when there are two peaks with distinctive amplitudes.

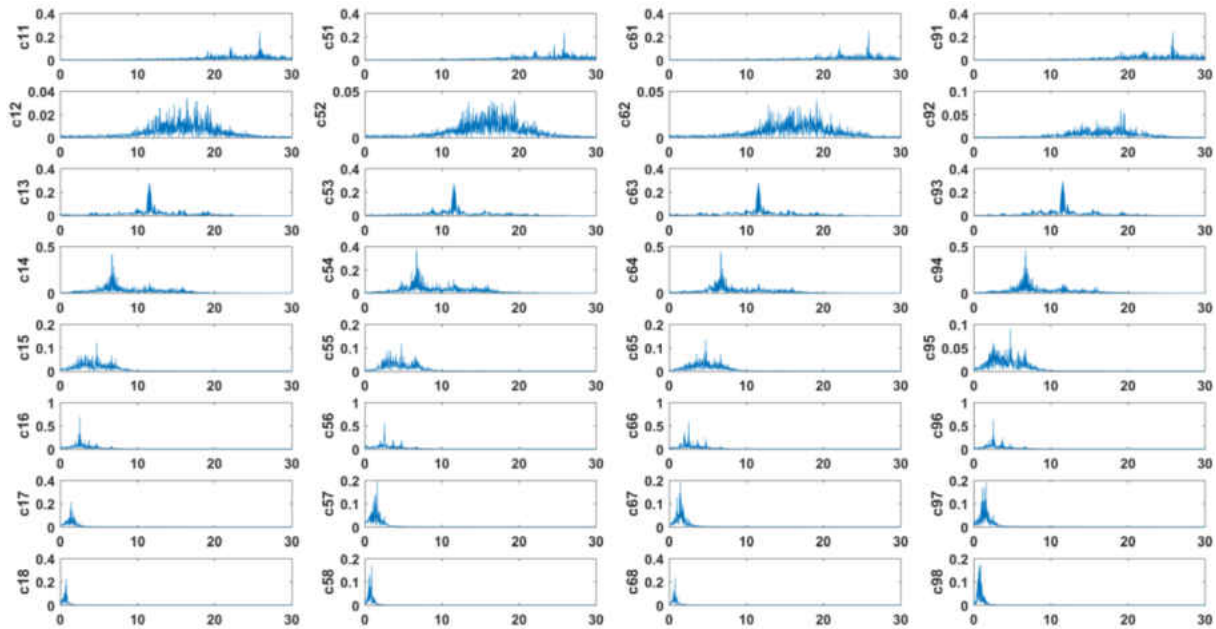
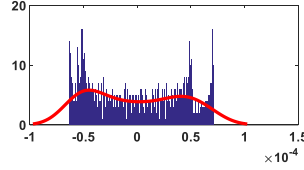
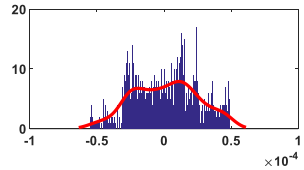
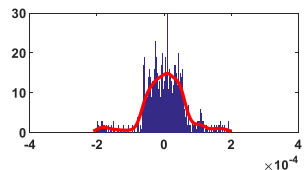
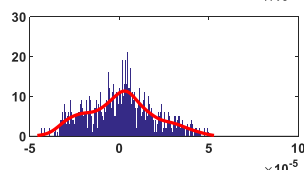
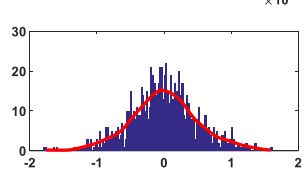
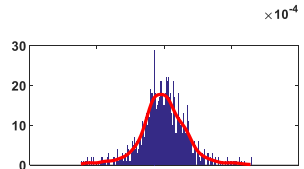
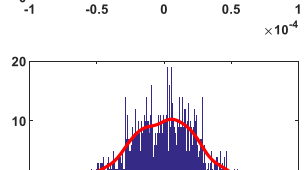
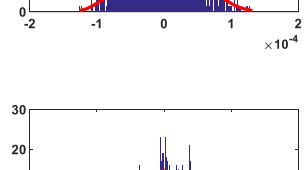


Figure 43 Extracted IMFs from the footbridge experiment

Table 6 is a summary of the findings from the footbridge test. The data set that belong to this identification study is captured under a random walk of a group of people. From the observations of PDF and kurtosis, the modes related to operational walking modes are successfully identified.

Table 6 A summary of the identification results for the footbridge

	Mode shapes			Probability Density Function
<b>Mode 1</b>	$\omega = 0.78$ $\kappa = 1.60$	$\zeta = 1.88$	$\sigma = 0.00$	
<b>Mode 2</b>	$\omega = 1.42$ $\kappa = 2.12$	$\zeta = 3.02$	$\sigma = 0.007$	
<b>Mode 3</b>	$\omega = 2.54$ $\kappa = 4.81$	$\zeta = 6.36$	$\sigma = 0.0032$	
<b>Mode 4</b>	$\omega = 4.74$ $\kappa = 2.76$	$\zeta = 0.01$	$\sigma = 0.0012$	
<b>Mode 5</b>	$\omega = 6.74$ $\kappa = 3.47$	$\zeta = 0.01$	$\sigma = 0.0011$	
<b>Mode 6</b>	$\omega = 11.59$ $\kappa = 2.60$	$\zeta = 0.01$	$\sigma = 0.0011$	
<b>Mode 7</b>	$\omega = 15.76$ $\kappa = 4.67$	$\zeta = 0.01$	$\sigma = 0.0011$	
<b>Mode 8</b>	$\omega = 25.88$ $\kappa = 3.55$	$\zeta = 0.01$	$\sigma = 0.0011$	

### Concluding Remarks

Flexible structures such as stadiums and footbridges are prone to narrowband excitations generated by occupants. Since the frequency response of the excitation and the fundamental dynamic response of the structure lie within the same band, there is a probability that their coupling may generate excessive vibration levels that may undermine the serviceability limits. Both the excitation and the response are of non-stationary nature that is not suitable for conventional time and frequency based analyses. In this regard, an investigation on the use of multivariate empirical mode decomposition (MEMD) for human-structure interaction problem is presented. The method uses a noise assisted version of the MEMD along with an adaptive projection algorithm to extract mono-component intrinsic mode functions (IMFs); to reduce mode misalignment and mixing and to account for power imbalances among channels as well as benefiting from correlations at an intrinsic level. The time-frequency representation of the response is provided by incorporating Hilbert-Huang spectrum (HHS). By utilizing HHS, the instantaneous changes in the energy, frequency, phase, and amplitude are realized as well as nonlinearities. The method is then expanded to structural identification relying on operational data. The performance of the application along with its limitations are reported in light of several examples conducted on a laboratory grandstand as well as on a real-life stadium and a footbridge.

## **CHAPTER FOUR: COMPUTER VISION BASED HUMAN COMFORT ASSESSMENT OF STADIA**

### Introduction

The current well known and widely used assessment methodologies for vibration level measurements are [30]–[32]. These standards were originally developed to evaluate human exposure to vibrations caused by operation of machinery and vehicles, but the same procedures are accepted to be applicable to civil engineering structures as well. The assessment measures used in these standards, such as root mean square (RMS), running RMS, maximum transient vibration value (MTVV), fourth power vibration dose value (VDV) or root mean quad (RMQ), have slight differences in their calculations of measurement directions, subjects' posture, application of frequency weightings, etc. Detailed information on the application of these measures have already been given in the review study by [1] mentioned above.

The research in the last decade focuses on the application of health, perception, motion sickness and comfort classification measures for sporting events [33], [33]–[35], concerts [36], [37] or for a long term monitoring [38]–[41]. [42] utilizes a psychophysical experimental method, called subjective scaling to study occupants' comfort and perception levels, while either sitting or standing. [43] studied the often-confused relationship between human vibration-perception and comfort levels using a controlled occupied grandstand that is gradually excited with different RMS powered sine wave vibrations from 2-6 Hz. The subjects are asked to choose their subjective vibration-perception and comfort levels from a bank of provided text descriptors. Their responses are compared with frequency weighted acceleration of two particular standards [32], [44]. Following the same experimental psychophysical methodology, [42] proposes a new approach for

perception assessment that considers the relation between human comfort and either the root mean square (RMS) of the normalized ground reaction forces (GRF) time history, or the normalized foot point acceleration time history [45]. The idea is that the GRFs obtained with stationary measurements are different from those of a moving grandstand [3].

Although the weighting of acceleration record seemed to favor the calculation of primary assessment measure (RMS), the method's outcomes are not drastically different from those of other methods. Reported RMS values are likely to vary within the time window that they are calculated; unfortunately, it is still unknown how long the duration should be. Although the evaluation via MTVV (derived from running RMS) is independent from duration and is mostly the case for grandstands considering the excessive vibration exceeding crest factor (CF) threshold, the information on the event causing the extreme values cannot be extracted. VDV and RMQ calculations experience the same problems. These alternative measures have not been given specific limits in the standards. However, VDV measures of perception can be made referring to a scale given in previous studies, which has proven to be the most reliable method among the others so far. In most cases, measures of perception or human discomfort levels from the measurement scale do not match with the actual, observed behavior of the occupants; raising questions of its appropriateness for application on grandstands.

Of all the preceding research, the main point of discussion is on the applicability and compatibility of the operating machinery based standards for the grandstand serviceability problem; as the excitation type have different inherence compared to machinery based vibrations.

### Calculation of Human Comfort Indices

In scope of this part of the dissertation, the procedures given in ISO 2631-1 are followed for the assessment of comfort levels. Although there are other standards for obtaining human comfort levels in literature, based on the reasonable results of previous studies, ISO 2631-1 is chosen. For this standard to be applicable, vibration should be measured in compliance with basicentric coordinate systems and placement of transducers should be orthogonal to each other. Vibration levels measured in this study are in “z” (vertical axes) direction as comfort levels along this direction are often more dominant and easy to measure for stadia.

Prior to the calculation of comfort indices, vibration records are filtered in the frequency domain with prescribed filtering weights categorized under different clauses as health, human comfort and perception and motion sickness Table 7.

Table 7 Guide for the application of frequency-weighting curves for principal weightings

<b>Frequency weighting</b>	<b>Health</b>	<b>Comfort</b>	<b>Perception</b>	<b>Motion sickness</b>
$W_k$	z-axis, seat surface	z-axis, seat surface z-axis, standing vertical recumbent (except head) x-, y-, z-axes, feet (sitting)	z-axis, seat surface z-axis, standing vertical recumbent (except head)	-
$W_d$	x-axis, seat surface y-axis, seat surface	x-axis, seat surface y-axis, seat surface x-, y- axes, standing horizontal recumbent y-, z-axes, seat-back	x-axis, seat surface y-axis, seat surface x-, y- axes, standing horizontal recumbent	-
$W_f$	-	-	-	vertical

Once the decision is made on the type of weighting - $W_k$  in this study-, frequency filter is designed with respect to the parameters shown in Table 8. Multiplication of each applied filtering gives the total weighting function to be applied on the frequency domain data:

$$H(p) = H_h(p)H_l(p)H_t(p)H_s(p) \quad (50)$$

Table 8 Parameters of the transfer functions of the principal frequency weightings

Weighting	Band-Limiting		Acceleration-velocity transition			Upward step			
	f <sub>1</sub>	f <sub>2</sub>	f <sub>3</sub>	f <sub>4</sub>	Q <sub>4</sub>	f <sub>5</sub>	Q <sub>5</sub>	f <sub>6</sub>	Q <sub>6</sub>
W <sub>k</sub>	0.40	100	12.50	12.50	0.63	2.37	0.91	3.35	0.91
W <sub>d</sub>	0.40	100	2	2	0.63	∞	-	∞	-
W <sub>f</sub>	0.08	0.63	∞	0.25	0.86	0.0625	0.80	0.10	0.80

Equation 50 shows a hybrid design comprised of high, low, bandpass filters and its illustration can be seen in Figure 44, along with its counterpart shown in ISO. This weighting is incorporated to account for the 5-8 Hz frequency range that the human body is deemed to be more susceptible.

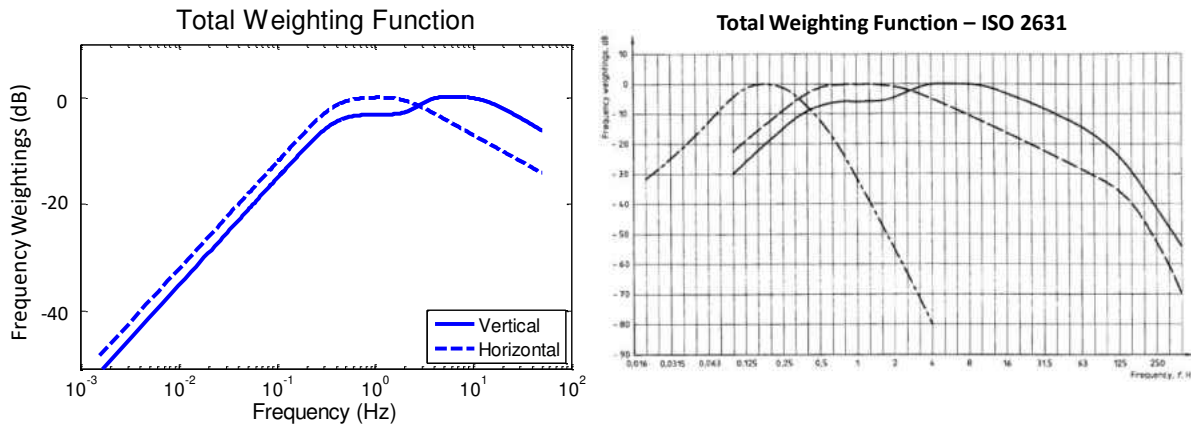


Figure 44 Architectural and structural details of a stadium as a demonstration of their slender nature

The next step is the computation of comfort indices. Two most commonly used and well-known indices namely RMS and VDV are incorporated. For a discrete time signal, RMS is calculated over the weighted time domain as follows:

$$a_{rms} = \left( \frac{1}{N} \sum_{i=1}^N a_i^2 \right)^{1/2} \quad (51)$$

where  $a_i$  is the discrete magnitude of the vibration and  $N$  is the number of samples. VDV is deemed to be more sensitive to transient accelerations since it is calculated over the fourth power of the vibration record:

$$VDV = \left( \frac{1}{f_s} \sum_{i=1}^N a_i^4 \right)^{1/4} \quad (52)$$

where  $f_s$  is the sampling rate of the vibration record and  $N$  is the number of samples. Calculated RMS values can be compared with the comfort scale in ISO guidance (Table 9). As to VDV, there is no comfort scale pointed out in the guideline but several previously suggested scales in the literature can be used. The justification on the comfort levels that are given in ISO guidance is unclear whereas VDV scale is based on limited number of studies. However, these measure are just going to be used to be used as a means of comparison.

Table 9 RMS Values and corresponding comfort levels (ISO 1997)

RMS Level (m/s <sup>2</sup> )	RMS Level (%g)	Comfort Level
<0.315	<3.2	Not Uncomfortable
0.315-0.63	3.2-6.4	A little Uncomfortable
0.5-1	5.1-10.2	Fairly Uncomfortable
0.8-1.6	8.2-16.3	Uncomfortable
1.25-2.5	12.7-25.5	Very Uncomfortable
>2	>20.4	Extremely Uncomfortable

Table 10 RMS Values and corresponding comfort levels [141]

RMS Level (m/s <sup>2</sup> )	RMS Level (%g)	Comfort Level
<0.315	<5	Reasonable for passive
0.315-0.63	5-18	Disturbing
0.5-1	18-35	Unacceptable
0.8-1.6	>35	Probably causing panic

Table 10 is an improved version of the comfort levels after the observation of [141]. The improvements should be continuously made so as to create a statistical and more accurate perception judgement.

Similarly, Table 11 shows and improved assessment levels that is put forward by [142]. This scale makes a distinction between concert and football events as the psychological state of the humans regarding the environment may heavily influence their judgement.

Table 11 VDV Values and corresponding comfort levels [142]

<b>VDV (m/s<sup>1.75</sup>) - Concert</b>	<b>VDV (m/s<sup>1.75</sup>) -</b>	<b>Comfort Level</b>
<0.66	<0.37	Reasonable for passive
0.66-2.38	0.37-1.32	Disturbing
2.38-4.64	1.32-2.58	Unacceptable
>4.64	>2.58	Probably causing panic

The most recent study that was carried out by [41] suggesting modified comfort levels. Modification is established based on the linear relationship between the peak acceleration and the VDV. According to the real events presented in the paper, the modified comfort assessment chart seems to yield better results. Comfort assessments made within this study are based upon this modified scale in Table 12.

Table 12 RMS & VDV Values and corresponding comfort levels [41]

<b>RMS (m/s<sup>2</sup>)</b>	<b>VDV (m/s<sup>1.75</sup>)</b>	<b>Comfort Level</b>
<0.49	<1.4	Reasonable for passive
0.49-1.77	1.4-4.8	Disturbing
1.77-3.43	4.8-9.3	Unacceptable
>3.43	>9.3	Probably causing panic

### Computer Vision Based Displacement Measurement

Displacement is a critical indicator to evaluate the structural response under human load and also it can be convert to load index to assess the structural loading condition. In this study, a computer vision based displacement measurement method is used as an alternative to accelerometer based comfort measurements. Figure 45 illustrates the procedure for the proposed method. The first step is camera calibration, which calculates the relationship between the image and the real world, and obtain the scale ratio between the actual spatial coordinates and the image pixel coordinates.

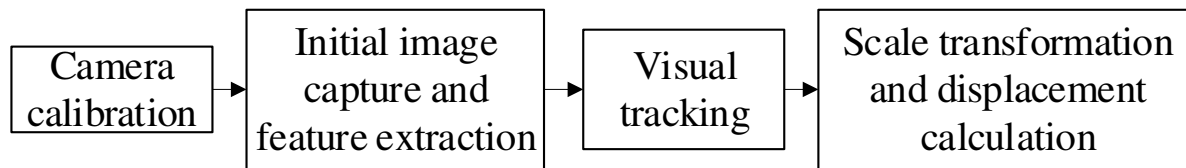


Figure 45 Procedure for vision-based displacement measurement

There are many different methods to carry out camera calibration for the application of vision-based displacement measurements [51], [143]–[152]. In this study the scale ratio introduced in [144] is used to convert the motion in image to the real world. The second step is to capture an initial image of the regions monitored on the structure, from which the initial pixel coordinates of these regions are obtained. Generally, such regions encompass areas of the structure with visible surface textures to establish a vibration measurement point. In this study, Speeded-Up Robust Features (SURF) [153] are chosen to be the visual trackers, as illustrated in Figure 46a.

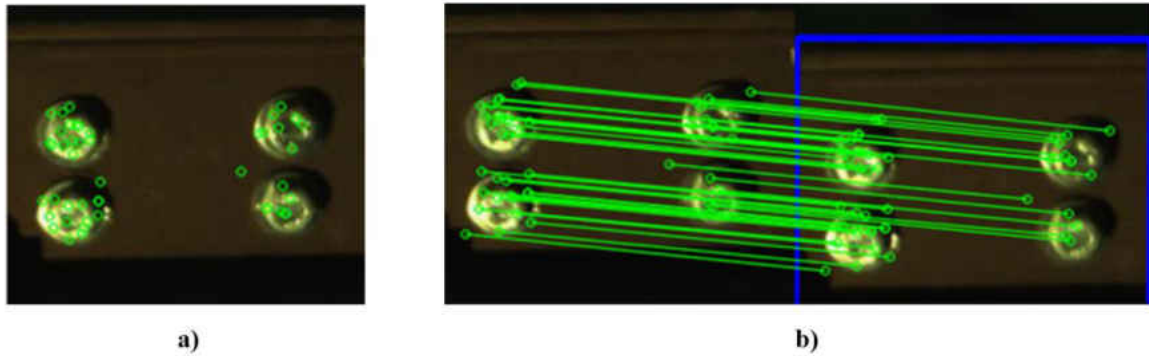


Figure 46 SURF feature and Lucas-Kanade tracking: a) extracted SURF features; b) Feature tracking using Lucas-Kanade tracking algorithm

In the third step, the original image and succeeding images captured by the camera are continuously tracked. The Lucas-Kanade algorithm [57] is used to calculate the optical flow and execute the visual tracking task. Through visual tracking, the virtual markers from the original image are located in each successive image (Figure 46b). Displacements are obtained in pixel coordinates by subtracting the location of the original coordinates in images from the coordinate locations of the most recent monitoring regions. The actual displacements of each selected region of the image which represents the measure target are obtained, by multiplying the average displacements at the feature points in each selected region in pixel coordinates with the scale ratio calculated during the first step. Lucas-Kanade algorithm calculates the sparse optical flow and assures that only the displacements at the feature points are obtained. The method is good for tracking small number of objects -in this study multi-point displacement measurement- and tracking sparsely distributed people. As the number of people increases towards forming a crowd, the full field dense optical flow calculation is needed where each pixel might represent one person. As a result, when crowd tracking is of concern, Farneback algorithm [58], [59], [68] is employed

to calculate the optical flow of each pixel in the image and finally the optical flow of each pixel is converted to the practical displacement in real world.

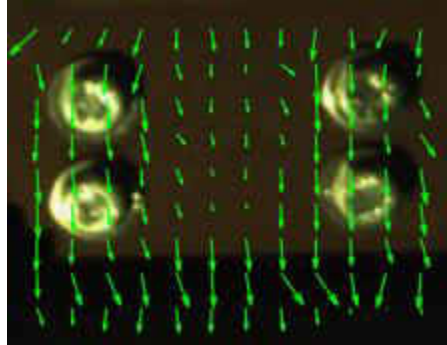


Figure 47 A demonstration of full field dense optical flow using Farneback algorithm

### Experimental Studies

To test the applicability of the proposed method, the flexible grandstand setup described in chapter 2 is used. Node number 2 that is seen in Figure 28 is selected to track. Five different cases are arranged to see the change in comfort levels. Table 13 summarizes the test scenarios.

Table 13 Test scenarios for the measurement of comfort levels

<b>Test Case</b>	<b>Frequency</b>	<b>Win/Lose</b>
Case 1	1.5 Hz	Jump
Case 2	2 Hz	Jump
Case 3	2.34 Hz	Zombie Nation Song
Case 4	2.5 Hz	Jump
Case 5	3 Hz	Jump

The motion of the structural node is tracked as seen in Figure 47 along with the subject standing on that node. Figure 48 shows the comparison between the two displacement measurements that are captured with the camera and the displacement sensor. Figure 49 is the acceleration record by taking the second numerical derivative of the same displacement record. Both figures show great correlation and almost an exact match. Even from this observation it can

be inferred that the same comfort measures are expected to be found. The comfort measures are firstly applied on the accelerometer records and subsequently the displacement acquired from the camera for the same node. Lastly, the same comfort measures are calculated using the normalized force record of the subject jumping over the node 2. The force record used here are also the same records presented in Chapter 2 for the same test.

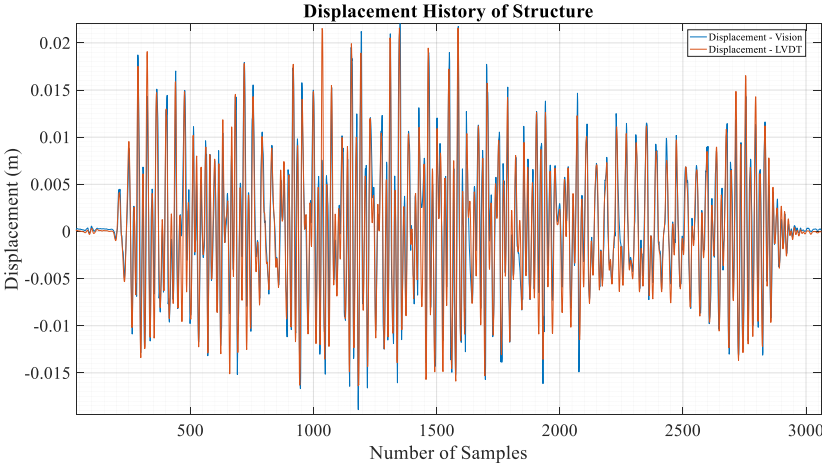


Figure 48 Comparison of the displacement records between the camera and the displacement sensor

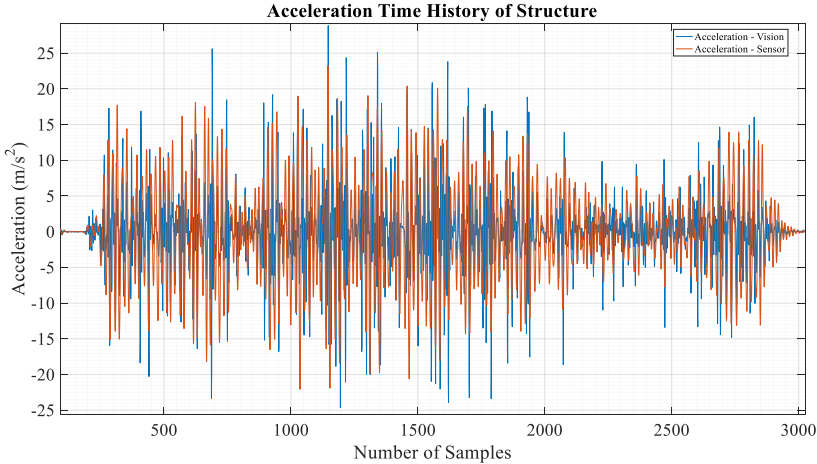


Figure 49 Comparison of the acceleration records between the camera and the displacement sensor

Table 14 and Table 15 show that except Case 1, comfort measures are increasingly disturbing as the jumping frequency increases. As it is pointed out earlier, the aim here is not to critique the accuracy of the levels but to be able to acquire the same levels by the use of computer vision. The direct acceleration records and camera recordings show almost the same levels. Besides, the use of computer vision based estimation also provides an additional information about displacement. Therefore, some displacement measures can also be defined and incorporated into the comfort assessment. The RMS and VDV values calculated from normalized ground reaction forces seem to indicate the comfort levels better because of the fact that these levels comply well with the statements of the jumping subject at node 2 as to how they feel.

Table 14 Comparison of the Evaluation of Each Case Based on RMS Acceleration for the grandstand

	Mx. Disp. (mm)	RMS (%g)					
		Sensor	Perception	Camera	Perception	Camera-Jumper	Perception
Case 1	9.80	2.34	Reasonable	2.47	Reasonable	0.46	Reasonable
Case 2	15.10	3.78	Reasonable	3.82	Reasonable	0.59	Reasonable
Case 3	16.02	3.86	Reasonable	3.92	Reasonable	0.63	Reasonable
Case 4	20.00	7.24	Disturbing	7.20	Disturbing	1.23	Reasonable
Case 5	21.05	7.27	Disturbing	7.54	Disturbing	0.74	Reasonable

Table 15 Comparison of the Evaluation of Each Case Based on VDV Perception Ranges for the grandstand

	VDV (m/s <sup>1.75</sup> )					
	Sensor	Perception	Camera	Perception	Camera-Jumper	Perception
Case 1	8.02	Panic	8.14	Panic	1.40	Reasonable
Case 2	12.03	Panic	12.22	Panic	1.70	Disturbing
Case 3	13.5	Panic	13.7	Panic	1.87	Disturbing
Case 4	21.68	Panic	21.94	Panic	4.55	Disturbing
Case 5	21.37	Panic	22.59	Panic	2.10	Disturbing

After acquiring successful results in laboratory, the stadium described in the previous sections is tested. Figure 50 shows two beams with different stiffness and almost at the same location under the lively audience. Displacement gauges are placed with the help of tripods and camera recordings for both locations. In the closest possible vicinity of displacement sensors, accelerometers are attached to confirm and compare the results.



Figure 50 Two structural members monitored for human comfort

The abbreviation of event and location seen in Table 16 stands for song (S) and target (T). For instance, S1T1 indicates the results from target 1 as the “Zombie Nation” song is played. Table 16 and Table 17 shows the results acquired from these measurements. There is a significant deflection difference between the members since they have different bending stiffness. This is an indication that the comfort measures can show different values even if they are taken from almost the same vicinity. On the other hand, RMS and VDV values are almost the same for both the camera and the physical sensor.

Table 16 Comparison of the Evaluation of Each Case Based on RMS Acceleration for the stadium

Event & Location	Mx. Disp. (mm)	Sensor	Perception	Camera	Perception
S1T1	2.08	0.02	Reasonable	0.01	Reasonable
S1T2	3.83	0.02	Reasonable	0.02	Reasonable
S2T1	2.86	0.03	Reasonable	0.03	Reasonable
S2T2	8.6	0.08	Reasonable	0.08	Reasonable

Table 17 Comparison of the Evaluation of Each Case Based on VDV Perception Ranges for the stadium

<b>Event &amp; Location</b>	<b>Sensor</b>	<b>Perception</b>	<b>Camera</b>	<b>Perception</b>
S1T1	0.09	Reasonable	0.08	Reasonable
S1T2	0.09	Reasonable	0.08	Reasonable
S2T1	0.11	Reasonable	0.10	Reasonable
S2T2	0.29	Reasonable	0.29	Reasonable

### Concluding Remarks

In this chapter, a new measurement method for human comfort assessment levels for stadia is proposed. The method is based on a specific computer vision and image processing algorithm called optical flow. The motion of both the structure and lively individuals can be tracked and well-known human comfort indices as root mean square (RMS) and vibration dose value (VDV) can be computed accordingly. The implementation is carried out using simple off-the-shelf cameras and the results are compared with conventional accelerometers. The analyses from tracking structural elements return almost the same results as accelerometers. As to the implementation of the same method on the individuals, the same indices are applied on the normalized ground reaction forces (GRFs) generated by tracking the motion of individuals. The magnitude of indices turns out much less than that of structure and seem to be reflecting the comfort levels more realistic. Along with the comfort indices calculated, one additional information is also given in terms of contactless displacement. For reasons such as perception levels can change from person to person, they are dependent on the type of events and also their magnitudes may not reflect the real situation due to the stiffness differences of the members, this new evaluation can become quite useful as a possible replacement in place of comfort indices. Instead of human comfort levels, allowable displacement of individual critical members can be monitored.

## CHAPTER FIVE: CONCLUSIONS

For the load quantification of individuals and crowd, two alternative load time history measurement techniques using advanced computer vision algorithms along with their applications in both laboratory and real life are introduced. The laboratory tests are carried out on a stiff force platform along with a grandstand simulator that could be set up in flexible and stiff configurations. The force measurements from conventional sensors and camera show acceptable match with more than 95% correlation as long as the structures is stiff and dynamic effects are not significant. It is evident to state that vision based methods are quite a good alternative for conventional methods. As the structure goes into flexible state to the point where dynamic magnification becomes prominent, the harmonics of the loading may be coupled with the resonant frequencies of the structure and differences start to emerge especially in amplitude. However, correlation is still high and the overall morphology is reasonable. The literature states that the force patterns on flexible structures are distorted and may be unreliable. The measurement series conducted in this study may be a significant example of such cases. The structural shape and the interaction of the supports with the load cells are also thought to influence this distortion in flexible setup. The performance of the vision based methods on the stiff simulator setup and the comparison of FE results (utilizing forces from camera measurements) with conventional sensors indicate that computer vision methods could be as reliable of an alternative as to conventional methods and may be even more so for flexible structures. However, more research to eliminate other possibilities by taking an issue by issue approach are needed to fully support this claim.

The results of a sample field study at a stadium hosting a fairly large crowd is also provided. The monitored section is not a typical flexible cantilever section and it resembles of the stiff setup

in the laboratory. The vibration level acquired by the comparison of FEM and accelerometers is a good match in the first narrowband frequency but not so much as to further harmonics. Although the accuracy is not quite as good as of the laboratory, it is evident that the same accuracy levels could be achieved if the methods are to be improved. More collaborative research needs to be conducted by taking advantage of computer vision discipline as crowd tracking stands as a challenging and active research interest therein. There are issues such as illumination changes, occlusion, etc. to be resolved. Besides, it should also be noted that each problem has its specific difficulties and these improvements on algorithms should be made with that specific problem oriented for better accuracy.

In the era of computer vision and artificial intelligence, structural engineers start using more of the useful tools that computer and data science are to offer. There are now many applications of such methods for local and global monitoring. This study along with few others in literature start shifting that focus by reflecting the same idea on human structure interaction. There are now successful synthetic load time history creation methods for individuals. In order for those to be implemented on crowd load modeling, successful real measurements need to be done. The use of computer vision methods can free researchers from limited laboratory conditions and pave the way for creating accurate databases of real, large crowds to be used for robust serviceability design. Utilization of these algorithms can further be expanded to an integrated camera based full scale monitoring contactless framework that could monitor both crowd and structure. Such a framework can provide real time condition assessment of the structure along with the human comfort assessment which is another research area that is left vastly untouched. The future work of the authors includes making improvements in all these areas.

For a specific problem of structural engineering when human-structure interaction is present on flexible structures and significantly alters dynamic behavior, an adaptive data-driven time history analysis is presented with laboratory and field applications. The method consists of set of algorithms based on NA-APIT-MEMD and its expansion to structural identification under operational conditions.

As to the utilization of the algorithm, in almost all the experiments, NA-APIT-MEMD algorithm is successful in aligning the modes of multivariate signals. On the other hand, although the mixing issue is reduced, it is not completely eliminated. When there are closely spaced modes ( $<1\text{Hz}$ ), consecutive peaks with significant power difference and weakly excited modes within the higher frequency band where noise is more dominant, the mode mixing issue seems to be more prevalent. If the modes are mixed but aligned, NA-MEMD can iteratively be applied across multiple channels whereas for other cases such as separating closely spaced modes, the CEEMDAN algorithm can be implemented. It is seen that the convenient selection of power for additional independent Gaussian white noise channels is 2-5% of the processed signal as it is also indicated in the literature. The selection of condensation factor  $\alpha$  is generally made between 0.3-0.5. The results seem to be worse below or over this range mentioned here.

As to the adaptation for modal analysis, the method is easy and extremely convenient for structures where the excitation is non-stationary, the wave forms deviate significantly from sinusoidal form and when the local nonlinearities are of concern. As long as the extracted IMFs comply with the rule of being mono-component, modal parameters can successfully be extracted as they are orthogonal vectors. By incorporating the HHT and its HHS representation, the identification can be made in terms of the modulated amplitude and the associated instantaneous

frequencies. This representation renders the realization of intra personal nature of the human excitation, frequency drifts of the structural modes and their interaction which are named after inter or intra wave modulations. These changes when realized over time, can give valuable information such as the detection of where the most of the energy resides, the condition and time when the amplitudes change, the existence of anomalies and either transient or steady state characteristics of the response. or shapes can be successful in understanding and tracking the temporal changes as well as identifying the system in question.

For the human comfort assessment, visual tracking procedure explained in Chapter 2 is applied on both the structure and the jumping individuals. The comfort levels acquired from the camera measurements correlate well with accelerations records. Besides, in addition to the computation of vibration acceptability measures, the specific displacement information of critical members are also acquired which can be compared with allowable displacement levels as an alternative to comfort indices. On the other hand, a possible comfort measurement by tracking the passive or active audience is also proposed by means of gravity normalized reaction forces. When compared with current comfort scales, more reasonable perception levels are achieved. However, new and better scales can be defined by conducting more tests and surveys with groups varying in different age, demographics, etc. This sort of comfort level monitoring methodology can be implemented in stadiums to track both the crowd and the structure simultaneously so that events that are likely to create panic could be prevented.

## LIST OF REFERENCES

- [1] C. A. Jones, P. Reynolds, and A. Pavic, "Vibration serviceability of stadia structures subjected to dynamic crowd loads: A literature review," *J. Sound Vib.*, vol. 330, no. 8, pp. 1531–1566, Apr. 2011.
- [2] J. Sim, A. Blakeborough, M. S. Williams, and G. Parkhouse, "Statistical Model of Crowd Jumping Loads," *J. Struct. Eng.*, vol. 134, no. 12, pp. 1852–1861, Dec. 2008.
- [3] S. Yao, J. R. Wright, A. Pavic, and P. Reynolds, "Experimental study of human-induced dynamic forces due to jumping on a perceptibly moving structure," *J. Sound Vib.*, vol. 296, no. 1–2, pp. 150–165, Sep. 2006.
- [4] Canadian Commission on Building and Fire Codes, "Canadian Commission on Building and Fire Codes, User's guide--NBC 2005 Structural Commentaries (Part 4 of Division B)," 2006.
- [5] ISO/TC/98/SC 2, "ISO 10137:2007, Bases for design of structures - Serviceability of buildings and walkways against vibrations," 2007.
- [6] IStructE/DCLG/DCMS Joint Working Group, "Dynamic performance requirements for permanent grandstands subject to crowd action," 2008.
- [7] A. J. Comer, A. Blakeborough, and M. S. Williams, "Rhythmic crowd bobbing on a grandstand simulator," *J. Sound Vib.*, vol. 332, no. 2, pp. 442–454, Jan. 2013.
- [8] A. Comer, A. Blakeborough, and M. S. Williams, "Grandstand Simulator for Dynamic Human-Structure Interaction Experiments," *Exp. Mech.*, vol. 50, no. 6, pp. 825–834, Jul. 2010.
- [9] V. Racic, J. M. W. Brownjohn, and A. Pavic, "Measurement and Application of Bouncing and Jumping Loads Using Motion Tracking Technology," 2011, pp. 201–210.
- [10] V. Racic, J. M. W. Brownjohn, and A. Pavic, "Novel Experimental Characterisation of Human-induced Loading," in *Proceedings of the 27th International Modal Analysis Conference*, 2009.
- [11] V. Racic, J. M. W. Brownjohn, and A. Pavic, "Reproduction and application of human bouncing and jumping forces from visual marker data," *J. Sound Vib.*, vol. 329, no. 16, pp. 3397–3416, Aug. 2010.
- [12] A. Caprioli, S. Manzoni, and E. Zappa, "People-induced Vibrations of Civil Structures: Image-based Measurement of Crowd Motion," *Exp. Tech.*, vol. 35, no. 3, pp. 71–79, May 2011.

- [13] A. Caprioli, S. Manzoni, and E. Zappa, "Crowd Motion Measurement Based on Image Processing," in *Proceedings of the 26th International Modal Analysis Conference*, 2008.
- [14] A. Caprioli, A. Cigada, R. Sala, and E. Zappa, "Image based measurement of a stadium excitation due to jumping people," in *Proceedings of the 24th International Modal Analysis Conference*, 2006.
- [15] A. Cigada and E. Zappa, "Analysis of Jumping Crowd on Stadium Stands Through Image Processing to Security Purposes," in *2006 IEEE International Workshop on Measurement Systems for Homeland Security, Contraband Detection and Personal Safety*, 2006, pp. 56–61.
- [16] F. Zheng, V. Racic, J. M. W. Brownjohn, M. T. Elliot, and A. Wing, "Vision-Based Tracking of Human Body Motion," 2014, pp. 171–174.
- [17] C. A. Jones, P. Reynolds, E. Zappa, S. Manzoni, and A. Cigada, "Verification of Crowd Dynamic Excitation Estimated from Image Processing Techniques," 2011, pp. 205–216.
- [18] P. Mazzoleni and E. Zappa, "Vision-based estimation of vertical dynamic loading induced by jumping and bobbing crowds on civil structures," *Mech. Syst. Signal Process.*, vol. 33, pp. 1–12, Nov. 2012.
- [19] D. E. Newland, *An introduction to random vibrations, spectral and wavelet analysis*. New York, 1993.
- [20] J. M. . Brownjohn, A. Pavic, and P. Omenzetter, "A spectral density approach for modelling continuous vertical forces on pedestrian structures due to walking," *Can. J. Civ. Eng.*, vol. 31, no. 1, pp. 65–77, Jan. 2004.
- [21] M. Kasperski and E. Agu, "Prediction of Crowd-induced Vibrations via Simulation," in *Proceedings of 23rd International Modal Analysis Conference - IMACXXIII*, 2005.
- [22] B. R. Ellis and T. Ji, "Loads generated by jumping crowds: Numerical modelling," *Struct. Eng.*, vol. 82, no. 17, pp. 35–40, 2004.
- [23] V. Racic and A. Pavic, "Stochastic approach to modelling of near-periodic jumping loads," *Mech. Syst. Signal Process.*, vol. 24, no. 8, pp. 3037–3059, Nov. 2010.
- [24] V. Racic and A. Pavic, "Mathematical model to generate near-periodic human jumping force signals," *Mech. Syst. Signal Process.*, vol. 24, no. 1, pp. 138–152, Jan. 2010.
- [25] V. Racic and A. Pavic, "Mathematical Model to Generate Asymmetric Pulses due to Human Jumping," *J. Eng. Mech.*, vol. 135, no. 10, pp. 1206–1211, Oct. 2009.
- [26] B. Peeters, H. Van der Auweraer, F. Vanhollebeke, and P. Guillaume, "Operational Modal

Analysis for Estimating the Dynamic Properties of a Stadium Structure during a Football Game,” *Shock Vib.*, vol. 14, no. 4, pp. 283–303, 2007.

- [27] M. Prasenjit, P. Reynolds, and A. Pavic, “Statistical Analysis of Online Response Data of a Stadium Structure,” in *Proceedings of the 23rd International Modal Analysis Conference*, 2005.
- [28] P. Reynolds, M. Prasenjit, and A. Pavic, “Use of Operational Modal Analysis on Empty and Occupied Stadia Structures,” in *Proceedings of the 1st International Operational Modal Analysis Conference (IOMAC)*, 2005.
- [29] C. A. Jones and P. Reynolds, “Finite Element Modelling and Updating of a Stadium Structure Using In-service Data,” in *Proceedings of the 27th International Modal Analysis Conference*, 2009.
- [30] ISO/TC 108/SC 4, “ISO 2631-1, Mechanical Vibration and Shock-Evaluation of Human Exposure to Whole-body Vibration. Part 1: General Requirements,” 1997.
- [31] ISO/TC 108/SC 4, “ISO2631-2, Mechanical Vibration and Shock-Evaluation of Human Exposure to Whole-body Vibration. Part 2: Vibration in Buildings (1Hz to 80 Hz),” 2003.
- [32] General Mechanical Engineering Committee, “BS 6841, Guide to measurement and evaluation of human exposure to whole-body mechanical vibration and repeated shock,” 1987.
- [33] F. N. Catbas, M. Gul, and H. O. Sazak, “Dynamic Testing and Analysis of a Football Stadium,” 2011, pp. 195–203.
- [34] N. Catbas, M. Gul, and H. O. Sazak, “Dynamic Response Monitoring and Correlation to Crowd Movement at a Football Stadium,” in *Proceedings of the 27th International Modal Analysis Conference*, 2009.
- [35] K. A. Salyards and L. M. Hanagan, “Analysis of Coordinated Crowd Vibration Levels In a Stadium Structure,” in *Proceedings of the 25th International Modal Analysis Conference*, 2007.
- [36] A. Caprioli and P. Reynolds, “Evaluation of Serviceability Assessment Measures for Different Stadia Structures and Different Live Concert Events,” in *Proceedings of the 25th International Modal Analysis Conference*, 2007.
- [37] K. A. Salyards, L. M. Hanagan, and M. W. Trethewey, “Comparing Vibration Serviceability Assessment Measures for Stadium Rock Concert Data,” in *Proceedings of the 24th International Modal Analysis Conference*, 2006.
- [38] A. Cappellini, R. Fagiani, and M. Vanali, “Serviceability Assessment of Two Different

- Stadium Grandstand During Different Events,” 2015, pp. 299–310.
- [39] A. Caprioli and M. Vanali, “Comparison of Different Serviceability Assessment Measures for Different Events Held in the G. Meazza Stadium in Milano,” in *Proceedings of the 27th International Modal Analysis Conference*, 2009.
- [40] A. Caprioli, M. Vanali, and A. Cigada, “One Year of Structural Health Monitoring of the Meazza Stadium in Milan: Analysis of the Collected Data,” in *Proceedings of the 27th International Modal Analysis Conference*, 2009.
- [41] K. A. Salyards and L. M. Hanagan, “Evaluation of Vibration Assessment Criteria and Their Application to Stadium Serviceability,” *J. Perform. Constr. Facil.*, vol. 24, no. 2, pp. 100–107, Apr. 2010.
- [42] S. P. Nhleko, M. S. Williams, and A. Blakeborough, “Vibration Perception and Comfort Levels for an Audience Occupying a Grandstand With Perceivable Motion,” in *Proceedings of the 27th International Modal Analysis Conference*, 2009.
- [43] A. J. Comer, A. Blakeborough, and M. S. Williams, “Human-structure interaction in cantilever grandstands-design of a section of a full scale raked grandstand,” in *25th International Modal Analysis Conference*, 2007.
- [44] General Mechanical Engineering Committee, “BS6472, Guide to Evaluation of Human Exposure to Vibration in Buildings (1 Hz to 80 Hz),” 1992.
- [45] S. P. Nhleko, A. Blakeborough, and M. S. Williams, “Ground Reaction Forces on Vibrating Structures,” in *Proceedings of the 27th International Modal Analysis Conference*, 2009.
- [46] C. A. Jones, P. Reynolds, and A. Pavic, “Vibration serviceability of stadia structures subjected to dynamic crowd loads: A literature review,” *J. Sound Vib.*, vol. 330, no. 8, pp. 1531–1566, 2011.
- [47] O. Celik, N. T. Do, O. Abdeljaber, M. Gul, O. Avci, and F. N. Catbas, “Recent Issues on Stadium Monitoring and Serviceability: A Review,” 2016, pp. 411–416.
- [48] F. N. Catbas, O. Celik, O. Avci, O. Abdeljaber, M. Gul, and N. T. Do, “Sensing and Monitoring for Stadium Structures: A Review of Recent Advances and a Forward Look,” *Front. Built Environ.*, vol. 3, Aug. 2017.
- [49] L. Georgiou, V. Racic, J. M. W. Brownjohn, and M. T. Elliot, “Coordination of Groups Jumping to Popular Music Beats,” 2015, pp. 283–288.
- [50] V. Racic and J. M. W. Brownjohn, “Stochastic model of near-periodic vertical loads due to humans walking,” *Adv. Eng. Informatics*, vol. 25, no. 2, pp. 259–275, Apr. 2011.

- [51] T. Khuc and F. N. Catbas, “Computer vision-based displacement and vibration monitoring without using physical target on structures,” *Struct. Infrastruct. Eng.*, vol. 13, no. 4, pp. 505–516, Apr. 2017.
- [52] T. Khuc and F. N. Catbas, “Completely contactless structural health monitoring of real-life structures using cameras and computer vision,” *Struct. Control Heal. Monit.*, vol. 24, no. 1, p. e1852, Jan. 2017.
- [53] A. Caprioli, S. Manzoni, and E. Zappa, “Crowd Motion Estimation by Means of a PIV Algorithm,” in *Proceedings of Eurodyn*, 2008.
- [54] X. Zheng and J. M. W. Brownjohn, “Modeling and simulation of human-floor system under vertical vibration,” 2001, pp. 513–520.
- [55] J. L. Barron, D. J. Fleet, and S. S. Beauchemin, “Performance of optical flow techniques,” *Int. J. Comput. Vis.*, vol. 12, no. 1, pp. 43–77, Feb. 1994.
- [56] S. S. Beauchemin and J. L. Barron, “The computation of optical flow,” *ACM Comput. Surv.*, vol. 27, no. 3, pp. 433–466, Sep. 1995.
- [57] B. D. Lucas and T. Kanade, “An Iterative Image Registration Technique with an Application to Stereo Vision,” in *Proceedings of the 7th International Joint Conference on Artificial Intelligence - Volume 2*, 1981, pp. 674–679.
- [58] G. Farneback, “Very high accuracy velocity estimation using orientation tensors, parametric motion, and simultaneous segmentation of the motion field,” in *Proceedings Eighth IEEE International Conference on Computer Vision. ICCV 2001*, 2001, vol. 1, pp. 171–177.
- [59] G. Farneäck, “Two-Frame Motion Estimation Based on Polynomial Expansion,” 2003, pp. 363–370.
- [60] A. Alahi, R. Ortiz, and P. Vandergheynst, “FREAK: Fast Retina Keypoint,” in *2012 IEEE Conference on Computer Vision and Pattern Recognition*, 2012, pp. 510–517.
- [61] H. Bay, A. Ess, T. Tuytelaars, and L. Van Gool, “Speeded-Up Robust Features (SURF),” *Comput. Vis. Image Underst.*, vol. 110, no. 3, pp. 346–359, Jun. 2008.
- [62] M. Calonder, V. Lepetit, C. Strecha, and P. Fua, “BRIEF: Binary Robust Independent Elementary Features,” 2010, pp. 778–792.
- [63] C. Harris, C. Harris, and M. Stephens, “A combined corner and edge detector,” in *In Proceedings of Fourth Alvey Vision Conference*, 1988, pp. 147--151.
- [64] D. G. Lowe, “Distinctive Image Features from Scale-Invariant Keypoints,” *Int. J. Comput. Vis.*, vol. 60, no. 2, pp. 91–110, Nov. 2004.

- [65] E. Rosten and T. Drummond, “Machine Learning for High-Speed Corner Detection,” 2006, pp. 430–443.
- [66] E. Rublee, V. Rabaud, K. Konolige, and G. Bradski, “ORB: An efficient alternative to SIFT or SURF,” in *2011 International Conference on Computer Vision*, 2011, pp. 2564–2571.
- [67] J. Shi and C. Tomasi, “Good features to track,” in *Proceedings of IEEE Conference on Computer Vision and Pattern Recognition CVPR-94*, 1994, pp. 593–600.
- [68] G. Farneback, “Fast and accurate motion estimation using orientation tensors and parametric motion models,” in *Proceedings 15th International Conference on Pattern Recognition. ICPR-2000*, 2000, vol. 1, pp. 135–139.
- [69] T. Wang, O. Celik, F. N. Catbas, and L. M. Zhang, “A frequency and spatial domain decomposition method for operational strain modal analysis and its application,” *Eng. Struct.*, vol. 114, pp. 104–112, May 2016.
- [70] T. Wang, O. Celik, and F. Catbas, “Damage detection of a bridge model based on operational dynamic strain measurements,” *Adv. Struct. Eng.*, vol. 19, no. 9, pp. 1379–1389, Sep. 2016.
- [71] F. N. Catbas, D. L. Brown, and A. E. Aktan, “Parameter Estimation for Multiple-Input Multiple-Output Modal Analysis of Large Structures,” *J. Eng. Mech.*, vol. 130, no. 8, pp. 921–930, Aug. 2004.
- [72] F. N. Catbas, O. Celik, O. Avci, O. Abdeljaber, and M. Gul, “Stadium Monitoring and Sensing : A Review of Recent Advances and A Forward Look,” *Front. Built Environ.*, pp. 1–29, 2017.
- [73] O. Celik *et al.*, “Issues, Codes and Basic Studies for Stadium Dynamics,” *Proc. Second Int. Conf. Infrastruct. Manag. Assess. Rehabil. Tech.*, 2016.
- [74] O. Celik, N. T. Do, O. Abdeljaber, M. Gul, O. Avci, and F. N. Catbas, “Recent Issues on Stadium Monitoring and Serviceability: A Review,” 2016.
- [75] B. Peeters, H. Van Der Auweraer, F. Vanhollebeke, and P. Guillaume, “Operational modal analysis for estimating the dynamic properties of a stadium structure during a football game,” *Shock Vib.*, vol. 14, no. 4, pp. 283–303, 2007.
- [76] B. Peeters, H. Van der Auweraer, F. Vanhollebeke, and P. Guillaume, “Operational Modal Analysis for Estimating the Dynamic Properties of a Stadium Structure during a Football Game,” *Shock Vib.*, vol. 14, no. 4, pp. 283–303, 2007.
- [77] C. a Jones and P. Reynolds, “Finite Element Modelling and Updating of a Stadium Structure using In-Service Data,” *Imac Xxvii*, 2009.

- [78] P. Reynolds, A. Pavic, and J. Carr, “Experimental dynamic analysis of the Kingston Communications Stadium,” *Struct. Eng.*, vol. 85, no. 8, pp. 33–39, 2007.
- [79] P. Reynolds, P. Mohanty, and A. Pavic, “Use of Operational Modal Analysis on Empty and Occupied Stadia Structures,” *1st Int. Oper. Modal Anal. Conf.*, pp. 26–27, 2005.
- [80] P. Reynolds and A. Pavic, “MODAL TESTING OF A SPORTS STADIUM,” pp. 1037–1043.
- [81] P. Mohanty, P. Reynolds, and A. Pavic, “Statistical Analysis of Online Response Data of a Stadium Structure,” *Imac 2005*, no. October, pp. 1–8, 2005.
- [82] F. Magalhães and Á. Cunha, “Explaining operational modal analysis with data from an arch bridge,” *Mech. Syst. Signal Process.*, vol. 25, no. 5, pp. 1431–1450, 2011.
- [83] G. F. Sirca and H. Adeli, “System identification in structural engineering,” *Sci. Iran.*, vol. 19, no. 6, pp. 1355–1364, 2012.
- [84] S. Nagarajaiah and B. Basu, “Output only modal identification and structural damage detection using time frequency & wavelet techniques,” *Earthq. Eng. Eng. Vib.*, vol. 8, no. 4, pp. 583–605, 2009.
- [85] S. R. Ibrahim and E. C. Mikulcik, “A method for direct identification of vibration parameters from the free response,” *Shock Vib. Bull.*, vol. 47, no. 4, pp. 183–196, 1977.
- [86] J.-N. JUANG and R. S. PAPPA, “An eigensystem realization algorithm for modal parameter identification and model reduction,” *J. Guid. Control. Dyn.*, vol. 8, no. 5, pp. 620–627, Sep. 1985.
- [87] P. Van Overschee and B. De Moor, “Subspace algorithms for the stochastic identification problem,” *Automatica*, vol. 29, no. 3, pp. 649–660, May 1993.
- [88] P. Van Overschee and B. De Moor, *Subspace Identification for Linear Systems*. Boston, MA: Springer US, 1996.
- [89] G. H. James III, T. G. Carne, and J. P. Lauffer, “The natural excitation technique (NExT) for modal parameter extraction from operating wind turbines,” Albuquerque, New Mexico, 1993.
- [90] S. R. Ibrahim, “Random Decrement Technique for Modal Identification of Structures,” *J. Spacecr. Rockets*, vol. 14, no. 11, pp. 696–700, Nov. 1977.
- [91] P. Guillaume, P. Verboven, and S. Vanlanduit, “Frequency-domain maximum likelihood identification of modal parameters with confidence intervals,” in *ISMA 23 The International Conference on Noise and Vibration Engineering*.
- [92] P. Guillaume, P. Verboven, S. Vanlanduit, H. Van Der Auweraer, and B. Peeters, “A poly-

- reference implementation of the least-squares complex frequency-domain estimator,” in *IMAC 21*, 2003, no. 2.
- [93] R. Brincker, L. Zhang, and P. Andersen, “Modal identification from ambient responses using frequency domain decomposition,” *Proceedings of SPIE - The International Society for Optical Engineering*, vol. 4062. 2000.
- [94] H. Van der Auweraer and J. Leuridan, “Multiple input orthogonal polynomial parameter estimation,” *Mech. Syst. Signal Process.*, vol. 1, no. 3, pp. 259–272, Jul. 1987.
- [95] B. Peeters, H. Van der Auweraer, P. Guillaume, and J. Leuridan, “The PolyMAX Frequency-Domain Method: A New Standard for Modal Parameter Estimation?,” *Shock Vib.*, vol. 11, no. 3–4, pp. 395–409, 2004.
- [96] W. Tong, Z. Lingmi, and T. Yukio, “An operational modal analysis method in frequency and spatial domain,” *Earthq. Eng. Eng. Vib.*, vol. 4, no. 2, pp. 295–300, 2005.
- [97] C. Y. Shih, Y. G. Tsuei, R. J. Allemang, and D. L. Brown, “Complex mode indication function and its applications to spatial domain parameter estimation,” *Mech. Syst. Signal Process.*, vol. 2, no. 4, pp. 367–377, Oct. 1988.
- [98] T. Wang, O. Celik, F. N. Catbas, and L. M. Zhang, “A frequency and spatial domain decomposition method for operational strain modal analysis and its application,” *Eng. Struct.*, vol. 114, pp. 104–112, May 2016.
- [99] T. Wang, O. Celik, and F. Catbas, “Damage detection of a bridge model based on operational dynamic strain measurements,” *Adv. Struct. Eng.*, vol. 19, no. 9, pp. 1379–1389, Sep. 2016.
- [100] A. Sadhu, S. Narasimhan, and J. Antoni, “A review of output-only structural mode identification literature employing blind source separation methods,” *Mech. Syst. Signal Process.*, vol. 94, pp. 415–431, 2017.
- [101] W. J. Staszewski and D. M. Wallace, “Wavelet-based Frequency Response Function for time-variant systems—An exploratory study,” *Mech. Syst. Signal Process.*, vol. 47, pp. 35–49, 2014.
- [102] A. Klepka and T. Uhl, “Identification of modal parameters of non-stationary systems with the use of wavelet based adaptive filtering,” *Mech. Syst. Signal Process.*, vol. 47, pp. 21–34, 2014.
- [103] X Xu, Z. Y. Shi, and Q. You, “Identification of linear time-varying systems using a wavelet-based state-space method,” *Mech. Syst. Signal Process.*, vol. 26, pp. 91–103, 2011.
- [104] K. Dziedziech, W. J. Staszewski, and T. Uhl, “Wavelet-based modal analysis for time-variant systems,” 2014.

- [105] A. Sadhu and S. Narasimhan, “A decentralized blind source separation algorithm for ambient modal identification in the presence of narrowband disturbances,” *Struct. Control Heal. Monit.*, vol. 21, no. 3, pp. 282–302, Mar. 2014.
- [106] A. Sadhu, A. Goldack, and S. Narasimhan, “Blind Modal Identification of a Pedestrian Bridge under Narrowband Disturbances.”
- [107] D. O’Donnell *et al.*, “Modelling and testing of a historic steel suspension footbridge in Ireland,” *Proc. Inst. Civ. Eng. - Bridg. Eng.*, no. January, pp. 1–17, 2017.
- [108] A. Sadhu, A. M. Asce, ; S Narasimhan, M. Asce, and A. Goldack, “Decentralized Modal Identification of a Pony Truss Pedestrian Bridge Using Wireless Sensors.”
- [109] J. F. Jimenez-Alonso, A. Saez, E. Caetano, and F. Magalhaes, “Vertical Crowd – Structure Interaction Model to Analyze the Change of the Modal Properties of a Footbridge,” *J. Bridg. Eng.*, vol. 21, no. 8, pp. 1–19, 2016.
- [110] S. Živanović, A. Pavić, and P. Reynolds, “Probability-based prediction of multi-mode vibration response to walking excitation,” *Eng. Struct.*, vol. 29, no. 6, pp. 942–954, 2007.
- [111] S. Živanović, A. Pavic, and P. Reynolds, “Modal testing and FE model tuning of a lively footbridge structure,” *Eng. Struct.*, vol. 28, no. 6, pp. 857–868, 2006.
- [112] A. Gheitasi, O. E. Ozbulut, S. Usmani, M. Alipour, and D. K. Harris, “Experimental and analytical vibration serviceability assessment of an in-service footbridge,” *Case Stud. Nondestruct. Test. Eval.*, vol. 6, pp. 79–88, 2016.
- [113] E. Shahabpoor, A. Pavic, V. Racic, and S. Zivanovic, “Effect of group walking traffic on dynamic properties of pedestrian structures,” *J. Sound Vib.*, vol. 387, pp. 207–225, 2017.
- [114] F. Venuti and L. Bruno, “Crowd-structure interaction in lively footbridges under synchronous lateral excitation: A literature review,” *Phys. Life Rev.*, vol. 6, no. 3, pp. 176–206, 2009.
- [115] S. Živanović, “Benchmark Footbridge for Vibration Serviceability Assessment under the Vertical Component of Pedestrian Load,” *J. Struct. Eng.*, vol. 138, no. 10, pp. 1193–1202, 2012.
- [116] N. Huang, Z. Shen, S. Long, M. Wu, and H. Shih, “The empirical mode decomposition and the Hilbert spectrum for nonlinear and non-stationary time series analysis,” *Proc. R. Soc. A-Mathematical Phys. Eng. Sci.*, vol. 454, no. 1971, pp. 903–995, 1998.
- [117] D. P. Mandic, N. ur Rehman, Z. Wu, and N. E. Huang, “Empirical Mode Decomposition-Based Time-Frequency Analysis of Multivariate Signals: The Power of Adaptive Data Analysis,” *IEEE Signal Process. Mag.*, vol. 30, no. 6, pp. 74–86, Nov. 2013.

- [118] G. Rilling, P. Flandrin, and P. Es, “On Empirical Mode Decomposition and Its Algorithms.”
- [119] N. E. Huang *et al.*, “A confidence limit for the empirical mode decomposition and Hilbert spectral analysis,” *Proc. R. Soc. A Math. Phys. Eng. Sci.*, vol. 459, no. 2037, pp. 2317–2345, 2003.
- [120] Z. Wu and N. E. Huang, “Ensemble Empirical Mode Decomposition: A Noise Assisted Data Analysis Method,” *Adv. Adapt. Data Anal.*, vol. 1, no. 1, pp. 1–41, 2009.
- [121] M. E. Torres, M. A. Colominas, G. Schlotthauer, and P. Flandrin, “A complete ensemble empirical mode decomposition with adaptive noise,” *ICASSP, IEEE Int. Conf. Acoust. Speech Signal Process. - Proc.*, pp. 4144–4147, 2011.
- [122] M. A. Colominas, G. Schlotthauer, and M. E. Torres, “Improved complete ensemble EMD: A suitable tool for biomedical signal processing,” *Biomed. Signal Process. Control*, vol. 14, no. 1, pp. 19–29, 2014.
- [123] T. Tanaka and D. P. Mandic, “Complex empirical mode decomposition,” *IEEE Signal Process. Lett.*, vol. 14, no. 2, pp. 101–104, 2007.
- [124] G. Rilling, P. Flandrin, P. Goncalves, and J. M. Lilly, “Bivariate Empirical Decomposition,” *IEEE Signal Process. Lett.*, vol. 14, no. 12, pp. 936–939, Feb. 2007.
- [125] M. U. Bin Altaf, T. Gautama, T. Tanaka, and D. P. Mandic, “Rotation Invariant Complex Empirical Mode Decomposition,” in *2007 IEEE International Conference on Acoustics, Speech and Signal Processing - ICASSP '07*, 2007, p. III-1009-III-1012.
- [126] N. ur Rehman and D. P. Mandic, “Empirical Mode Decomposition for Trivariate Signals,” *IEEE Trans. Signal Process.*, vol. 58, no. 3, pp. 1059–1068, Mar. 2010.
- [127] N. Rehman and D. P. Mandic, “Multivariate empirical mode decomposition,” *Proc. R. Soc. A*, vol. 466, pp. 1291–1302, 2010.
- [128] J. Cui, W. Freeden, and S. J. C. Sci, “Equidistribution on The Sphere,” vol. 18, no. 2, pp. 595–609, 1997.
- [129] D. Looney, A. Hemakom, and D. P. Mandic, “Intrinsic multi-scale analysis: a multi-variate empirical mode decomposition framework,” *Proc. R. Soc. A Math. Phys. Eng. Sci.*, vol. 471, no. 2173, pp. 20140709–20140709, Dec. 2014.
- [130] N. ur Rehman and D. P. Mandic, “Filter Bank Property of Multivariate Empirical Mode Decomposition,” *IEEE Trans. SIGNAL Process. IEEE Trans. Signal Process. IEEE Trans. Signal Process. IEICE Tech. Rep. Signal Process. IEEE Trans. Signal Process. Stat. Neerl.*, vol. 5947, no. 4, pp. 584–587, 2006.

- [131] D. P. Mandic, A. Hemakom, V. Goverdovsky, and D. Looney, “Adaptive-projection intrinsically transformed multivariate empirical mode decomposition in cooperative brain–computer interface applications.”
- [132] A. Sadhu, “An integrated multivariate empirical mode decomposition method towards modal identification of structures,” *J. Vib. Control*, Dec. 2015.
- [133] K. Motte, W. Weijtjens, C. Devriendt, and P. Guillaume, “Operational Modal Analysis in the Presence of Harmonic Excitations: A Review,” 2015, pp. 379–395.
- [134] P. Van Overschee and B. De Moor, *Subspace Identification for Linear Systems*. Boston, MA: Springer US, 1996.
- [135] Michael Ohler N and L. Mevel, “Fast multi-order computation of system matrices in subspace-based system identification,” *Control Eng. Pract.*, vol. 20, pp. 882–894, 2012.
- [136] N. U. Rehman, C. Park, N. E. Huang, and D. P. Mandic, “EMD via MEMD: Multivariate Noise-Aided Computation of Standard EMD,” *Adv. Adapt. Data Anal.*, vol. 525, no. 2, 2013.
- [137] N. E. HUANG, Z. WU, S. R. LONG, K. C. ARNOLD, X. CHEN, and K. BLANK, “On Instantaneous Frequency,” *Adv. Adapt. Data Anal.*, vol. 1, no. 2, pp. 177–229, Apr. 2009.
- [138] N. E. Huang and S. S. P. Shen, *Hilbert–Huang Transform and Its Applications*, vol. 16. WORLD SCIENTIFIC, 2014.
- [139] P. F. Pai, “Hilbert-Huang decomposition of time signals for structural damage detection,” *Proc. SPIE*, vol. 6177, p. 61770Q–61770Q–12, 2006.
- [140] Z. Shi and T. Y. Hou, “Extracting a shape function for a signal with intra-wave frequency modulation,” 2017.
- [141] M. Kasperski, “Actual problems with stand structures due to spectator-induced vibrations,” in *EURODYN’96 European Conference on Structural Dynamics*.
- [142] B. R. Ellis and J. D. Littler, “Response of cantilever grandstands to crowd loads. Part 2: load estimation,” *Proc. Inst. Civ. Eng. - Struct. Build.*, vol. 157, no. 5, pp. 297–307, Oct. 2004.
- [143] J. M. W. Brownjohn, Y. Xu, and D. Hester, “Vision-Based Bridge Deformation Monitoring,” *Front. Built Environ.*, vol. 3, p. 23, Apr. 2017.
- [144] C. Z. Dong, X. W. Ye, and T. Jin, “Identification of structural dynamic characteristics based on machine vision technology,” *Measurement*, Sep. 2017.
- [145] T. Khuc and F. N. Catbas, “Completely contactless structural health monitoring of real-life structures using cameras and computer vision,” *Struct. Control Heal. Monit.*, vol. 24, no. 1, p. e1852, Jan. 2017.

- [146] T. Khuc and F. Catbas, “Non-target displacement measurement of structures using vision based approaches,” in *Bridge Maintenance, Safety, Management and Life Extension*, no. July 2014, CRC Press, 2014, pp. 668–675.
- [147] H. Yoon, H. Elanwar, H. Choi, M. Golparvar-Fard, and B. F. Spencer, “Target-free approach for vision-based structural system identification using consumer-grade cameras,” *Struct. Control Heal. Monit.*, vol. 23, no. 12, pp. 1405–1416, Dec. 2016.
- [148] X. W. Ye, C. Z. Dong, and T. Liu, “Force monitoring of steel cables using vision-based sensing technology : methodology and experimental verification,” vol. 18, no. 3, pp. 585–599, 2016.
- [149] X. W. Ye, T. Yi, C. Z. Dong, T. Liu, and H. Bai, “Multi-point displacement monitoring of bridges using a vision-based approach,” vol. 20, no. 2, pp. 315–326, 2015.
- [150] X. W. Ye, C. Z. Dong, and T. Liu, “A Review of Machine Vision-Based Structural Health Monitoring: Methodologies and Applications,” *J. Sensors*, vol. 2016, pp. 1–10, Nov. 2016.
- [151] X. W. Ye, C. Z. Dong, and T. Liu, “Image-based structural dynamic displacement measurement using different multi-object tracking algorithms,” *Smart Struct. Syst.*, vol. 17, no. 6, 2016.
- [152] X. W. Ye, T.-H. Yi, C. Z. Dong, and T. Liu, “Vision-based structural displacement measurement: System performance evaluation and influence factor analysis,” *Meas. J. Int. Meas. Confed.*, vol. 88, 2016.
- [153] H. Bay and A. Ess, “Speeded-Up Robust Features (SURF),” vol. 110, no. September, pp. 346–359, 2008.